MULTISPECIES EVALUATION OF ANTIRETROVIRAL DISPOSITION IN A PUTATIVE TISSUE RESERVOIR OF HIV: IMPLICATIONS FOR ERADICATION

Corbin G. Thompson

A dissertation submitted to the faculty of the University of North Carolina at Chapel Hill in partial fulfillment of the requirements for the degree of Doctor of Philosophy in Pharmaceutical Sciences in the Eshelman School of Pharmacy (Pharmacotherapy and Experimental Therapeutics).

Chapel Hill
2017

Approved by:

Angela D.M. Kashuba

Philip C. Smith

David C. Muddiman

Amanda H. Corbett

David Margolis

ABSTRACT

Corbin G. Thompson: Multispecies Evaluation of Antiretroviral Disposition in a Putative Tissue Reservoir Of HIV: Implications For Eradication
(Under the direction of Angela D.M. Kashuba)

Ongoing HIV replication within gut lymphoid tissues may contribute to the persistence of HIV despite treatment with antiretrovirals (ARVs). ARVs may have reduced exposure in certain tissue areas, but current methods for assessing ARV tissue concentrations cannot test this hypothesis. The goal of this project was to characterize how ARVs distribute within gut tissue, and determine whether or not they concentrate in areas of local HIV gene expression. Drug transporter expression and localization were also evaluated in these tissues to determine what factors influence ARV distribution.

Using mass spectrometry imaging (MSI), the ileum and rectum of humanized mice (n=49), non-human primates (NHP, n=12) and humans (n=5) were evaluated for ARV distribution. The co-localization of ARV distribution with CD3+ T cells, drug efflux transporters, and HIV RNA expression was assessed. ARV correlation with CD3+ T cells ranged from -0.09 to 0.32 and was not significantly different between species. HIV RNA was not co-localized with ARV exposure in any species (r range -0.09-0.2). ARV-transporter co-localization was highest for MDR1 in all species, and not significantly different between the ileum and rectum. MSI provided previously unobtainable distributional data, showing ARV localization to specific tissue sites and no co-localization with HIV gene expression.

Drug transporters affect ARV tissue disposition and can be exploited to maximize ARV exposure, but quantitative measures of drug transporter protein expression across preclinical species are not available. Gene and protein expression of ARV efflux and uptake transporters were evaluated using qPCR, Western blot, and LC-MS proteomics. Gene and protein expression were generally consistent between infected and uninfected animals and between ileum and rectum. There was poor correlation between methods, and no single method significantly predicted tissue ARV concentrations in a stepwise regression model. We also show that the contribution of human transporter isoforms in humanized mice can significantly affect interspecies comparisons. Human protein expression data was most consistent with humanized mice (1-9 fold different) over NHPs (1-21 fold different). By completing these experiments in two animal species and in humans, we can better understand how HIV persists in tissues and inform the development of targeted therapies for HIV eradication.

To My Family

ACKNOWLEDGEMENTS

I have to recognize the support of many individuals who contributed both professionally and personally to completion of this dissertation. First and foremost, I would like to acknowledge and thank my advisor Dr. Angela Kashuba for her mentorship over the past five years. The scientific and professional guidance she has provided has been invaluable, and I would not have been able to accomplish this goal without her continued push for excellence. I appreciated her willingness to let me work through problems independently while providing appropriate support and oversight. She truly made graduate school an enjoyable experience.

My dissertation committee has been incredibly generous with their time and effort, and I thank them for contributing their expertise and insight. As committee chair, Dr. Smith did a wonderful job of making sure I was comfortable with the state of my project and was always willing to listen to any concerns I had. I admired his approachability and candor during our discussions and thank him for taking on the responsibility of chairing the committee. Dr. Muddiman's willingness to share his technology and collaborate with our group made this entire project possible. His passion for science and excitement about pushing this technology forward made him a valuable resource over the past several years. Dr. Corbett was a fantastic clinical advisor, and gave me the opportunity to experience first-hand what clinical practice in an HIV setting is like. Her consistent mindfulness about how the results of this project may be applied in a real-world setting forced me to consider alternative approaches to data analysis and presentation. Finally, Dr. Margolis's expertise helped me frame this project in the broader context of HIV eradication. As a world-renowned expert in this field, Dr. Margolis generously

provided feedback and suggestions at every stage of this dissertation. His depth of knowledge and insight improved the quality and impact of this work.

I have been privileged to be mentored by and work with many exceptional individuals before and during graduate school. Drs. Crossgrove, Rorabaugh, and Black allowed me to explore my initial interests in research and I am very grateful for their patience and encouragement. Dr. Eli Rosen was a terrific resource and his knowledge, creativity, and resourcefulness came in handy more times than I can count. His willingness to take time to teach trainees and troubleshoot problems was very welcomed. Craig Sykes was critical to moving this project forward and always provided thoughtful perspective on problems that arose during this process. The clinical knowledge I gained from Dr. Marx helpful in framing my project. Heather Prince did a terrific job helping me coordinate the clinical study portion of this project. She sets high standards for herself and others, and the quality of clinical data generated in the lab is a direct reflection of that.

Many collaborators and core facilities have participated in this work. Michelle Mathews at the translational pathology core and Dr. John Fallon were instrumental in method development for numerous aspects of my project, and their tenacity in getting these methods off the ground is appreciated. Our collaborators in Garcia lab here at UNC, the Akkina lab at Colorado State, and the Luciw lab at UC Davis were always willing to share data and samples and this project would not have been possible without their help. I also want to thank the nurses and staff at the CTRC for their hard work, and the women who participated in the clinical study for their altruism and selflessness.

It has been my pleasure to work and train alongside a fantastic group of scientists. All of the members of the Kashuba lab deserve recognition for the hard work they do every day, and for

making the lab a great place to work and learn. Melanie Nicol, Cindi Emerson, Mackenzie Cottrell, Nithya Srinivas, Erin Burgunder, Kuo Yang, Katy Garrett, Mike Weber, John Dohnal, Amanda Schauer, Nicole White, and Kimberly Handy have been great friends and colleagues and I am thankful to have gone through this experience with them. Nancy Gillis has been a great friend and was always willing to give me honest feedback and opinion, and there is an element of perfection in all of her work.

Finally, I want to thank my family and friends for their continued support. I could not ask for a better partner and friend than Anastasia, who loves, challenges, and inspires me every day. I thank Mom, Dad, Connor, all of my grandparents, Aunt Denise, and Uncle David and Eva for their unwavering love and encouragement. I also thank the Barkett family for welcoming me into their lives and providing me with a new batch of siblings. The friendship of John and Diana, Mike and Laura, Alan and Lydia, Andrew, Rabea, Hadiya, and others is valued and appreciated.

TABLE OF CONTENTS

LIST OF FIGURES

LIST OF TABLES

LIST OF ABBREVIATIONS

ABCB1	ATP-binding cassette subfamily B member 1
ABCC1	ATP-binding cassette subfamily C member 1
ABCC2	ATP-binding cassette subfamily C member 2
ABCC4	ATP-binding cassette subfamily C member 4
AIDS	Acquired Immunodeficiency Syndrome
ARV(s)	Antiretroviral(s)
ATZ	Atazanavir
BCRP	Breast cancer resistance protein
BLT	Bone marrow, liver, thymus humanized mouse model
cART	Combination antiretroviral therapy
CYP450	Cytcochrome P450
DTG	Dolutegravir
DTT	Dithiothreitol
EFV	Efavirenz
ENT1	Equilibrative nucleoside transporter 1
FGT	Female genital tract
FTC	Emtricitabine
FTC-tp	Emtricitabine triphosphate
GALT	Gut-associated lymphoid tissue
GI	Gastrointestinal
HIV	Human Immunodeficiency Virus
IHC	Immunohistochemistry
IR-MALDESI	Infrared matrix assisted laser desorption electrospray ionization
ISH	In situ hybridization

LC	Liquid chromatography
LRA	Latency reversing agent
MDR1	Multidrug resistant protein 1
MNC	Mononuclear cell
MRM	Multiple reaction monitoring
MRP1	Multidrug resistance-associated protein 1
MRP2	Multidrug resistance-associated protein 2
MRP4	Multidrug resistance-associated protein 4
MS	Mass spectrometry
MSI	Mass spectrometry imaging
MVC	Maraviroc
NBF	Neutral buffered formalin
NHP	Non-human primate
NRTI	Nucleotide reverse transcriptase inhibitor
NNRTI	Non-nucleotide reverse transcriptase inhibitor
OAT1	Organic anion transporter 1
OAT3	Organic anion transporter 3
OATP2A1	Organic anion transporting polypeptide 2A1
OCT	Optical coherence tomography
OCT2	Organic cation transporter 2
OCT3	Organic cation transporter 3
PBMC	Peripheral blood mononuclear cell
PD	Pharmacodynamics
PEG	Polyethylene glycol
P-gp	P-glycoprotein

PK	Pharmacokinetics
PrEP	Pre-exposure prophylaxis
PVDF	Polyvinylidene difluoride
qPCR	Quantitative polymerase chain reaction
QTAP	Quantitative targeted absolute proteomics
RAL	Raltegravir
RS	Raman spectrometry
SHIV	Simian-human (chimeric) immunodeficiency virus
SLC22A2	Solute carrier family 22 member A2
SLC22A3	Solute carrier family 22 member A3
SLC29A1	Solute carrier family 29 member 1
SLCO2A1	Solute carrier organic anion transporter protein family member 2A1
SIV	Simian immunodeficiency virus
STI	Sexually-transmitted infection
SubQ	Subcutaneously
TBS-T	Tris-buffered saline with Tween 20
TDF	Tenofovir disoproxil fumarate
TFV	Tenofovir
TFV-dp	Tenofovir diphosphate
TPL	Translational Pathology Laboratory
WB	Western blot
ZDV	Zidovudine

Chapter I: HIV Persistence in GALT: Pharmacological Challenges and Opportunities

Summary

An increasing amount of evidence suggests that HIV replication persists in gut-associated lymphoid tissues (GALT) despite treatment with combination antiretroviral therapy (cART). Residual replication in this compartment may propagate infection at other sites in the body and contribute to sustained immune dysregulation and delayed immune recovery. Therefore, it is important to focus efforts on eliminating residual replication at this site. There are several challenges to accomplishing this goal, including low antiretroviral (ARV) exposure at specific tissue locations within GALT, which might be overcome using the tools of clinical pharmacology. Here, we summarize the evidence for GALT as a site of residual HIV replication, highlight the consequences of persistent infection in tissues, identify current pharmacologic knowledge of drug exposure in GALT, define the challenges that hinder eradication from this site, and propose several avenues for pharmacologic intervention.

Introduction

The ability to suppress HIV replication with combination antiretroviral therapy (cART) permanently changed the landscape of HIV/AIDS. Since the introduction of cART in 1996, the life expectancy of HIV-infected individuals has continued to climb to levels near those of non-HIV infected populations, showcasing the dramatic effect of cART on reducing viral load and preventing or reversing AIDS.[1] Despite this, studies evaluating the need for continued cART in the setting of undetectable plasma virus have demonstrated rebound viremia as soon as 2-3 weeks after drug discontinuation.[2–4] Using ultra-sensitive assay techniques, HIV DNA is detectable in resting CD4+ T cells even in patients who have had undetectable plasma viral loads for years.[5] Utilizing decay rates of HIV RNA in plasma and DNA in peripheral blood mononuclear cells (PBMCs), Perelson et al developed a mathematical model which estimated the overall half-life of viral decay to be approximately 44 months.[6] Given this extremely long rate of viral decay , it has been estimated that it would take 73 years of cART to fully eradicate HIV from the body.[7] Therefore, HIV persistence despite cART is a hallmark of HIV infection and represents a significant barrier to cure.

It is well established that HIV latency is a primary driver of persistence in humans. The latent reservoir, comprised of long-lived memory and potentially follicular helper T cells, is established early in infection and is unaffected by current antiretroviral (ARV) therapies.[8,9] However, it also has been hypothesized that ongoing viral replication from productively-infected CD4+ T cells in certain tissue reservoirs may contribute to persistence. While this hypothesis remains controversial, mounting evidence suggests that active replication may be occurring in sites such as the central nervous system, genital tract, and lymphoid tissue.[10–13] Gut-associated lymphoid tissue (GALT) is perhaps the most likely source of ongoing HIV replication given its

high concentration of HIV target cells and its role as a site of initial HIV exposure and early infection. Given the extensive distribution of GALT and its important role in immune function, ongoing replication in this compartment may have clinical consequences not observed from other tissue reservoirs.

As the evidence for ongoing replication in tissue reservoirs continues to grow, so does the need for interventions aimed at eradicating HIV from these sites. Clinical pharmacology can play a large role in understanding how these reservoirs persist in the face of cART, and in the development of targeted interventions for HIV eradication. The tools of pharmacology can also help to clarify the mechanisms of persistence in GALT (e.g. active replication, latency, or both). The pharmacologic mechanisms influencing HIV tissue reservoirs have been previously reviewed[14,15], but none have focused on the unique challenges faced in eradicating HIV replication in GALT. The purpose of this chapter is to summarize the evidence for ongoing HIV replication in GALT, address the challenges associated with current eradication strategies, and propose opportunities for pharmacologic intervention.

HIV Persistence in GALT

GALT is the largest component of the lymphoid system, comprised of the tonsils, Peyer's patches, lymphoid aggregates in the stomach and small intestine, and lymphoid cells in the lamina propria. GALT contains the highest concentration of CD4+ T cells, making it an ideal target for HIV infection.[16,17] GALT is also one of the first tissues to become infected after exposure, with T cell decreases observed as soon as four days after infection.[17–19] Given this early establishment of infection and the large number of target cells, this compartment may be a natural candidate for HIV persistence. Clinical observations support this hypothesis, where HIV

RNA shedding from the rectum of HIV positive, STI uninfected men, was reduced but not eliminated with cART.[20,21] In addition, gut immune activation after initial infection has also been shown to persist despite long-term treatment, suggesting persistent exposure to viral antigens.[22] Further, the amount of infectious virus in active CD4+ T cells (many of which are located in the GALT) was found to be 1.6-fold higher than in resting CD4+ T cells, suggesting that latently-infected cells do not account for all of the residual virus.[23]

Given the lymphoid nature of GALT and the corresponding clinical evidence of persistent replication at this site, several groups have looked for molecular evidence of HIV persistence and compartmentalization in the gut. HIV RNA and DNA have been shown to concentrate in the gut compared to PBMCs, and that this distribution changes along the length of the GI tract (e.g. unspliced RNA in the ileum and rectum were increased 10.2 and 2.4-fold over blood, respectively).[24] In addition, the ratio of RNA/DNA (as high as 4.6) throughout the gut suggests low level replication.[24] Additional work found that HIV DNA concentrations were on average 5-fold higher in the gut versus PBMCs in patients on suppressive cART, even after correcting for T-cell population differences between these compartments.[25] In a study in which DNA was isolated from the rectum, PBMCs, and plasma of patients not receiving cART, greater diversity was observed among gut-derived HIV variants versus those derived from PBMCs, and these variants were interspersed among all three compartments, suggesting movement between sites.[26] Further, no evidence of compartmentalization was observed in a study using DNA isolated from the ileum, colon, and PBMCs of HIV positive patients with undetectable plasma viral loads.[27] This finding was corroborated in further work showing HIV envelope sequences were not significantly different between cells derived from GALT and PBMCs, however the authors did not find evidence of HIV evolution in GALT.[28] In addition, recent phylogenetic work

has shown that viral sequences derived from PBMCs were phylogenetic offspring from sequences derived from lymph nodes in patients with undetectable plasma viral loads.[29] Though this study was not performed in GALT, it demonstrates that focal HIV replication in lymphoid tissue can maintain PBMC infection during suppressive therapy. Together, these data support persistent HIV replication within the GALT, and that this local replication can maintain infection in the plasma through free movement of infected cells or virions between these compartments.

Despite these results, several investigations suggest that GALT is not the sole source of rebound viremia upon treatment cessation. For example, a cross-sectional evaluation of multiple T cell subsets by McBride et al showed that less than 20% of total HIV DNA was found in memory T cells with gut migratory capacity.[30] Further, sequence analysis of rebound plasma virus from three HIV-infected patients who experienced treatment interruption demonstrated that the post-interruption viral sequences were not GALT-derived, suggesting an alternative source of rebound viremia.[31] This hypothesis is supported by a recent study that sampled GALT and lymph nodes before and after treatment interruption and found that rebounding HIV variants likely arise from many anatomic sites, rather than from a small viral population from a single location (e.g. GALT).[32]

Nonetheless, the studies discussed above provide convincing evidence of persistent HIV replication in GALT, although the contribution of this replication to viral rebound remains unclear. Clinical observations are supported by genetic analyses, which indicate that viral gene expression in GALT is maintained even in the setting of undetectable plasma viral loads, and that there is likely cross-talk between plasma and tissue that may propagate infection in PBMCs. Though direct evidence is still needed (since attempts at isolation of replication competent virus

from durably suppressed patients have failed[33]), these data provide a foundation for exploring the mechanisms of HIV persistence in this tissue compartment.

Consequences of HIV GALT Persistence

Immune Dysregulation in Acute Infection As an early site of HIV exposure and infection, GALT plays an important role in the pathogenesis of HIV infection. The interplay between immune cell depletion and activation, local viral dynamics, and systemic immune dysregulation is complex and is the focus of thorough reviews.[34,35] It was observed early in the HIV epidemic that infection resulted in severe GI complications and was associated with increased mortality in AIDS patients.[36,37] This was caused by severe depletion of specific T cell populations within GALT that occur rapidly after infection (27% reduction within 4 weeks).[19] Specifically, IL-17 expressing T helper cell (Th17) populations were found to be preferentially depleted in SIV infection, which may lead to decreased immune function and disruption of gut epithelial integrity.[38] Studies in macaques and humans have shown these T cell decreases to occur within the first week of infection.[17–19] The importance of T cell depletion within GALT has been supported by studies showing that elite controllers do not experience specific depletion of Th17 cells, suggesting that this immune dysregulation is a main driver of disease progression.[39]

Delayed Immune Reconstitution Persistent replication within GALT also represents a large obstacle to restoring immune function in HIV positive patients. It is well documented that immune reconstitution is delayed in GALT following initiation of cART[19], and that a systemic inflammatory state is maintained even after plasma viral loads are undetectable.[40] This persistent inflammation, likely driven by continued GALT disruption, has been associated with poor outcomes and the development of comorbid conditions in these patients.[41] The mechanisms

responsible for this delay have not been fully determined, but several studies have implicated ongoing $CD8^+$ T cell activation, fibrosis, or impaired mucosal homing as contributing factors.[22,42,43] Importantly, ongoing viral replication in GALT could help explain this delay in immune recovery regardless of the specific mechanism(s) involved. Persistent exposure of viral antigen to antigen-presenting cells in the gut can increase inflammatory markers[44], decrease epithelial integrity[45], and increase microbial translocation[46], continuing the cycle of local immune dysregulation and systemic inflammation. Microbial translocation is of particular concern, as this is associated with increased incidence of comorbidities and hastened disease progression.[47,48] The profound immune depletion in GALT, with subsequent clinical complications, underscore the importance of eradicating residual viral replication in this compartment.

Challenges to Eradicating HIV GALT Replication

As introduced above, there are a number of factors that make GALT an ideal reservoir for HIV. The first line of defense against cART lies in the anatomy and location of GALT. Blood perfusion to the GALT via the extensive mesenteric arterial network is more variable than perfusion to other sites, and may be reduced in situations where blood is needed in other organs (e.g. skeletal muscle during exercise, brain during shock). Further, the proximity of GALT to the colorectum, a site of HIV exposure, and the high density of target cells make it a site of initial infection and viral propagation. Clinical evidence suggests that the HIV reservoir is established within days after infection[49], and it is reasonable to expect that this may happen in GALT. Clinical studies show that initiation of cART during the acute-phase reduces, but does not

eliminate, the HIV reservoir,[49,50] likely due to the very early establishment of the latent reservoir before cART can be initiated. Thus, alternative strategies for HIV elimination are required.

A critical obstacle to achieving HIV eradication in GALT is the potential for inadequate ARV distribution into this compartment. ARV penetration into gut tissues is highly variable, both between and within drug classes[51], and is not easily predicted based on chemical structure or standard pharmacokinetic properties.[52] The lack of complete immune restoration in GALT following cART administration and the isolation of HIV RNA from tissues in patients with suppressed plasma HIV RNA levels provides indirect evidence that ARVs may not achieve adequate concentrations in certain areas of GALT. This is supported by tissue homogenate data showing that GI exposures of ARVs such as dolutegravir are 83% lower than plasma.[53] Additionally, studies evaluating the utility of intensified ARV dosing regimens on the size of the viral reservoir have shown little effect, suggesting that anatomic or pharmacokinetic barriers may exist that prevent ARV penetration into GALT.[54,55] A study by Fletcher et al compared ARV concentrations between PBMCs and mononuclear cells (MNCs) isolated from the lymph nodes, ileum, and rectum.[56] It was found that ARV concentrations in gut MNCs were up to 100% lower than PBMC concentrations, and that lower concentrations correlated with slower HIV decay rate in these tissues. These data suggest that ARVs retain their efficacy provided they are able to reach an as-yet unidentified threshold concentration in target cells. However, the interplay between active replication secondary to reduced ARV exposure and latent infection remains unknown, as does the relative contribution of each of these processes to HIV persistence.

Despite the direct and indirect evidence that a lack of ARV tissue penetration contributes to HIV persistence, this idea remains controversial. The most frequently cited counterargument is the lack of observed drug resistance that would be expected to develop in the setting of

subtherapeutic ARV exposure.[57] Given that resistance is known to develop rapidly when ARV concentrations drop below therapeutic concentrations in plasma, it is reasonable to question this pharmacologic assertion. In the absence of widespread resistance developing in patients, some have interpreted the continued detection of HIV gene expression as simply random egress from latency, having little to do with drug penetration.[57] However, it has recently been suggested that ARV exposure in tissue reservoirs may be so low that the threshold for resistance development is never met.[29] In other words, minimal ARV exposure allows for continued replication of wild-type virus which can outcompete resistance variants that could otherwise emerge. In this way, inadequate ARV penetration into tissues may contribute to ongoing replication congruent with clinical observations of low level viremia in patients receiving cART.

In addition to propagating immune dysfunction and systemic inflammation, inadequate ARV penetration into target cells may also hinder efforts of latency reversal and blunt the corresponding host immune response.[22] Reversal of HIV latency in quiescent memory T cells using small molecule drugs represents a promising approach for reduction or eradication of the HIV reservoir, and several drug candidates are currently undergoing clinical evaluation.[58,59] A key assumption underlying these efforts is that virions produced from these re-activated T cells will be unable to infect nearby healthy cells and stimulate new rounds of HIV replication. However, this assumption is valid only if ARVs are present at sufficient concentrations to inhibit viral replication. However, if enough healthy T cells remain unexposed to ARVs[56] in the setting of latency reversal, reactivation of quiescent cells could result in no effect, or possibly an *increase* in the size of the viral reservoir through new rounds of infection.

There are several barriers that complicate the optimization of ARV therapy for HIV eradication in GALT. First and foremost is the limited knowledge of the specific factors that

influence ARV disposition in GALT. ARV penetration into tissues is variable and dependent on several physicochemical and pharmacokinetic characteristics.[51] Volume of distribution and plasma protein binding are important variables and vary widely from drug to drug. Drug transporters and metabolizing enzymes are also known to affect the absorption and distribution of ARVs, and there are many examples of clinically significant drug-drug interactions involving these proteins.[60] Though the specific transporters or enzymes utilized by ARVs vary between drug classes, the metabolizing enzymes of the CYP450 family, particularly CYP3A4, and the efflux transporters p-glycoprotein (P-gp), breast cancer resistance protein (BCRP), and the multi-drug resistance proteins (MRP) are responsible for a significant portion of ARV transport and metabolism.[61] As such, alterations in the expression and/or activity of these proteins can have a dramatic effect on local ARV concentrations. As an example, the penetration of atazanavir (ATZ) into the brain was increased by 5.4-fold in P-gp/BCRP knockout mice compared to wild-type, showing that a lack of functional efflux transporters at the blood brain barrier allows more drug to enter tissue.[62] Other groups have shown that the expression of the uptake transporter family OAT1 at this site also modulates TFV brain penetration.[63] These findings have been corroborated in other tissues such as the testes, where it was shown that inhibition of P-gp and BCRP in human Sertoli cells increases the testicular uptake of ATZ,[64] and in in P-gp/BCRP knockout mice, where ATZ concentrations in testicular tissues were increased by 4.6-fold compared to wild-type mice.[62] A recent paper by Bendayan showed that the penetration of protease inhibitors into human testes was variable and may be dependent on drug transporter expression and localization.[65]

Expression and activity of these proteins is variable along the GI tract.[66,67] For example, protein expression of P-gp and BCRP was found to be 3-fold higher in the ileum versus the

colorectum, with the opposite being true for the efflux transporter MRP2 (1.5-fold lower in ileum vs colorectum).[67] CYP3A4, an enzyme responsible for the metabolism of protease inhibitors, has been shown to be expressed at varying levels in GI tissue, and is highest in the duodenum.[66,68] In combination, these factors may explain the large differences observed in ARV exposure in tissues, including the GI tract. For example, the exposure of the P-gp substrate RAL in the splenic flexure was shown to be 2.8-fold higher than the terminal ileum or colorectum.[69] This is inversely related to the expression patterns of P-gp in the GI tract,[67] suggesting that decreased RAL efflux out of enterocytes secondary to focal decreases in efflux transporter expression can result in compartment-specific increases in RAL exposure along the GI tract. This complicates attempts to achieve maximum drug exposure in tissue, as the local expression of drug transporters and enzymes may be the primary driver of tissue concentration. To date there has been no evaluation of the relationship between these variables and ARV GALT exposure, however given the numerous examples of altered plasma pharmacokinetics secondary to drug transporter or metabolizing enzyme interactions in the gut, it is reasonable to expect that changes in these variables will also have an effect on local ARV exposure in GALT.

An additional barrier to ARV optimization in GALT is the lack of target concentrations for efficacy in this setting. Plasma target concentrations are well established and are easily achievable by standard dosing regimens (derived from early dose finding studies), but similar target concentration values for eradication of residual HIV replication in tissues have not been determined. HIV RNA has been detected in the GI tract of patients receiving cART who had detectable ARV concentrations in these same tissues, providing evidence that current regimens are not sufficient to stop residual replication, although these patients had only been receiving cART for several months.[20] The lack of efficacy observed in ARV intensification studies[54,55]

shows that more sophisticated methods of determining effective concentrations are needed to define pharmacokinetic targets in this compartment, as higher concentrations may be needed for a longer period of time in tissues compared to plasma. In a study of pre- and post-cART reverse transcriptase (RT) sequences in 8 HIV-infected participants, it was found that sequence diversity decreased 1.5-2 fold throughout the gut during treatment, and that zidovudine (ZDV)-resistant variants were concentrated in the gut versus PBMCs, demonstrating that efficacy targets may be different between these compartments.[70] The ability to define exposure-response relationships in GALT and other tissue reservoirs, as has been done in the female genital tract for HIV prevention efforts[71], will be critical to overcoming HIV replication in this compartment. Defining these relationships is unlikely to change current dosing strategies (though dose intensification studies suggests this would have little effect), however a well-defined PK target in tissues would inform the development, or selection, of targeted therapies to stop replication.

The challenges described above highlight the difficulty in eliminating HIV persistence in GALT. While some barriers are unavoidable (e.g. high target cell concentration, size and complexity of GALT, etc.) others, such as inadequate drug penetration or the contribution of drug transporters or metabolizing enzymes, can be acted on in a rational way to improve therapeutic success in this area. The next section focuses on ways that clinical pharmacology approaches can inform the design of targeted therapies for HIV eradication in GALT.

Opportunities for Pharmacologic Intervention

Emerging Technologies to Understand ARV Distribution

The ability to accurately quantify ARV concentrations in tissue reservoirs like GALT is critically important in understanding the distribution of these drugs. To date, most evaluations of

ARV tissue concentrations have used liquid chromatography-mass spectrometry (LC-MS) analysis of tissue homogenates.[51] Though traditional LC-MS methodology can provide clinically useful quantitative data, it does not have the ability to identify distributional patterns within the tissue, as the entire sample is consumed in the homogenization process. This is a critical limitation of the technology, as it has been shown for other drugs that distribution across tissue is not uniform.[72] For example, if the majority of a particular ARV were located in a specific tissue compartment (e.g. epithelial layer) with no distribution into the rest of the tissue, LC-MS may overestimate the penetrative ability of this ARV. This is particularly concerning if HIV replication is occurring in focal areas within a tissue that cannot be reached by ARVs. Further, because the majority of ARVs have intracellular sites of action, concentrations within cells are the largest determinant of antiviral efficacy. MNC isolation from reservoir tissues overcomes the limitations of LC-MS by reporting ARV concentrations only in the cells of interest.[56] However, this method cannot easily or completely account for drug lost during the isolation process which can significantly underestimate true intracellular concentrations,[73] nor can it distinguish cell populations derived from different areas within a tissue. Therefore, it is crucial to use alternative technologies to define ARV distribution into tissues and cells.

Mass spectrometry imaging (MSI) is a growing field that has numerous potential biological applications and is already being implemented in the drug development process.[74] MSI combines the sensitivity and specificity of LC-MS with the ability to visually observe distributional patterns within tissue. Using infrared matrix assisted laser desorption/electrospray ionization (IR-MALDESI), a novel MSI method, we have demonstrated that the distribution of ARVs like efavirenz is heterogeneous within the colorectum, concentrating in the mucosa and lamina propria and corresponding to areas of high CD3+ T cell density.[75] Tissue drug imaging

can be particularly powerful when combined with other techniques such as *in situ* hybridization (ISH) or immunohistochemistry (IHC). Leveraging all of these methods in combination, it is possible to compare ARV distribution to that of HIV target cells (IHC) or to HIV itself (ISH) to determine whether ARV localization corresponds with areas of local HIV replication.[76] Because IR-MALDESI is quantitative[76–78], it is also possible to determine what local concentrations are needed within a tissue compartment to effectively suppress HIV replication, aiding in the search for target concentrations in tissues.

Raman spectroscopy (RS) is another promising imaging technique that has the potential to provide ARV distributional data within unperturbed tissues like GALT. Utilizing the principles of Raman scattering and confocal microscopy, RS can identify exogenous substances, such as small molecule ARVs, in heterogeneous tissue matrices.[79] Like IR-MALDESI, RS can potentially identify areas of ARV localization. Unlike IR-MALDESI, however, RS is able to temporally analyze small molecule distribution, providing spatial information in real time.[80] Recently, RS has been combined with optical coherence tomography (OCT) technology to identify tenofovir distribution in mucosal tissues at various tissue depths.[81] Another advantage of RS, and one that is shared with IR-MALDESI, is the high spatial resolution these technologies can provide. Both technologies have been demonstrated to accurately detect drug at resolutions of 100 microns or lower.[79,82] This is especially important for distinguishing ARV distribution among different cell populations in heterogeneous tissues like GALT. As these technologies improve, it may be possible to distinguish ARV concentrations at different cellular locations[83], providing even more specific PK information in the cytosol (relevant for most ARVs) versus the nucleus (relevant for integrase inhibitors).

Droplet microfluidics is a pioneering technology that allows for high-throughput, single cell assays.[84] In the case of HIV persistence, where proviral DNA may be found in a relatively small number of cells, understanding how the exposure of a current or novel therapy exerts its PD effect *ex vivo* would provide a foundation for optimization of therapy. By encapsulating single cells inside small volume (1pL) droplets and performing reactions within each droplet, microfluidics overcomes the disadvantages of current techniques.[85] This technology has been used previously to perform cellular screening assays for drug effect and genetic analysis to link genotype to phenotype in a single cell population.[86,87] Though this technique has not yet been used to evaluate small molecule concentrations, it shows promise in the area of cellular ARV PK, as differential exposure between and among cell types can be evaluated with high frequency (2000Hz), with simultaneous evaluation of PD effects (protein or gene expression changes).

Evaluation of small molecule tissue and cellular distribution using novel technologies is a burgeoning field. IR-MALDESI and RS have a growing body of evidence demonstrating their utility in this arena. Microfluidics shows additional promise for performing cellular PK/PD evaluations. The advantages and disadvantages of each of these technologies is summarized in Table 1.1. One limitation that is shared by all of these methods is the difficulty in accounting for synergy among ARVs, which may result in adequate control of replication despite suboptimal exposure of the individual drugs. Additionally, though IR-MALDESI has been used to evaluate ARVs from multiple classes[88], RS and microfluidics have had limited or no use in ARV pharmacology to date and it is unknown whether or not these methods will have widespread utility. However, exploring the use of these techniques and others to evaluate ARV distribution in GALT is an important step toward HIV eradication.

Table 1.1: Potential Technologies to Evaluate Small Molecule Tissue Distribution

Method	Quantitative	Visual Inspection of Analyte Distribution	Changes in Exposure Over Time	Resolution	Flexible Workflow/Sample Preparation
LC-MS/MS of Tissue Homogenates [56,89]	Absolute quantitation possible	Not possible	Not possible with a single tissue	Averaged concentrations within an isolated cell population	Validated methods available for most tissue or fluid matrices
Mass Spectrometry Imaging [75-78,86]	Absolute quantitation possible	Yes, across a single tissue cross-section	Not possible with a single tissue	≤ 100 micron spatial resolution	Sample preparation and imaging parameters must be optimized for each tissue
Raman Spectroscopy [79–81]	Absolute quantitation possible	Yes, coupled with optical coherence tomography	Possible in a single transwell experiment	≤ 100 micron spatial resolution	Requires setup of transwell assay system and optimization of analyte detection
Droplet Microfluidics [85]	Quantitation possible with labelled analytes	Not possible in tissue	Not possible with cells from a single tissue	Single cell resolution	Requires specialized cellular isolation and preparation

Defining the Factors Influencing ARV Disposition

When viewed in isolation, drug exposure in tissues is limited in its ability to inform development of HIV therapies targeted at GALT or other tissue reservoirs. Beyond simply defining and describing the problem (e.g. a certain drug is sequestered in the gut mucosa, allowing for ongoing HIV RNA expression in submucosal T cells), distributional data needs to be evaluated from the perspective of improving ARV exposure. As above, ARV disposition in the GALT is dependent on many factors affecting absorption and distribution (Figure 1.1). The physicochemical characteristics of the ARVs themselves likely play an important role in tissue exposure. It has already been shown, for example, that drugs with low plasma protein binding penetrate better into mucosal tissues.[52] Further, the retention time of these drugs (as a function of

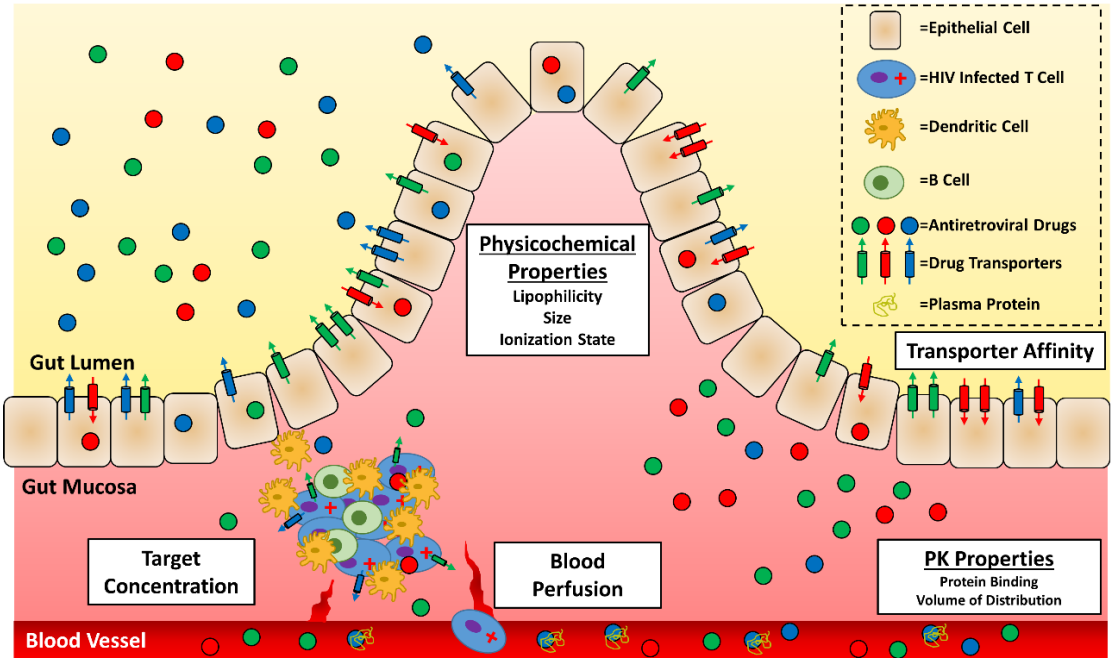

Figure 1.1: Factors influencing Antiretroviral Disposition and Efficacy in GALT Solubilized drugs (green, red, and blue circles) can penetrate into intestinal tissue from peripheral blood supply or directly from the intestinal lumen. Penetration arising from blood is dependent on the amount of local perfusion as well as pharmacokinetic properties of the drug, i.e. drug bound to plasma protein (shown in yellow) cannot enter tissue. Penetration from the gut lumen is dependent on physicochemical properties of each drug as well as affinity for drug efflux (blue, green) or uptake (red) transporters on the surface of epithelial cells. GALT-specific exposure is also dependent on local blood perfusion and drug transporter expression on the surface of lymphocytes.

their half-life in tissues) is also critical, as it has been shown that ARVs like indinavir are rapidly cleared from the lymph compartment despite achieving equilibrium with plasma concentrations.[90] In addition, there may be certain components of the molecular structure of ARVs that favor increased GALT exposure, and these features can potentially be utilized in the development of nanoformulations targeted at tissue reservoirs.[91,92] Targeted nanoformulations have shown success in cancer therapeutics, and several nanoformulated drugs are approved for use in breast and pancreatic cancer, achieving increased exposure into tumors and increasing survival rates.[93] Among ARVs, a nano-formulated version of indinavir was shown to achieve a 6-fold increase in lymph node concentrations and greater exposure in plasma.[94] Additional formulations for drugs such as abacavir, rilpivirine, and efavirenz are already in development,

masking unfavorable PK characteristics to maximize ARV tissue exposure.[95–97] For example, a dimeric prodrug formulation of abacavir, which functions as a P-gp inhibitor when dimerized but that can still exert anti-HIV activity when cleaved to its monomer form, has been developed to increase abacavir penetration into the CNS.[95] Similar approaches for other ARVs to increase GALT exposure should be considered.

Another important step toward eradication is to identify which drug transporters or metabolic enzymes either adversely or favorably affect ARV exposure in the GALT. Exploiting these factors to increase ARV GALT penetration from the lumen (e.g. P-gp inhibition on enterocytes to decrease efflux) or systemic circulation (e.g. CYP3A4 inhibition in the liver to increase half-life) may overcome the inherent challenges in treating GALT persistence. Several studies have shown drug transporter expression to be inconsistent along the GI tract[67], but transporter localization in relation to GALT has not been evaluated in this context. A potential explanation for this gap in knowledge is the lack of consistency with which transporter expression is evaluated and reported, as the methodology used in these studies is highly variable, with groups using qPCR, immunoblot, LC-MS proteomics, IHC, or some combination of these methods.[98–101] Further, there has been no formal analysis of the agreement of these techniques with one another. Gene expression has been shown to vary drastically from end protein expression, and even measures of transporter proteins may give very different results.[101] In order to fully characterize which drug transporters or metabolic enzymes affect local ARV concentrations in GALT, a consensus should be reached on the best expression measures in tissues. Studies formally comparing these methods to each other and examining which method of measurement provides the most useful comparisons to ARV distribution are greatly needed.

Leveraging ARV distribution data against the biologic factors that influence these distribution patterns will provide the most informative data for the design of novel therapies targeted at tissue reservoirs, including GALT. In addition to identifying which ARVs achieve the highest exposure in GALT and if the exposure occurs where latent and/or reactivated HIV virus is located is critical. Further, defining which drug characteristics, transporters, or enzymes should be targeted or avoided when developing new therapies or optimizing existing ones would refine novel strategies to pursue. Importantly, defining the characteristics that affect ARV exposure in GALT is likely to also inform the exposure of LRAs and other small molecules compounds in GALT. While specific factors may differ between drug classes, the lessons learned from evaluation of ARVs in this tissue can be easily translated to LRAs, for which GALT exposure is equally important.

Utilizing Pre-Clinical Models to Streamline Drug Development

The location and nature of many active HIV reservoirs make them difficult to sample in human participants. Limited repeat sampling can be accomplished in some sites including GALT, but extensive evaluation of human GALT tissue remains a challenge, particularly for the ability to recover virus from tissue biopsies. These limitations necessitate the use of pre-clinical animal models to study HIV persistence. Unfortunately, it has been shown that ARV distribution can be variable between species, with tissue ARV penetration varying greatly between humanized mice, non-human primates, and humans. This is especially problematic when plasma data from animal models are used to select effective doses for humans, potentially adversely affecting clinical trials. The reasons for these discrepancies are multifactorial, but species differences in drug transport and metabolism are likely contributors. An extensive review by J.

Lin summarizes some of these differences, including that the concentrations of CYP3A and CYP2C are increased by 1.8 and 12-fold in rats compared to humans,[102] which can lead to increased metabolism of substrates (e.g. protease inhibitors, NNRTIs) and decreased plasma or tissue exposure over time. Further, our group has shown substantial differences in gene and/or protein expression of several drug transporters between humanized mice and non-human primate models, which may affect local concentrations of ARVs transported be these proteins, particularly those affected by P-gp (e.g. abacavir) and BCRP (e.g. dolutegravir) [101,103]

The challenges in reconciling data from pre-clinical species as it relates to HIV persistence have been recognized by the field.[104] However, it is obvious that an animal model that accurately reflects ARV tissue distribution in humans or that can be accurately scaled to predict human distribution would be helpful in the evaluation of candidate ARVs for targeting GALT. The generation of reliable interspecies scaling factors for ARV distribution and metabolism would streamline ARV development when tissue targeting is required. To accomplish this, studies evaluating ARV distribution and metabolism across multiple species including humans, and particularly focusing on GALT, should be conducted. These data can form the foundation for quantifying the variability of ARV distribution across models and developing models to accurately predict these endpoints in humans, and greatly inform eradication strategies, including anticipated combination strategies in which drug-drug interactions are possible.

Conclusion

HIV persistence represents the largest obstacle in the search for a cure. If ongoing replication in GALT is to be eliminated, an understanding of how this reservoir propagates is needed. Although this compartment presents unique challenges to eliminating replication, the

pharmacologic tools described here offer promising solutions. Tissue imaging provides distributional data that has been previously unattainable, and will allow the field to assess whether or not ARVs have a significant presence in reservoirs by identifying and quantifying within-tissue localization. This has enormous implications for HIV persistence; heterogeneous ARV distribution in the GALT would provide convincing evidence that current therapies are simply not present where they are needed, while reproducibly broad distributional patterns would suggest alternative reasons for persistent infection. Demonstrating that HIV replication is occurring in areas or cells with low ARV exposure would provide further evidence that inadequate ARV tissue exposure contributes to HIV persistence.

In addition to clarifying the mechanisms driving HIV persistence in GALT, the tools of pharmacology can be used to inform the development of targeted therapies for HIV eradication. Defining the factors governing ARV exposure in GALT will help to identify which variables to target or avoid during the development of novel small molecules, particularly once preferred methodologies for measuring these factors are identified. Additionally, performing these evaluations in multiple pre-clinical species will provide foundational knowledge of interspecies tissue distribution differences. This will be critical for the evaluation of candidate ARVs and latency reversing agents for targeting reservoirs by preventing the inappropriate interpretation of data from one species to another. Ultimately, these data will allow for a more directed design of therapies aimed at eradicating HIV reservoirs and potentially curing HIV.

Specific Aims

AIM 1: Define ARV distribution within a putative viral reservoir from 2 animal species using IR-MALDESI imaging and LC-MS/MS methods

1a: Using IR-MALDESI imaging, characterize and quantify the spatial distribution of ARVs from 5 therapeutic classes within the gastrointestinal-associated lymphoid tissue (GALT) of non-human primates (NHP), and 2 humanized mouse models. This will allow for determination of whether ARVs concentrate in certain tissue sub-compartments, and whether this differs across pre-clinical species. *Discussed in Chapter II*

1b: Utilizing tissues collected in Aim 1a, identify the distribution of HIV target cells and HIV RNA, and quantify their co-localization with ARV distribution. By co-localizing ARV distribution with these variables, deficiencies in exposure at the site of action can be identified. This will provide critical data to clarify the mechanisms of HIV persistence. *Discussed in Chapter II*

AIM 2: Identify the physiologic factors that influence ARV distribution and activity in tissues suspected of being active viral reservoirs.

2a: Quantify the gene and protein expression of relevant drug transporters in the GALT of humanized mice and NHPs using qPCR, Western blotting, and LC-MS proteomics. Quantify cross-species variability and identify any species-specific features which may influence drug transporter activity. This will be the first comprehensive comparison of commonly-used methodologies for drug transporter expression across species. *Discussed in Chapter III*

2b: Utilizing tissues collected in Aim 1a, evaluate the potential effect of drug efflux transporters on ARV distribution by quantifying ARV/transporter co-localization along the gastrointestinal

tract. Determine whether or not these effects are differential between transporters, between species, or between anatomic sites. *Discussed in Chapter III*

AIM 3: Identify ARV regimens that concentrate within active viral reservoirs and assess their impact on HIV persistence in humans.

3a: Characterize and quantify the distribution of four commonly used ARV regimens within the GALT of virologically suppressed HIV positive patients using IR-MALDESI quantify co-localization with target cells and HIV RNA. Define the relationship between data from humans and animal models. These interspecies comparisons will inform the development of novel targeted therapies. *Discussed in Chapter IV*

3b: Using tissues collected in Aim 3a, quantify drug transporter gene and protein expression by qPCR and LC-MS proteomics, and assess co-localization of drug efflux transporters with observed ARV distribution. Quantify the agreement in transporter expression data between species and identify differential effects of drug transporters on ARV distribution between animals and humans. *Discussed in Chapter IV*

Chapter II: Mass Spectrometry Imaging to Determine Antiretroviral GALT Exposure in Preclinical Models of HIV Infection

Summary

HIV replication within the gut may be propagated by reduced antiretroviral (ARV) exposure. Mass spectrometry imaging (MSI) provides biodistribution data that LC-MS cannot. Here, we use MSI to visualize ARV distribution within gut tissues from two species, and assess co-localization with HIV target cells, HIV RNA, and drug efflux transporters. Two humanized mouse (n=49) and one primate (NHP, n=12) models were given combination ARVs. One 10μm slice from frozen ileum and rectum was analyzed by MSI. Serial slices were analyzed for CD3+ T cell and efflux transporter localization by IF/IHC, and HIV RNA by ISH. Co-localization of ARV and IF/IHC/ISH imaging was performed in Matlab using Pearson correlation (r). ARV distribution was heterogeneous in NHP tissues with 2-fold greater mucosal accumulation in NHP vs mice, where the majority of ARV detection was secondary to heme. ARV-T cell correlation ranged from -0.09 to 0.32, was consistent between species and up to 4-fold higher in the NHP ileum versus the rectum. HIV RNA was preferentially detected in areas of low TFV and MVC exposure in both species (overall range -0.09-0.2). ARV-transporter co-localization was variable between ARVs and highest for MDR1 (range -0.09-0.54) in both species. Co-localization suggests efflux transporter expression results in lower ARV exposure in HIV target cells in the ileum, which may contribute to low level HIV replication. This is supported by HIV RNA detection in the absence of ARV signal. These data support the hypothesis that GALT may act as an HIV reservoir, and will inform the development of targeted therapies for HIV eradication.

Introduction

The persistence of HIV despite treatment with combination antiretroviral therapy (cART) is the major obstacle to eradication of this disease, necessitating lifelong therapy in infected individuals. Rebound plasma viremia after treatment cessation is thought to be secondary to reactivation of multiple latently-infected memory T cell populations.[4,5,8,9] The elimination of this latent cellular reservoir has received most of the focus of HIV eradication research to date, however it has been hypothesized that residual HIV replication from active T cells within tissue reservoirs may also contribute to viral rebound upon treatment interruption.

The evidence for continued production of replication-competent virions within certain anatomic sites continues to grow and has been extensively reviewed.[14,15] Several tissue compartments, such as the central nervous system[10], male and female genital tracts[11,12], gut-associated lymphoid tissue, and peripheral lymph nodes[13] have been implicated as potential tissue reservoirs. The contribution of these tissue reservoirs to persistent replication was recently investigated by Lorenzo-Redondo et al, who showed that viral sequences isolated from the lymph nodes of suppressed patients were genetic descendants of peripheral blood mononuclear cell (PBMC)-derived variants and vice versa, demonstrating viral evolution during cART and supporting the active reservoir hypothesis.[29] Additionally, several groups have used *in situ* hybridization to show localized HIV RNA expression in tissues from cART-treated individuals.[32,56] While it is unlikely that all of this RNA represents replication-competent virus[105], these data suggest that the latent reservoir is not the sole contributor to HIV persistence.

The extensive immune network contained within GALT and its role as a site of early infection make it an important target for HIV eradication efforts. The consequences of HIV persistence in GALT, such as prolonged immune dysregulation and delayed reconstitution during

cART, are unique from other anatomic compartments and have been previously reviewed in Chapter I.[106] The mechanism(s) underlying propagation of tissue reservoirs like GALT is unclear, but suboptimal antiretroviral (ARV) penetration into tissues has been suggested as a potential cause.[56] Inadequate ARV exposure at the site of action would help explain the persistence of HIV replication and provide an avenue to develop targeted therapies. Unfortunately, traditional methods of analyzing small molecule penetration into tissues are limited in their capacity to measure within-tissue distribution. Liquid chromatography-mass spectrometry (LC-MS) of tissue homogenates has been the gold standard for ARV tissue analysis, but provides only an averaged concentration over the entire tissue. If HIV replication is occurring focally (e.g. in a single lymphoid follicle), this method may misrepresent ARV exposure at the site of action. Some groups have isolated the mononuclear cell (MNC) population from tissues before performing LC-MS.[56] While this method is an improvement over homogenate analysis, it does not account for drug lost during MNC isolation[73] and cannot distinguish between MNCs from different sites within the tissue.

Mass spectrometry imaging (MSI) allows for the visual inspection of small molecule analytes within a tissue section, while simultaneously providing absolute quantitation.[77,107] We have previously demonstrated our ability to detect efavirenz (EFV) distribution within several putative tissue reservoirs, including gastrointestinal tissues, and showed that its distribution was heterogeneous.[75] An advantage of MSI that has yet to be explored is the ability to co-localize ARV distribution with other targets from adjacent tissue slices. Understanding ARV disposition as it relates to HIV target cells, drug transporters, and HIV RNA expression would greatly inform the eradication field, as focal HIV RNA expression in areas of low ARV exposure would provide convincing evidence that suboptimal ARV penetration propagates tissue reservoirs. In

addition to the lack of within-tissue distributional data, there is a paucity of data on how ARV distribution differs among pre-clinical species and between animals and humans. The development of any new therapeutic agent requires testing in animal models, but efficacy measures for these studies can be greatly skewed if within-tissue distribution is different from humans. Defining the differences in ARV distribution, if any exist, between animal models will inform the development of novel therapies for use in humans.

In this study, we use MSI to visualize the distribution of ARVs from multiple therapeutic classes in two GI tissues from three animal models. We quantify concentration in the mucosal compartment, and assess the co-localization of ARVs with HIV target cells and with viral RNA expression. Additionally, we assess whether ARV localization is correlated with HIV RNA expression, or whether focal RNA expression occurs in the absence of ARV exposure. Finally, we evaluate the effect of drug transporters on observed distribution patterns, and quantify the differences between species. The data generated here provide insight into the mechanisms of HIV persistence in GALT, and will form the basis of studies aimed at optimizing cART to eradicate HIV.

Methods

Animal Models

Uninfected Animals

Three commonly used animal models from two species were employed in this study: the hu-HSC-Rag (n=20) and bone marrow-liver-thymus (BLT; n=6) humanized mouse models and a rhesus macaque non-human primate model (NHP; n=6). Humanization protocols used to generate both mouse models have been described previously.[108,109] Female hu-HSC-Rag mice

aged 3-6 months underwent humanization as previously described, and were then dosed with one of several ARV regimens for 10 days: EFV 10mg/kg (n=6) alone; atazanavir (ATZ) 140mg/kg (n=6) alone; or tenofovir (TFV) 208mg/kg, emtricitabine (FTC) 240mg/kg, raltegravir (RAL) 56mg/kg, maraviroc (MVC) 62mg/kg (n=6) in combination. Each drug was given once per day (QD). A single cohort of female BLT mice also underwent humanization and received a combination of TFV, FTC, RAL, ATZ, and MVC at equivalent doses for 6 days (toxicity has been observed with longer dosing periods). All drugs were administered by oral gavage, and dosing solutions were prepared by solubilizing formulated drug. Dosing regimens for each animal model are summarized in Table 2.1.

Table 2.1: Sample size and ARV administration schematic

Dosing Regimen	MICE				MACAQUES			
	BLT		hu-HSC-Rag		TFV/FTC/ATZ/MVC		TFV/FTC/EFV/RAL	
	+	-	+	-	+	-	+	-
EFV			N=6	N=6				
ATZ			N=6	N=6				
TFV/FTC/RAL/MVC			N=6	N=6				
TFV/FTC/RAL/MVC/ATZ	N=7	N=6						
CONTROL	N=2	N=2	N=3	N=2				
TFV/FTC/ATZ/MVC					N=3	N=3	N=3	N=3
TFV/FTC/EFV/RAL					N=3	N=3	N=3	N=3

The extent of humanization for both mouse models was assessed by quantifying human T cell populations using flow cytometry as previously described.[109] Male rhesus macaques (*Macaca mulatta*) between 3 and 7 years of age were dosed for 10 days with TFV 30mg/kg subcutaneously (SubQ), FTC 16mg/kg (SubQ) and one of the following regimens: MVC 270mg/kg twice daily (BID) with ATZ 150mg/kg BID OR EFV 200mg QD with RAL 100mg/kg

BID. Doses for all drugs in all animal models were chosen based on commonly used treatment doses for HIV infection in these models.[110–114] Two animals from each mouse model were not dosed with ARVs and used as controls. Dosing periods for all animals were chosen to achieve pharmacokinetic steady-state in tissues based on known half-lives of the drugs used and previous studies with these models.

Infected Animals

To assess the effect of infection on drug distribution and transporter expression, three additional cohorts of animals (n=21 hu-HSC-Rag, n=18 BLT, n=6 macaques) were infected and dosed with identical ARV regimens. Flow cytometry was used to quantify the extent of humanization at baseline and at 4 weeks post-infection. The hu-HSC-Rag animals were infected intraperitoneally with 200µL 2.1 x 10^6 IU/mL of $HIV_{Bal\ D7}$. Plasma HIV RNA was measured weekly beginning two weeks after inoculation and continuing for 4 weeks. ARV dosing commenced once 4 weeks of durable HIV infection was established, and a final viral load was measured during therapy. BLT mice were infected intravenously with 200µL 90,000 TCIU of HIV_{JRcsf}, with plasma HIV RNA being measured 1, 2 and 4 weeks after inoculation to confirm durable infection, and once after starting therapy. Macaques were infected intravenously with $10^{4.5}$ $TCID_{50}$ of RT-$SHIV_{mac239}$, with viral loads measured weekly after inoculation.

Tissue Collection

One day after the final ARV dose was administered, animals were euthanized and underwent necropsy. Whole blood was collected via retroorbital or cardiac puncture for mice and venipuncture for macaques. Several tissues suspected of being HIV reservoirs were collected from all animals, including the ileum and rectum. After removal from the body, tissues were cut

into two approximately equal sized pieces (~100mg for the mice ileum, ~10mg for the mice rectum, and ~2g for non-human primate (NHP) ileum and rectum), placed into separate aluminum foil pouches and snap frozen on dry ice. Total time from euthanization to tissue freezing was less than 60 minutes for all tissues. After freezing, tissues were stored at -80˚C for further analysis. All animal experiments were performed in accordance with locally-approved IACUC protocols.

Tissue Slicing

To generate serial sections for multi-modal analysis, tissues were sliced frozen at 10µm thickness using a cryostat (Leica Biosystems, Wetzlar, Germany) and thaw mounted onto glass microscope slides in the following order: 8 slices for immunohistochemistry (IHC), 2 slices for MSI (one for analysis and one backup), 2 slices for LC-MS, 15-20 slices for ISH. NHP tissues were mounted on optimal cutting temperature (OCT) compound and sliced individually, however the small size of the mouse tissues (3-5mm cross sections) precluded this method. Instead, mouse tissues were grouped by dosing cohort and mounted within a 50:50 gelatin carboxymethylcellulose gel block, which was snap frozen and stored at -80°C. Each frozen gel block was mounted on OCT, sliced and thaw mounted, allowing for mounting and analysis of up to 6 mouse tissues simultaneously.

Mass Spectrometry Imaging and Absolute Quantitation

ARV distribution within each tissue was assessed using infrared matrix-assisted laser desorption electrospray ionization (IR-MALDESI) as previously described.[75,107] The glass microscope slide containing the thaw mounted tissue was placed into the source chamber and

maintained at -10˚C. Relative humidity inside the chamber was reduced to <6% to allow for sample cooling without condensation of water vapor, then humidity was increased to deposit a layer of ice across the entire stage. Tissues were ablated with two pulses of a mid-IR laser (IR-Opolette 2371, Opotek, Carlsbad, CA) with a 100um spot-to-spot distance. Ablated molecules were ionized by orthogonal electrospray using 0.2% formic acid in 50:50 methanol water as an electrospray solvent and sampled into a Thermo Fisher Scientific Q Exactive mass spectrometer (Bremen, Germany) for analysis in positive ion mode. Raw data from each voxel were converted to the mzXML format with MSConvert (ProteoWizard), then to the imzML format for interrogation using MSiReader, which allows for generation of images of ARV distribution across the tissue slice.[115]

Absolute quantitation of ARV concentration was achieved by spotting a series of calibration standards (of known ARV concentration) onto a non-dosed "blank" NHP tissue slice from identical tissue matrices (ileum or rectum; Bioreclamation IVT, Baltimore, MD). 100nL of each calibration standard was spotted onto the tissue, allowed to air dry, then placed inside the source chamber and analyzed in an identical manner to the samples. A new calibration tissue was analyzed every day that sample analysis occurred to account for inter-day variability run conditions (electrospray stability, relative humidity, thickness of ice layer, etc.). Calibration tissues were analyzed in MSiReader, where the summed pixel intensity over each calibration spot was plotted against the known ARV concentration to generate a calibration curve. The slope and intercept of this curve was applied to the summed pixel intensity value for each ARV over the entire area of the corresponding sample to generate an absolute concentration.[77] To quantify ARV concentration in mouse tissues, a single calibration spot was applied to a blank mouse tissue and analyzed in tandem with NHP calibration tissues. The pixel intensity value for the

mouse calibration spot was used to adjust the slope and intercept of the NHP calibration curve (to account for response differences between tissues from different species), and the adjusted calibration curve was applied to mouse samples. Resulting ng/slice concentrations were converted to µg/g using the known area of each tissue slice, depth of each tissue (10um), and an assumed tissue density of 1.06g/mL.

LC-MS Analysis and Comparison to MSI

Plasma and tissue ARV quantitation of each sample was performed using LC-MS methods as described previously.[75] Plasma samples, calibration standards, and quality control samples underwent protein precipitation followed by LC-MS/MS. Internal standard was added to plasma and mixed with 600µL of acetonitrile. Samples were vortexed and centrifuged, then the supernatant was diluted with 50:50 methanol:water. For tissues, 1 mL of ice cold 70:30 acetonitrile-water was added to sample tubes containing a serial 10µm section from each sample. Samples were sonicated for 10 minutes with calibration standards and quality control samples. Separation for both matrices occurred on a Shimadzu high-performance liquid chromatography system, and an AB SCIEX API 5000 mass spectrometer (AB SCIEX, Foster City, CA, USA) equipped with a turbo spray interface was used as the detector. The dynamic range of the plasma assay ranged from 1-20,000ng/mL for TFV, ATZ and EFV, 1-8,000ng/mL for MVC, 8-20,000ng/mL for FTC and RAL. The dynamic range for tissues range from 0.1-50ng/mL. The precision and accuracy of the calibration standards and QC samples were within the acceptable range of 15%. Tissue concentrations were reported as ng/slice and converted to µg/g using an assumed tissue density of 1.06 g/mL.

In order to assess the agreement of the experimental MSI and reference LC-MS methods, tissue ARV concentrations from both methods were normalized for the corresponding plasma concentrations to generate tissue penetration ratios (TPRs; duplicate LC-MS samples were averaged before normalization). Bland-Altman plots were used to evaluated the agreement between methods for each ARV evaluated.

Immunofluorescence (IF)/Immunohistochemistry(IHC)

Dual IF on frozen humanized mouse and NHP sections were performed in the Bond fully-automated slide staining system (Leica Microsystems) using Bond Polymer Refine Detection kit (DS9800). Slides were allowed to sit at room temperature for 15 minutes, then fixed in 10% NBF for 15 minutes. They were then placed in Bond wash solution (AR9590). Antigen retrieval was done at 100°C in Bond-epitope retrieval solution 2 pH9.0 (AR9640) for 10 minutes. Staining was performed first using CD4 1F6 antibody (Abcam clone BC/ 1F6) at 1:50 dilution for 1h with Bond Polymer and Post-Primary reagents and Cy5 fluorochrome (Perkin Elmer) for 15 minutes. Antigen retrieval was done at again 100°C in Bond-epitope retrieval solution 2 pH9.0 (AR9640) between protocols. Slides were then stained with CD3 (Leica clone LN10) Ready-to-Use antibody for 15 minutes and Dako Envision mouse secondary for 30 minutes. Cy3 fluorochrome (Perkin Elmer) was applied for 15 minutes. IF slides were counterstained with Hoechst 33258 (Invitrogen, Carlsbad, CA) and mounted with ProLong Gold antifade reagent (P36934, Life Technologies).

Drug efflux transporter localization was analyzed using IHC. Frozen serial sections were stained with primary antibody for MDR1 (1:50; Abcam, Cambridge, MA), MRP2 (1:50, Kamiya Biomedical, Seattle, WA), MRP1 (1:100, Santa Cruz Biotechnology, Santa Cruz, CA), or BCRP

(1:50; Santa Cruz) for 15-60 minutes followed by pH antigen retrieval (Leica). DAB (3,3'-diaminobenzidine) was used as a substrate-chromagen for detection. All staining was performed on a Leica Bond automated tissue stainer (Leica). Mouse and NHP liver tissues were used as a positive control for all antibodies, and negative staining was performed using secondary antibody only. Samples were visually evaluated for transporter localization.

In Situ Hybridization (ISH)

15-20 serial sections from each tissue were evaluated for HIV/SHIV RNA expression using RNAscope.[116] Before beginning the RNAscope procedure, slides were fixed in 4% paraformaldehyde at 4˚C for 15min followed by dehydration with graded ethanol washes (50%, 70%, 100% ethanol for 5 minutes each). Detailed methodology for the RNAscope procedure is described elsewhere[117], but briefly, slides were boiled to retrieve epitopes in P2 ACD buffer for 30 minutes followed by peroxidase blocking for 10 minutes at room temperature, rinsing with double distilled water, dehydrating with 100% ethanol for 5 minutes, then air drying. Slides were then incubated for 20 minutes at 40˚C with protease digestion solution from ACD (P3). After protease digestions, slides were rinsed with double distilled water and incubated with HIV clade B or SIV_{mac239} ACD probes for 2 hours at 40˚C. Slides were then washed in 0.5X ACD wash buffer and incubated in amplification reagents according to RNAscope 2.5 HD detection protocol[117]. All reagents used in the hybridization process were obtained from Advanced Cell Diagnostics (ACD, Newark, CA) and used according to manufacturer's protocol with some minor adaptations. After counterstaining slides with Hematoxylin, slides were mounted in clear mount and cover slipped.

Image Co-localization

Image manipulation and co-registration was performed using the Matlab v. R2015a Image Processing Toolbox (Mathworks, Natick, MA). A schematic of the co-localization workflow is shown in Figure 2.1. For a given sample (Figure 2.1a), MSiReader was used to export pixel intensity matrices for cholesterol, heme, and each ARV of interest across the entire tissue slice into Matlab; IF and IHC samples were scanned as described above and downsampled to match the resolution of the MSI data. Off-tissue response was eliminated by using cholesterol signal to mask ARV response, such that only on-tissue signal was shown. To eliminate the confounding effect of ARVs contained within the vasculature, ARV responses were again masked based on heme distribution (Figure 2.1b) to show only the ARV signal that localized outside the microvasculature. To ensure that MSI-derived images and IF/IHC/ISH images were appropriately aligned before co-localization, co-registration was performed on the cholesterol image using the

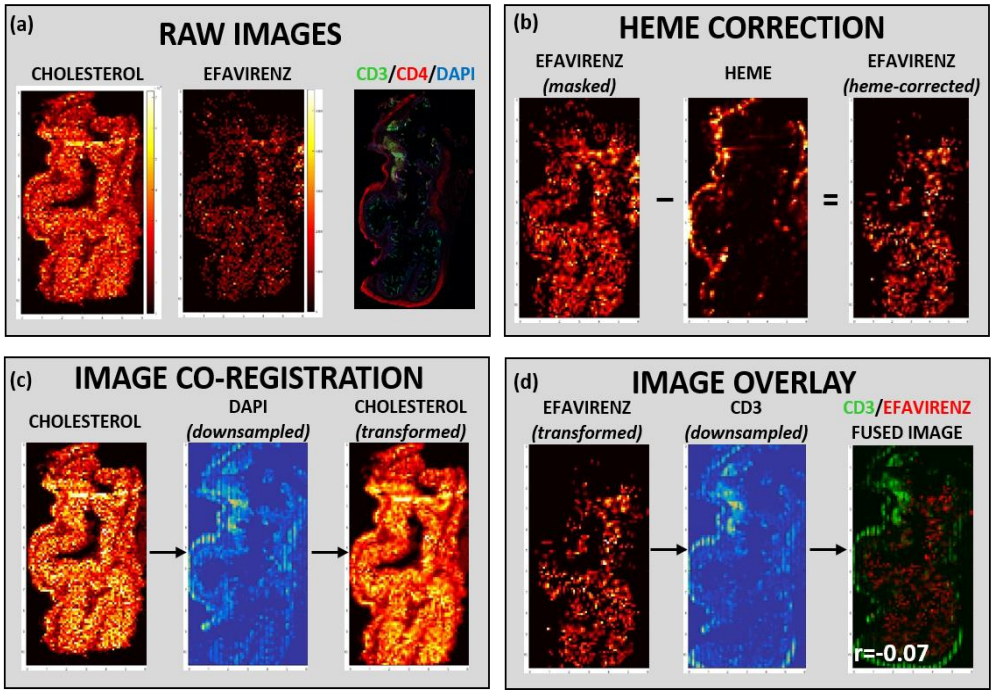

Figure 2.1: Image Co-localization Workflow Representative raw IR-MALDESI and IF (a). Total ARV signal is masked based on corresponding heme distribution (b). (c) Co-registration of cholesterol and DAPI image. (d) Overlay of ARV and variable of interest (CD3 in figure) to form fused image of ARV (red) and CD3 (green), with correlation coefficient shown.

background DAPI stain as a reference (Figure 2.1c). The resulting transform variable was applied to all ARV images so that every ARV image was identically-oriented. Finally, the heme-corrected transformed ARV images were overlayed with the variable of interest (CD3, MDR1, etc.) to generate a fused image (Figure 2.1d) containing both the ARV (in red) and the variable of interest (in green). After image overlay was performed, Pearson's correlation was performed to assess the co-localization of both variables.

Statistical Analysis

Descriptive statistics (median, range) of plasma and tissue concentrations as well as correlation coefficients were generated for each drug in each animal model. Pearson correlation was performed only on tissues where both variables were detected. Comparisons between animal models and between anatomic compartments were performed using Kruskal-Wallis ANOVA on ranks. $p<0.05$ was considered statistically significant.

Results

Plasma Exposure of Antiretrovirals

ARV concentrations in plasma collected at necropsy were measured to verify absorption of oral doses and to ensure consistency across animal models. ARV plasma concentrations were detectable in >90% of samples. Figure 2.2 compares plasma exposure between infected and uninfected animals from each model. No significant differences were observed between these groups. Given the overall lack of differences in plasma exposure, data were combined in Figure 2.3, which shows plasma data across all animal models. There were no statistically significant differences between the two humanized mouse models except for RAL, where plasma exposure showed a 10-fold increase in BLT mice over hu-HSC-Rag mice (p=0.03). Despite receiving different ARV dosing, the NHPs had plasma concentrations that were not significantly different than the humanized mice, with the exception of RAL which was 2-logs higher in NHPs over humanized mice (p<0.001).

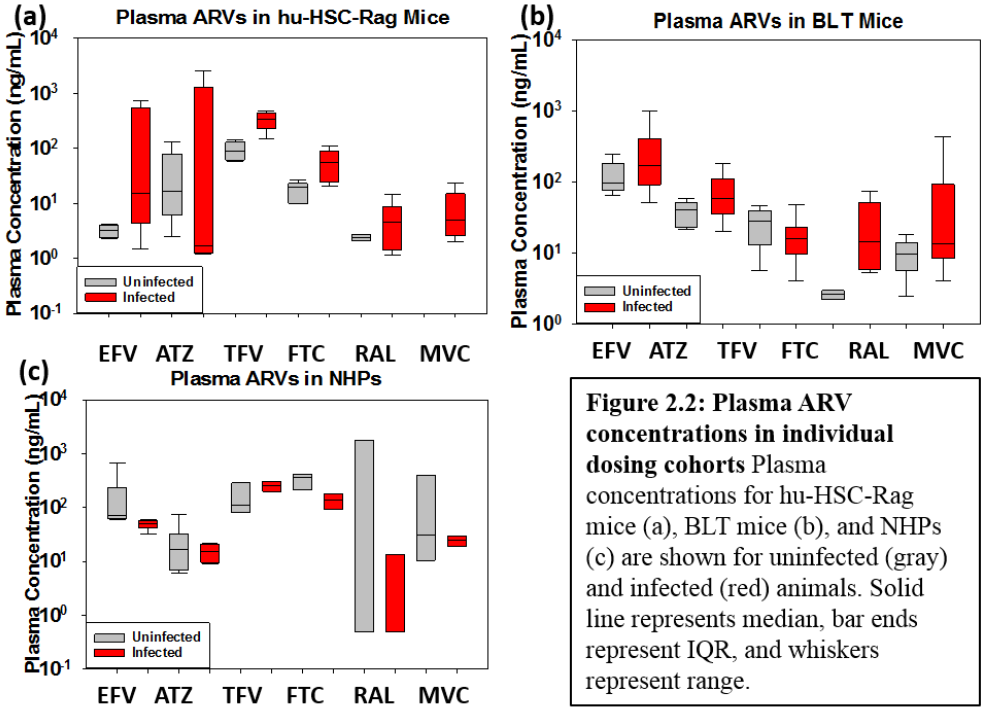

Figure 2.2: Plasma ARV concentrations in individual dosing cohorts Plasma concentrations for hu-HSC-Rag mice (a), BLT mice (b), and NHPs (c) are shown for uninfected (gray) and infected (red) animals. Solid line represents median, bar ends represent IQR, and whiskers represent range.

Quantitative Comparison of LC-MS and MSI

We have published LC-MS tissue concentrations from these animals using larger tissue samples (three 50 micron slices)[118], however here we utilize concentrations obtained from a single 10 micron serial slice to make a more direct comparison. In mice, tissue concentrations from serial slices were detected with far less frequency than larger samples, ranging from 8% detection for EFV to 77% detection for TFV. MVC was not detected in any hu-HSC-Rag tissue sample despite detection in plasma, but did achieve measurable concentrations in BLT ileum and rectum. Detection of ARVs in tissue slices by MSI was also sporadic in mice, with detection largely mimicking LC-MS results (ranging from 4% detection for EFV samples to 55% detection for TFV). Unlike LC-MS, MVC was detected in 50% of samples using MSI in both hu-HSC-Rag and BLT mice. Conversely, the NHP samples had detectable ARV concentrations in >85% of samples for every ARV evaluated by LC-MS, and 100% of samples by MSI.

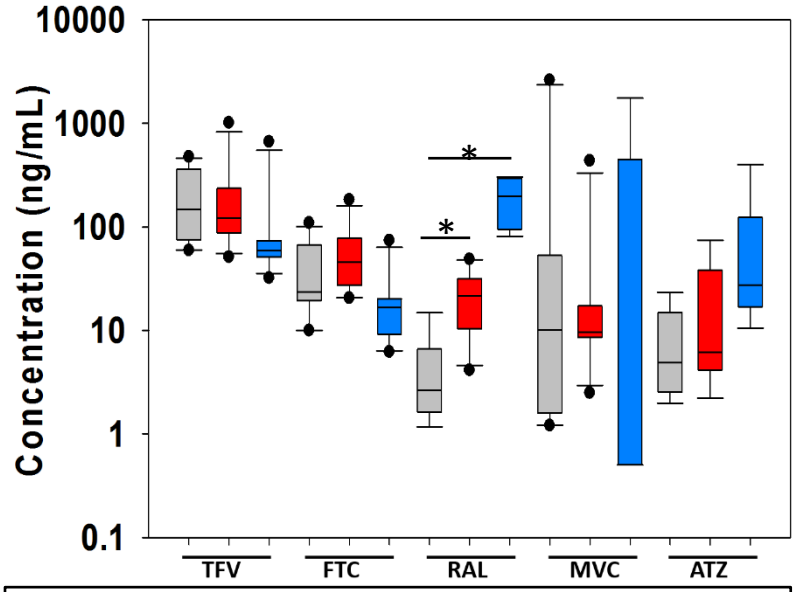

Figure 2.3: ARV Plasma Concentrations Across Animal Models Plasma concentrations are shown for hu-HSC-Rag mice (gray), BLT mice (red), and NHPs (blue) for each ARV. Solid line represents median, box ends represent IQR, and whiskers represent range. Solid dots are outlier values. *p<0.05

We have previously demonstrated our ability to obtain absolute quantitation of ARVs in tissue slices using IR-MALDESI and showed good agreement (with 15%) with LC-MS[75], however this was performed on tissues from a single animal. Here, we performed a more comprehensive comparison between these methods using Bland-Altman plots, which are shown in Figure 2.4. Mean bias between methods ranged from -0.06 for MVC to -8.65 for ATZ. TFV (Figure 2.4a), FTC (Figure 2.4b), and MVC (Figure 2.4e) did not demonstrate bias toward one method over

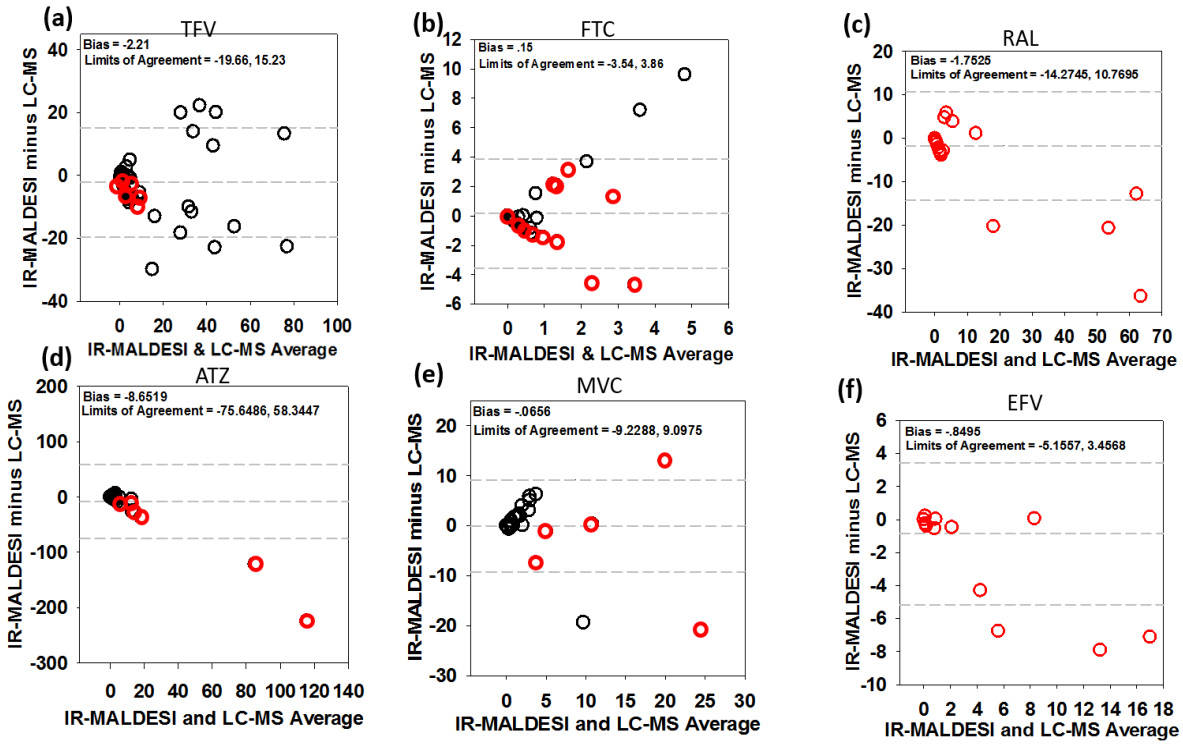

Figure 2.4: Comparison of LC-MS and IR-MALDESI Methods Comparison of paired tissue sample concentrations generated using each method are shown for each ARV (a-f), with method average along the x-axis and method difference along the y-axis. Middle dashed line represents mean bias; upper and lower dashed lines represent the upper and lower limits of agreement (i.e. confidence intervals). Red circles are NHP data; black circles are humanized mouse data.

another, with concentrations spread evenly above and below zero. For RAL (Figure 2.4c), ATZ (Figure 2.4d), and EFV (Figure 2.4f), the bias favored higher LC-MS concentrations over MSI as the average concentration increased, potentially indicating saturation of MSI detection at higher concentrations.

Heterogeneous ARV Distribution in Gastrointestinal Tissues and Co-localization with HIV Target Cells

Figure 2.5 showcases representative images of differential ARV distribution from a single NHP tissue slice. TFV (Figure 2.5b) and FTC (Figure 2.5c) showed disparate distribution patterns, with TFV giving the highest signal in the lumen, with low but consistent penetration into the mucosa and muscularis, while FTC was minimally detected in the mucosa. Consistent with previously published data[75], EFV distribution was not homogenous throughout the NHP ileum or rectum, instead localizing in the mucosal layer with little penetration into the muscularis (Figure 2.5d). RAL, on the other hand was localized to the lumen and showed less penetration into the mucosa (Figure 2.5e). The potential effect of these differences in ARV distribution on exposure in HIV target cells is reflected by the ARV-CD3+ T cell correlation coefficients in Figure 2.5g-j. For example, although RAL showed greater

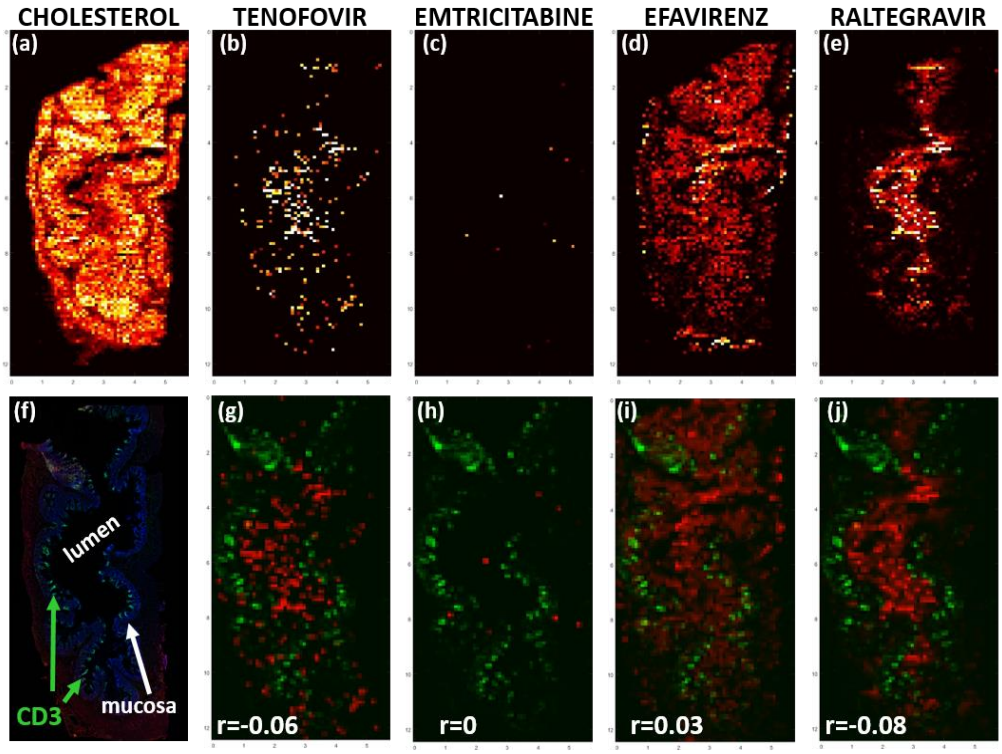

Figure 2.5: Differential ARV Localization Within a Single NHP Tissue Slice Representative heme-corrected IR-MALDESI and IF images from a NHP ileum (a-f). Overlay images (g-j) show ARV in red and CD3+ T cells in green.

sequestration to the luminal area of the tissue versus EFV, the co-localization of these drugs was not markedly different, with RAL showing a 3-fold increase compared to EFV. Further, when comparing T-cell co-localization between TFV and FTC in this tissue, the relative lack of FTC detection and subsequent lack of T-cell exposure results in no correlation with CD3+ T cells. TFV, on the other hand, demonstrated low but quantifiable correlation with an r value of 0.06.

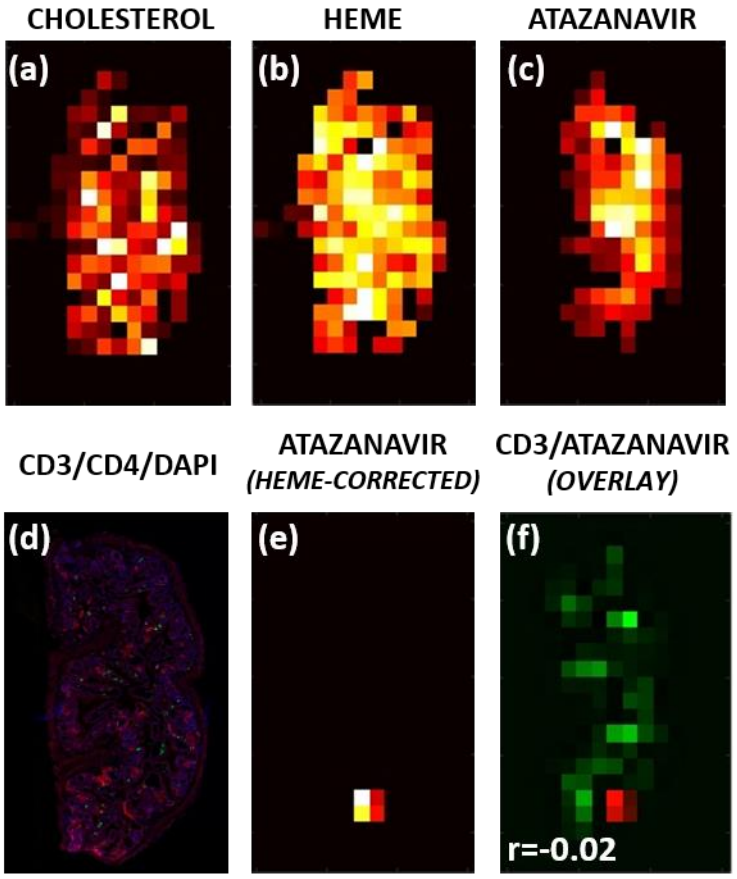

Figure 2.6: ARV Localization in Humanized Mouse Tissues Representative images from a single humanized mouse rectum. Raw IR-MALDESI and IF images are shown in a-d. (e) shows heme-corrected ATV distribution, with overlay of ARV (red) and human CD3+ T cells (green)

Representative images from humanized mouse tissue are shown in Figure 2.6. As previously mentioned, ARV detection by MSI of single slices was sporadic compared to NHP tissues. We were unable to detect RAL or FTC in any tissue slice from both mouse models, despite detection in plasma and tissue by LC-MS, and robust detection in NHP tissues. Figure 2.6a-c shows the distribution of cholesterol, heme, and ATZ, respectively. As shown in Figure 2.6b, we observed extensive heme distribution throughout these tissue cross-sections (IF slice

shown in Figure 2.6d), contrary to NHP results where heme was localized to discrete tissue areas. As a consequence, ARV detection was greatly reduced upon heme correction (compare Figure 2.6c to 2.6e), showcasing the importance of this step. We observed a large decrease in detectable CD3+ T cells in the humanized mouse samples (Figure 2.6d), probably owing to the fact that staining was specific for T cells of human origin only. Figure 4f shows the overlay for this tissue, where decreases in CD3+ detection and ARV signal result in low correlation (r=0.02).

T-cell co-localization for all animal models in both the ileum and rectum is summarized in Table 2.2. Co-localization with CD3+ T cells was variable but generally low, with r values ranging from -0.09 to 0.32. Lack of detection of many ARVs complicated within-species comparisons, however co-localization values were similar between BLT and hu-HSC-Rag mice for all detected ARVs. For NHPs, TFV co-localization with HIV target cells was 2-fold higher in the rectum over the ileum, with FTC and RAL also showing a similar trend. Conversely, EFV r values were 4-fold higher in the ileum. Interspecies comparisons were limited, but tended to show similar co-localization between mice and NHPs. The exception was EFV in the ileum, which showed some of the highest r values in NHPs despite being undetectable in hu-HSC-Rag mice after heme correction. MVC was also undetectable in hu-HSC-Rag mice despite detection in both BLT mice and NHPs, although correlation coefficients were low.

Table 2.2: Summary of ARV-CD3+ T Cell Correlation Coefficients Across Species

Drug	Ileum			Rectum		
	Mice		All Macaques	Mice		All Macaques
	BLT	hu-HSC-Rag		BLT	hu-HSC-Rag	
TFV	-	-	0.02 (-0.06,0.08)	0 (-0.04,0.29)	0 (-0.03-0.09)	0.04 (0,0.15)
FTC	-	-	0 (0,0)	-	-	0.02 (-0.01,0.11)
RAL	-	-	0 (-0.09,0.08)	-	-	-0.08 (-0.09,-0.03)
EFV		-	0.20 (-0.04,0.28)		0 (n=1)	-0.07 (-0.08,-0.04)
MVC	-0.01 (-0.09,0.13)	0 (0,0)	0.01 (0.01,0.02)	-0.01 (-0.09,0.11)	-	0.05 (0.04,0.06)
ATZ	0.02 (-0.02,0.32)	-0.01 (-0.03,0)	0.03 (-0.03,0.12)	0 (-0.05,0.07)	0 (-0.03,0.02)	0.05 (0.01,0.08)

*data shown are median and range

Mucosal Accumulation of Antiretrovirals Between Species

To determine the percentage of total ARV signal within each tissue slice that localized in the mucosal layer, an overlay workflow similar to Figure 2.1 was employed, where a region of interest was manually defined surrounding the mucosal layer and summed pixel intensities from this ROI were divided by the summed pixel intensity from the entire tissue slice. Results are reported in Table 2.3. Overall, mucosal accumulation was extremely variable within tissue slices, ranging from 0-100% of total ARV signal. Accumulation was similar between the humanized mouse models with the exception of ATZ in the rectum, which was 1.7-fold higher in hu-HSC-Rag versus BLT mice. ARV accumulation in NHP mucosa was 2-3 fold higher than mice in the ileum, but similar in the rectum.

Table 2.3: Summary of Mucosal Accumulation Across Species

Drug	Ileum			Rectum		
	Mice		All Macaques	Mice		All Macaques
	BLT	hu-HSC-Rag		BLT	hu-HSC-Rag	
TFV	-	-	70 (34, 80)	58 (48, 70)	49 (28, 73)	45 (5, 77)
FTC	-	-	61 (50, 84)	-	-	38 (27, 99)
RAL	-	-	55 (6, 97)	-	-	46 (20, 100)
EFV		-	53 (33, 96)		100 (n=1)	45 (1, 100)
MVC	18 (4, 27)	22 (20, 25)	57 (18, 80)	39 (28, 77)	-	56 (30, 65)
ATZ	20 (3, 39)	25 (0, 49)	45 (6, 69)	37 (35, 38)	66 (32, 38)	58 (11,100)

*data shown are median percent accumulation and range

HIV RNA Expression in Areas of Low ARV Signal

To determine whether or not low ARV-T cell co-localization translated to ongoing HIV gene expression in these cells, MSI images were co-localized with HIV RNA localization obtained from ISH. In NHPs, HIV RNA expression was detected preferentially in areas of low or no ARV signal (Figure 2.7). As shown in Figure 2.7k, detected HIV RNA was not diffusely distributed throughout tissues, but instead localized into discreet clusters within the submucosa (see insert of Figure 2.7k). These discreet areas of RNA expression tended to be observed only in tissue areas that corresponded to high T cell density (compare Figure 2.7k to 2.7f), showing that detected RNA likely represents real gene expression rather than non-specific response. The NRTIs TFV and FTC, though detected at low levels in this tissue, did not co-localize with RNA (r=0 for both). MVC and ATZ showed very similar distributions and were more readily detected in this sample, however even these ARVs showed poor correlation (r= -0.01 for both) when compared to HIV RNA. In mice (Figure 2.8), HIV RNA was again detected in tissue areas that

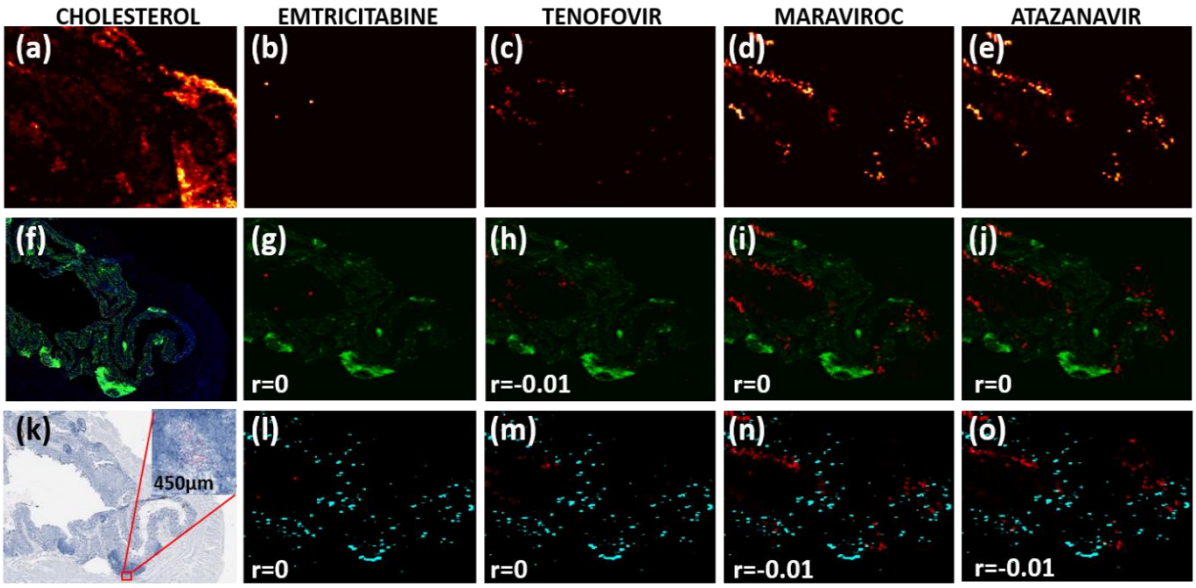

Figure 2.7: HIV RNA Localization in Areas of Low ARV Signal Representative images from a single NHP rectum. Raw IR-MALDESI images are shown in a-e. IF images showing CD3+ T cell distribution (green; f) were overlayed with ARV images in g-j. Raw ISH image is shown in k, with positive staining in red (insert in k provided to show positive cells). Co-localization of ARV images (red) and HIV RNA (cyan) are shown in l-o, with corresponding correlation coefficients.

corresponded to CD3+ T cells (Figure 2.8d & f). After correction for heme signal, ARVs were found to be poorly co-localized with detected RNA and resulting correlation coefficients were low.

When compared across species, corresponding correlation coefficients were low for every ARV evaluated (Table 2.4), and were not significantly different between species or between the ileum and rectum. HIV RNA was not detected several tissues where we had previously observed CD3+ T cell distribution (marked NV in table), resulting in a small number of samples available for analysis within each cohort. This was especially true in mice, where RNA was detected with greater frequency in BLTs versus hu-HSC-Rag animals, consistent with CD3+ T cell expression data. Though the range of correlation coefficients was wide (-0.09-0.20), TFV and MVC showed poor correlation with HIV RNA in both species. FTC and ATZ coefficients were more variable but still low. We were unable to detect SHIV RNA expression in

the three infected animals receiving EFV & RAL, however further analysis of RNA expression by qPCR of these tissues revealed that RNA expression in these animals was 2-3 logs lower than those receiving ATZ & MVC, which may explain the lack of detection (data not shown).

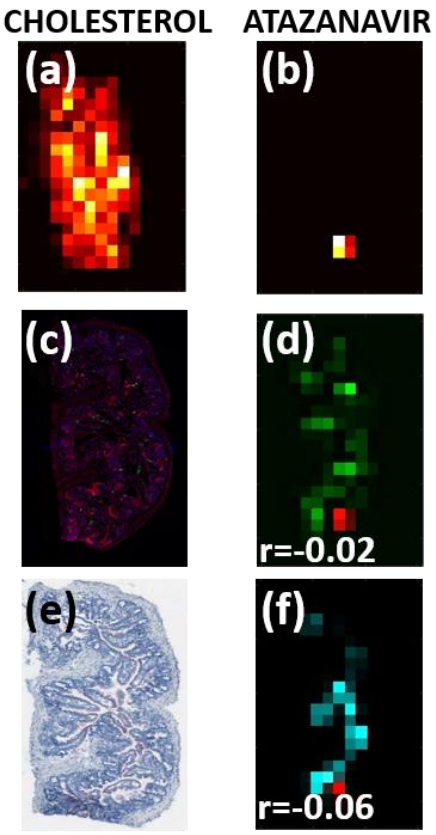

Figure 2.8: HIV RNA Localization in Areas of Low ARV Signal (Mice) Representative images from a single humanized mouse ileum. Heme-corrected IR-MALDESI images are shown in a & b. IF image showing CD3+ T cell distribution (green; c) was overlayed with ATZ in d. Raw ISH images is shown in e, with positive staining in red. Co-localization of ARV image (red) and HIV RNA (cyan) is shown in f, with corresponding correlation coefficient.

Table 2.4: Summary of ARV-HIV RNA Correlation Coefficients Across Species

Drug	Ileum			Rectum		
	Mice		All Macaques	Mice		All Macaques
	BLT	hu-HSC-Rag		BLT	hu-HSC-Rag	
TFV	-	-	0 (0,0)	-0.02 (-0.04, 0.03)	-0.01 (n=1)	0 (0, 0.12)
FTC	-	-	0.01 (0, 0.02)	-	-	0 (0, 0)
RAL	-	-	NV	-	-	NV
EFV		-	NV		NV	NV
MVC	-0.03 (-0.09, 0.16)	-0.02 (-0.04, 0)	-0.01 (-0.02, 0.10)	-0.04 (-0.06, 0.03)	-	-0.01 (-0.02, 0.08)
ATZ	0.06 (-0.03, 0.24)	-0.06 (n=1)	0 (-0.02, 0.09)	-0.01 (-0.04, 0.05)	0.20 (n=1)	0 (-0.01,0.07)

*data shown are median and range; NV=no virus detected

Drug Efflux Transporter Localization and Effect

Figure 2.9 shows representative images of ARV-efflux transporter co-localization, which demonstrates the potential influence of these transporters on observed distribution patterns. Figure 2.9a-e show raw MSI images with differential distribution between ARVs. Heme-corrected images are shown in Figure 2.9f-j, where a large decrease in ARV response is observed, though tissue localization patterns remain intact. EFV, for example, distributes through the mucosa and accumulates in the adipose layer of tissue (Figure 2.9i). When overlayed with MDR1, it does not appear that EFV disposition is significantly affected by the expression or localization of this transporter, as the two variables are not co-localized (Figure 2.9n). Conversely, RAL concentrates on the luminal surface of this tissue, with limited penetration into the submucosa (Figure 2.9j). Unlike EFV, MDR1 is highly co-localized with RAL (Figure 2.9o),

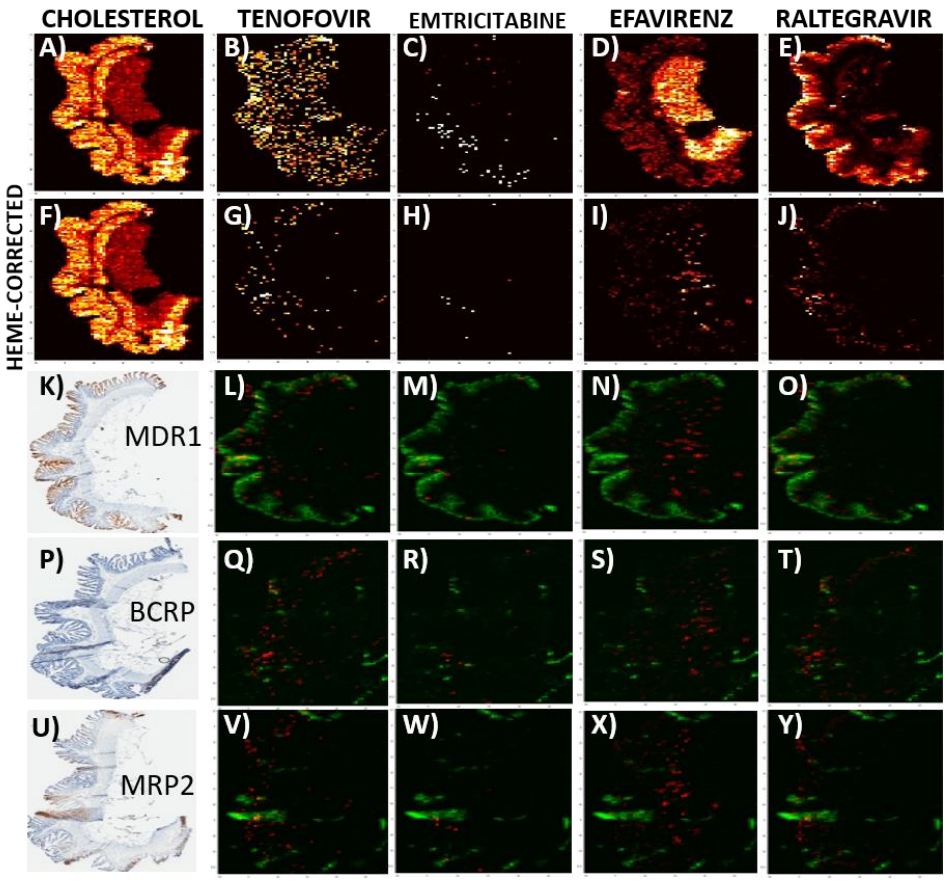

Figure 2.9: Efflux Transporter Correlation with ARV Localization Representative images from a single NHP ileum. Raw IR-MALDESI images are shown in a-e. (f-j) shows heme-corrected ARV distribution. Raw transporter IHC and subsequent ARV-transporter overlays are shown for MDR1 (k-o), BCRP (p-t), and MRP2 (u-y), with ARV in red and transporter in green.

suggesting that this efflux transporter may act as a barrier to RAL penetration into the submucosa from the gut lumen. Similarly, TFV (Figure 2.9g) and FTC (Figure 2.9h) show differential distribution in this tissue slice with corresponding differences in MDR1 co-localization (Figure 2.9l and 2.9m, respectively). BCRP (Figure 2.9p) and MRP2 (Figure 2.9u) were not extensively expressed in these tissues and thus significant differences on co-localization between drugs was not observed.

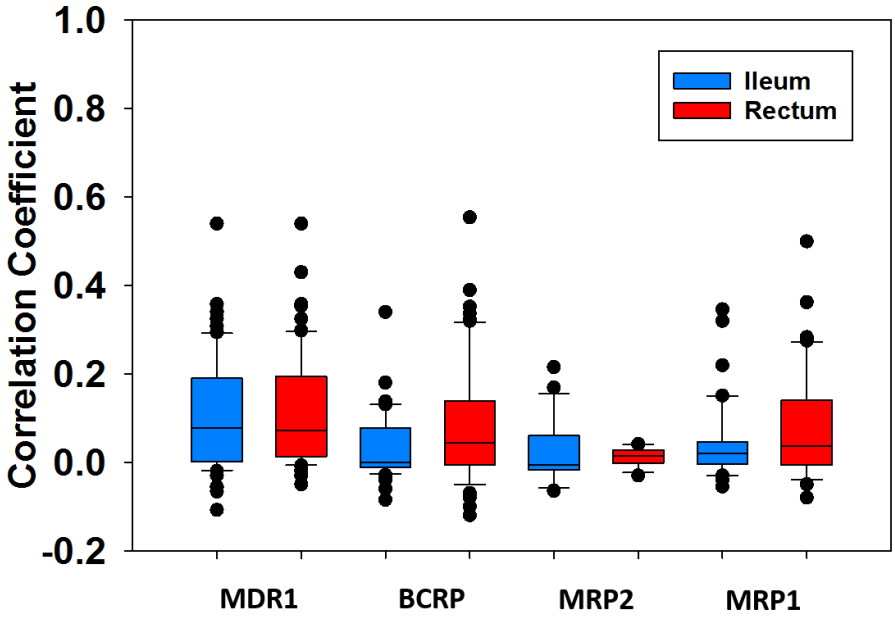

Figure 2.10: ARV-Efflux Transporter Co-localization Across Compartments Correlation coefficients for pooled ARVs-efflux transporters in the ileum (blue) and rectum (red). Solid lines represent medians, box ends represent IQR, and whiskers represent range. Solid black dots are outlier values.

A summary of correlation coefficients with all efflux transporters in all animals is shown in Appendix 2.1. Again correlation coefficients were low, ranging from -0.09 to 0.55, with most values below 0.2. ARV-efflux transporter co-localization was lower on average in NHPs compared to humanized mice for every transporter evaluated, though species comparisons could only be made for TFV, MVC, and ATZ. To compare the effect of drug transporters at different sites in the GI tract, animal models were pooled and compared between the ileum and rectum in Figure 2.10. No significant differences were observed in ARV-transporter co-localization between the ileum and the rectum for any of the transporters evaluated.

Discussion

This is the first study to demonstrate heterogeneous ARV distribution within tissues across pre-clinical models and relate this distribution to HIV RNA expression. Using mass spectrometry imaging, we show that ARV disposition in the NHP ileum and rectum is differential between drug classes. In particular, EFV and RAL localized to completely distinct tissue subcompartments despite being dosed orally and at the same time. Similarly, the relatively homogenous detection of TFV across NHP tissue slices was not observed with FTC, despite identical routes of administration. Co-localization with relevant biologic variables such as CD3+ T cells allowed us to interpret the implications of these differences. For instance, when looking at the tissue slice in Figure 2.5, the nearly 3-fold decrease in EFV-CD3 co-localization compared to RAL-CD3 suggests that, at standard treatment doses for these animals, EFV may not achieve adequate exposure at the site of action compared to RAL, which concentrates more in the mucosa.

Despite the large differences observed on an individual tissue level, aggregate T-cell correlation coefficients were not significantly different between ARVs in the NHP tissues (Table 2.2), with a large amount of intra-species variability in T cell co-localization. There are several potential explanations for this observation, namely the large variation in CD3+ T cell expression from animal to animal. Further, the differences in tissue slice morphology and approximate location along the GI tract likely contribute to observed variability. ARV localization into tissue subcompartments may not be consistent along the length of the GI tract, and even small variations in the local tissue environment can alter the disposition of drugs at these sites. This may help explain why EFV co-localization with CD3+ T cells was much higher in the NHP ileum than any other ARV.

In stark contrast to the NHP data, ARV distribution in both humanized mouse models initially appeared to be more homogenous in GI tissues, though heme-correction greatly decreased ARV detection (Figure 2.6) and subsequently lowered correlation coefficients (Table 2.2). Low ARV-T cell co-localization in mice suggests that these drugs may not achieve adequate exposure at the site of action. This suggestion is tempered, however, by the fact that CD3+ T cell detection was extremely low compared to NHPs, thus correlation coefficients are falsely lowered to some extent. The relative lack of detection in humanized mice can be explained by the fact that we stained only for human T cells rather than the entire T cell population. Though the gut tissues are known to substantially reconstitute human lymphocyte populations in humanized mouse models, particularly in the BLT model, the relative decrease compared to NHPs was not unexpected.

Low co-localization with T cells across animal models was a surprising result given that a large percentage of heme-corrected ARV signal was detected in the mucosal layer (Table 2.3), where the majority of activated T cells in the gut are localized.[119] Although few differences were observed between animal models with regard to T-cell co-localization, we observed higher mucosal accumulation in the NHP tissues versus either mouse model, though these differences were not statistically significant. Serial slicing revealed high-quality cross-sectional slices for most mouse tissues, so severely altered morphology cannot explain these differences. A possible explanation may be that the mucosal layer represents a greater proportion of the total tissue size in mice compared to NHPs (compare 2.5f to 2.6d), and that the very low ARV detection in mice after heme-correction drove these values down.

Importantly, we show that low ARV-T cell co-localization may result in continued HIV replication in this cell population. As shown in Figures 2.7 and 2.8 , HIV RNA was localized to

areas of low ARV exposure in both NHP and mouse tissues, with median correlation coefficients suggesting a low amount of drug exposure at the site of action. These findings agree with the low ARV-T cell co-localization previously observed, especially given that RNA detection was co-localized with only a small percentage of CD3+ T cells, consistent with viral gene expression in the smaller CD4+ T cell population. Given that only a small proportion of detectable HIV RNA from ARV-treated subjects represents replication-competent virus, and that these animals had only been receiving cART for 7-10 days, this pharmacodynamic endpoint is likely an overestimation of the true magnitude of persistent infection during treatment. Nevertheless, these findings provide support for the hypothesis that ongoing HIV replication in tissues like GALT is driven by low ARV penetration to the site of action, and that strategies to achieve therapeutic concentrations at these sites are needed.

The ultimate goal in generating these data are to develop target concentrations for efficacy at the site of action. Although concentrations within certain tissue sites (e.g. mucosa) can be estimated based on accumulation and total concentration of the entire slice, a reasonable first step may be to base efficacy target estimates on the limit of detection (LOD) for the ARVs that were not well correlated with RNA. Because we observed HIV gene expression almost exclusively in locations where no TFV or MVC signal was co-localized, we can assume that concentrations above the LOD for each drug are sufficient to suppress RNA expression at these sampling sites. Using maximum LOD estimates from calibration experiments run in tandem with our infected samples, these values are as follows: TFV, 4,503fg/voxel; MVC, 708fg/voxel. Importantly, these total drug values represent the most conservative estimate, as there may be ARV exposure in other tissue sites that is below current LODs, but still high enough to suppress viral gene expression. However, we provide a starting framework for defining exposure-response

at the site of action, as improvements in sensitivity will likely decrease the LOD in the future. Future work will refine this pharmacodynamic endpoint, with particular focus on translating per-voxel drug amounts to per-gram concentrations to generate specific target concentrations for HIV suppression in tissues, especially for those ARVs where HIV RNA expression was detected despite detectable signal (e.g. ATZ).

The potential contribution of drug efflux transporter localization to differences in ARV tissue distribution are substantial. MDR1 in particular demonstrated drastically different extents of co-localization depending on the ARV evaluated (2.8k-o), which may have implications for exposure at the site of action. For example, the higher MDR1 co-localization observed with RAL suggests that this transporter may act as a barrier to RAL distribution into the mucosa from the gut lumen. MDR1 appears less important for EFV distribution, as evidence by the lower co-localization values and concentration of EFV signal in the tissue submucosa. Importantly, these trends are supported by data showing that RAL, but not EFV, is a substrate for MDR1.[120] Further, existing transporter substrate data also support observed distribution of TFV, which is not an MDR1 substrate.[121]

Similarly to the T cell co-localization and mucosal accumulation comparisons, large variability in transporter co-localization data resulted in most comparisons within and between models showing non-significant differences (Appendix 2.1). This was particularly true for BCRP, which showed the largest range of any transporter, and MRP2, which was not detected in the mouse gut. MRP1 was more ready detected in tissues, and co-localization with this transporter was 2 to 4-fold higher in the mouse ileum versus NHPs. This is particularly important for drugs like ATZ or FTC, which may have decreased exposure in the mouse ileum secondary to increased efflux by MRP1. When ARV-transporter co-localization was compared across

efflux transporters and anatomic compartments, no significant differences were observed (Figure 2.9), suggesting that the four efflux transporters evaluated here contribute equally to ARV disposition, and that this contribution is continuous along the GI tract.

Importantly, we did not observe any significant difference between infected and uninfected animals for any variable measured in this study. Previous work has shown that HIV infection can alter the protein expression of drug transporters by as much as 3-fold[99], and that infection can alter several PK variables such as intestinal absorption and metabolism that may affect ARV disposition in tissues.[122] The ARVs examined here are known to utilize several of the drug transporters shown to be altered during infection (e.g. RAL by MDR1, TFV by BCRP), and we showed that these transporters may influence exposure in gut tissues (Figure 2.7). Nevertheless, it does not appear that HIV infection substantially contributes to ARV disposition in these tissues. A possible explanation for the disparity in results may be that the animals were not infected for a long enough time for these changes to become apparent, as previous work has utilized biopsy samples from humans that were infected for >12 months before tissue collection.[99] It may be the case that transporter or metabolic changes only manifest during chronic HIV infection, and we were unable to capture those changes here.

There are several limitations of this study which should be addressed, the primary one being lack of information gained from a single 10 micron tissue slice. As previously mentioned, the relative lack of ARV detection in many of these tissues despite detection with traditional LC-MS can be explained by the small amount of tissue available for analysis. It may be the case that because we analyzed such a small portion of tissue, we simply missed where drug is actually distributing. It is not unreasonable to expect that sampling at additional points along the GI tract of these animals would yield better detection of ARV and perhaps differential distribution

patterns. In other words, the distribution we observe in a single slice from the ileum may not reflect the distribution several centimeters, or even several millimeters, away. A related limitation is the lack of information on distributional changes over time. Because all of these tissues were collected during the plasma PK trough, it is unknown whether the tissue penetration of ARVs would be different at other PK time points. We attempted to minimize this possibility by dosing animals to plasma steady-state, and we have shown that tissue concentrations during PK steady-state have little variability and are unlikely to significantly differ based on sample collection time.[123,124]

The use of Pearson correlation on image overlays is a further limitation of this study. While T-cell or RNA co-localization is a crude measure that provides a general idea of ARV exposure at the site of action, this method cannot account for potency differences between drugs, and how this affects exposure-response relationships in tissue. For example, though in some cases EFV co-localization with CD3+ T cells was higher than RAL, this difference may not matter due to the potency differences between these drugs. This is supported by the fact that there is no clinical evidence that treatment with EFV delays viral rebound after treatment cessation more than RAL, or that RAL treatment results in greater tissue replication versus other therapies. To overcome these limitations, future work will focus on generating new image overlay workflows to account for potency differences between drugs and provide a more relevant pharmacodynamics endpoint.

As we demonstrated in Figure 2.6, masking ARV response on the basis of corresponding heme distribution resulted in drastic decreases in ARV signal, particularly in mouse and human tissues. This is an important step to reduce confounding from ARVs contained in the microvasculature or from blood contamination during tissue collection which could falsely

elevate correlation with biologic variables; however, this process of data censoring is imprecise and has several important limitations in its implementation. Application of this step underestimates true ARV tissue signal as there are likely cases where ARVs are present in tissue but happen to co-localize with a micro-vessel, making their masking unnecessary and falsely lowering correlation coefficients. Though we attempted to correct for this by applying heme masks to both MSI and IHC/ISH images, the true correlation values between these variables remain unknown.

The use of viral RNA as a surrogate of viral replication is another important limitation. As previously mentioned, RNA expression does not necessarily represent downstream protein expression or completion of the viral life cycle, thus detected RNA may be secondary to random egress from latency rather than productively infected T cells. Further, though the RNAscope method used here has improved specificity to detect HIV-specific genes versus traditional ISH[116] it may be the case that some of the RNA detected here originated from non-HIV sources, further overestimating the actual amount of potential viral replication. Future studies should examine downstream components of the HIV life cycle (e.g p24) by IHC, or potentially by IR-MALDESI itself.

Importantly, the ARV responses observed in this study represent total rather than unbound drug. As the efficacy of these agents is driven by free drug concentrations at the site of action, we are limited in our ability to estimate target concentrations in these tissues from total drug alone. It has been shown that the extent of protein binding, and thus free drug concentrations, can differ between plasma and tissues for anti-infective agents.[125,126] In some cases, estimates of the free drug in tissues can be accurately extrapolated from plasma data[127,128]; however, direct measurement of unbound tissue concentrations provide the most useful data for

comparison to IC_{50} values for a given pathogen. Strategies such as ultrafiltration or microdialysis have been utilized by others to measure unbound tissue concentrations directly and have been previously reviewed.[72] Performing similar analyses in replicate tissues from this study can provide insight into how much of the total ARV signal observed is due to unbound drug, as well as provide a framework for estimating target concentrations for efficacy at this site.

The resolution of ARV distribution images generated by MSI is the limiting factor in obtaining data at the cellular level. Despite the availability of high-resolution IHC/ISH images for HIV target cells, drug transporters, and RNA, the final image overlays are capped at 100 micron resolution, precluding our ability to observe ARV distribution within cells. Although understanding the distribution of these agents on a macro level in tissues is helpful, and still provides data that would otherwise be unobtainable with traditional LC-MS, the fundamental question of exposure in reservoirs is whether or not ARVs can achieve adequate concentration in cells to suppress viral replication. The lack of ARV signal in areas of HIV RNA detection would suggest this is not the case, but the limitation remains. A related limitation was our inability to detect the active metabolites of TFV (TFVdp) or FTC (FTCtp). These phosphorylated moieties act as chain terminators in reverse transcription rather than the parent compounds, and are sequestered within lymphocytes. Though analysis of parent TFV and FTC can show in general where these compounds distribute, it may be the case that the specific distribution of the metabolite differs drastically from that of the parent compound. We have demonstrated rapid degradation of these metabolites back to the parent compounds in tissue samples, and are currently optimizing methods to stabilize these metabolites for increased detection in this setting.

Despite these limitations, this work provides novel data demonstrating that the assumptions made when analyzing LC-MS concentrations from tissue homogenates may not be

valid, and that ARV distribution in tissues is not homogenous. ARV localization was similar between animal models, with low T-cell co-localization in all species despite a 1.5-fold increase in mucosal accumulation in NHPs that was not observed in humanized mice. We show that HIV RNA is expressed in areas of low TFV and MVC exposure, providing support for the hypothesis that suboptimal ARV tissue penetration may propagate tissue reservoirs. Drug transporter effects were differential between ARVs, but consistent between the ileum and rectum. Quantitatively, we observed good agreement between IR-MALDESI and the gold standard LC-MS, but showcased the advantage of visualizing drug distribution. Ultimately, these data can be used to inform the design of targeted therapies for HIV eradication.

Chapter III: Multimodal Analysis of Drug Transporter Expression and Localization in Gastrointestinal Tissue and Implications for Antiretroviral Disposition

Summary

HIV persistence in tissue reservoirs like the GI tract may be reduced with optimized exposure of antiretrovirals (ARVs). Drug transporters affect ARV tissue disposition, but quantitative measures of drug transporter protein expression across pre-clinical species are not available. Our objective was to use proteomics to obtain absolute transporter concentrations and assess agreement with corresponding gene and immunometric protein data. Ileum and rectum were collected from two ARV-dosed humanized mouse (hu-HSC-Rag (n=41); BLT (n=13)) and one primate (rhesus macaque, (NHP, n=12)) models and analyzed for gene (qPCR) and protein (LC-MS proteomics and Western blot) expression and localization (immunohistochemistry) of ARV efflux and uptake transporters. Drug concentrations were measured by LC-MS/MS. Multivariable regression was used to determine the ability of transporter data to predict tissue ARV penetration. We observed little agreement between analytical methods, with interspecies comparisons showing different trends for gene and protein expression. For example, qPCR analysis showed a 2-fold increase in permeability glycoprotein (Pgp) expression in NHPs versus mice, however proteomics analysis showed a 200-fold difference in the opposite direction. Proteomics results were supported by IHC staining showing extensive efflux transporter localization on the luminal surface of these tissues. ARV tissue concentration was variable between species, and multivariable regression showed that QTAP data best predicted these

values. Lack of agreement between analytical techniques, and better agreement between drug and transporter concentration in tissue, suggests that resources should be focused on generating downstream measures of protein expression to predict drug exposure. Taken together, these data inform the use of pre-clinical models for studying ARV distribution and the design of targeted therapies for HIV eradication.

Introduction

The introduction of combination antiretroviral therapy (cART) in the mid-1990s permanently altered the landscape of HIV infection, saving millions of lives and helping to increase the lifespan of HIV-infected individuals to levels near their uninfected counterparts.[1] However, early studies of cART showed persistent infection and rapid rebound viremia after drug removal even from patients with undetectable viral loads, necessitating lifelong therapy.[4,49] Today, viral rebound upon cART cessation is a well-established clinical phenomenon which has been shown to be secondary to the establishment of an HIV reservoir early in infection.[49] The latent reservoir, consisting of quiescent memory T cells containing proviral DNA, has been well characterized and has received the focus of most eradication research over the past 15 years. However, there is also evidence that HIV can persist within certain anatomic sites, or tissue reservoirs, including the central nervous system, lymphatic system, gut-associated lymphoid tissue (GALT), and genital tract.[129,130,29] Both latent and tissue reservoirs represent a substantial barrier to HIV eradication from the body, and an understanding of the factors that contribute to the propagation of these reservoirs, particularly in GALT (see Chapter I), is a necessary step toward HIV cure.

There is a growing body of evidence to support the existence of tissue HIV reservoirs. For example, several studies have demonstrated continued viral shedding from the gastrointestinal (GI) and genital tract despite undetectable plasma viral loads,[12,131,132] and additional studies have shown that replication-competent virus can be isolated from the tissues of patients long after cART initiation.[133] More recent work has demonstrated viral genetic evolution within the lymph nodes of patients fully suppressed on cART.[29] Given that this persistence has been observed in the setting of suppressive cART, it is reasonable to suspect that inadequate

antiretroviral (ARV) penetration into certain tissues may contribute to HIV persistence. It has been shown by our group and others that ARV tissue penetration is highly variable between anatomic sites and between ARVs within a single tissue.[51] Further, Fletcher et al demonstrated that higher tissue ARV concentrations were significantly associated with faster HIV decay within the lymph nodes and GI tract.[56] More recently, we have shown our ability to image ARVs within a tissue, and found heterogeneous efavirenz (EFV) distribution in several anatomic sites, particularly in the GI tract.[75] Further investigation into what factors govern these distribution patterns is critical for understanding how to increase ARV exposure in tissue reservoirs.

Drug transporters are known to play an important role in the disposition of many drugs, including ARVs. Not only does their activity help define a drug's pharmacokinetic profile (e.g. absorption in the intestine, excretion in the kidney), but they play a major role in drug interactions, particularly for ARVs.[60,61] Using tissue penetration data from multiple classes of drugs, including ARVs, we have previously shown that the likelihood of being a substrate for the efflux transporters MRP1 and MRP4 was significantly predictive of drug penetration into the female genital tract[52], suggesting a role for these transporters in overall ARV tissue exposure. Several groups, including our own, have published studies evaluating the expression and localization of drug transporters in tissues relevant for HIV prevention[98,134] and, more recently, cure.[65] However, there has been no consensus in the field on the optimal way to measure transporter expression. There is little agreement between publications with regard to what is being measured (i.e. gene vs protein expression), and there has been no assessment of the level of agreement between techniques (e.g. qPCR vs Western blot vs immunohistochemistry (IHC)). Further, although proteomics-based methods have been used to obtain absolute concentrations of specific proteins including drug transporters[135,136], this technology has not been compared against

other methods in the context of HIV infection. A comprehensive evaluation of transporter expression and localization using multiple techniques within the same study is greatly needed to inform the field as to the best way to measure transporter expression for their effect on ARV penetration into tissues.

In addition to methodological considerations, another important variable to address is expression differences between species. Animal models are commonly used to study HIV infection, and any evaluation of the tissue exposure of a new or existing ARV must first be performed in animals before moving into humans. While there are some data showing similarities in ARV exposure between humans and animals[114], there is a relative lack of data comparing important variables for drug distribution, such as drug metabolizing enzymes, drug transporters, and PK properties between animal models or between animals and humans. Further, the effect of HIV infection on these variables has not been elucidated. Identification and quantitation of these differences, if they exist, will help to prevent the inappropriate extrapolation of data from one species to another, determine whether pharmacokinetic information should be obtained during infection, and streamline the drug development process.

In the present study, we perform a comprehensive evaluation of drug transporter expression and localization in two tissues of the GI tract[24,130] using multiple methodologies and three animal models from two species. These data will help identify important variables for ARV exposure into tissue reservoirs, while at the same time identifying the best way to measure drug transporter expression. Finally, the generation of novel inter-species data can help determine the applicability of animal models to future ARV development.

Methods

ARV Dosing and Tissue Collection

Animal dosing and tissue collection were described in detail in Chapter II, but briefly, three commonly used animal models were employed in this study: the hu-HSC-Rag (n=41) and bone marrow-liver-thymus (BLT; n=13) humanized mouse models and a non-human primate model (n=12), with half of each cohort infected with HIV or SHIV as described previously.[108,137,138] Mice were dosed orally with one of several ARV regimens for 10 days: EFV 10mg/kg (n=6) alone; atazanavir (ATZ) 140mg/kg (n=6) alone; or tenofovir (TFV) 208mg/kg, emtricitabine (FTC) 240mg/kg, raltegravir (RAL) 56mg/kg, maraviroc (MVC) 62mg/kg (n=6) in combination. Male rhesus macaques (*Macaca mulatta*) were dosed for 10 days with TFV 30mg/kg subcutaneously (SubQ), FTC 16mg/kg (SubQ) and one of the following regimens: MVC 270mg/kg twice daily (BID) with ATZ 150mg/kg BID OR EFV 200mg QD with RAL 100mg/kg BID. Doses for all drugs were chosen based on commonly used treatment doses for HIV infection in these models.[110–114] ARV dosing combinations were chosen based on the limited resources available (i.e. NHPs) or on toxicity (e.g. EFV in BLT mice). Two animals from each mouse model were not dosed with ARVs and used as controls. Ileum and rectum were collected at necropsy and snap frozen. All animal experiments were performed in accordance with locally-approved IACUC protocols.

Gene Expression

Transporter gene expression was analyzed by quantitative polymerase chain reaction (qPCR) on five efflux and four uptake transporters (Table 3.1). These transporters were chosen

based on their relevance to ARV disposition and expression in the GI tract, though this is not an exhaustive list.[61] Approximately 30mg of tissue was homogenized in lysis buffer using a Precellys Tissue Homogenizer (Bertin Technologies, Montigny-le-Bretonneux, France) and RNA was extracted using a Qiagen RNAeasy Mini Kit (Qiagen, Valencia, CA) per manufacturer's protocol. RNA concentrations were measured using a NanoDrop 2000c (Thermo Fisher Scientific, Waltham, MA), and 200ng of RNA was reverse transcribed to cDNA using the VILO Superscript cDNA Synthesis Kit (Thermo Fisher). RNA integrity was confirmed using the 260/280 ratio for each sample. In order to obtain a large enough volume of cDNA to perform PCR in triplicate for 10 genes, cDNA was pre-amplified for 10 cycles using Taqman Pre-amplification Master

Table 3.1: Drug Transporters Evaluated for Gene and Protein Expression

Gene Name	Protein Name	ARV Substrates	ARV Inhibitors	ARV Inducers
ABCB1	MDR1	TFV, RAL, ATZ, MVC	TFV, FTC, EFV, ATZ, MVC	FTC, EFV, ATZ
ABCC1	MRP1	FTC, ATZ	TFV, FTC, EFV, ATZ	ATZ
ABCC2	MRP2	ATZ	TFV, FTC, EFV	RTV, NFV, MVC
ABCC4	MRP4	TFV		
ABCG2	BCRP	TFV	EFV, ATZ	RTV, NFV
SLCO2A1	OATP2A1			DRV
SLC29A1	ENT1	TFV, FTC		
SLC22A2	OCT2	3TC	ABC,FTC,TFV	
SLC22A3	OCT3			

Mix (Life Technologies, Carlsbad, CA) and Taqman Gene Expression Assays (Appendix 3.1) and then diluted 5-fold with Tris-EDTA buffer. Forty cycles of qPCR were performed on the pre-amplified cDNA using Taqman primers and probes on a QuantStudio6 (Life Technologies). Raw C_T values were calculated based on a threshold value of 0.2, and expression for all

transporters was normalized to the housekeeping gene GAPDH (which showed lower variability after pre-amplification versus beta-actin; data not shown) using the $2^{-\Delta CT}$ method.[139]

Protein Extraction and Western Blot

Protein used for Western blot and LC-MS proteomics was isolated using a modified version of an extraction method optimized for proteomics as described previously.[140,141] Briefly, tissues (10-100mg) were homogenized in 1.3mL hypotonic buffer containing 10mM NaCl, 1.5mM $MgCl_2$, 10mM Tris HCl pH 7.4, and 150uL of Complete Protease Inhibitor Solution (Sigma-Aldrich, St. Louis, MO) using the Precellys tissue homogenizer. Tissue homogenate was left on ice for 30 minutes, then sonicated for 5 minutes and centrifuged for 10min at 10,000g. Supernatant was saved and subjected to high-speed centrifugation at 55,000rpm for 1 hour. Supernatant was discarded and the pellet was resuspended in Complete Protease Inhibitor Solution. Protein concentrations were quantified using the BCA protein assay (Pierce, Rockford, IL). The total protein isolated from each tissue was split between Western blot and proteomics. At least 10 and up to 50µg was reserved for proteomics, with the remaining protein (up to 10µg) being used for Western blot.

For Western blot, up to 10µg of protein was combined with 7.5µL sample buffer (NuPage, ThermoFisher) and 0.5M dithiothreitol (DTT, Sigma-Aldrich) and heated at 70˚C for 10 minutes before being loaded onto a 4-12% electrophoresis gel (NuPage) and run for 110 minutes at 180V. Transfer onto a PVDF membrane (NuPage) occurred over 90 minutes at 30V. Once transfer was completed, membranes were rinsed with Tris-buffered saline with Tween-20 (TBS-T) and blocked for 1 hour at room temperature in 5% milk. After blocking, primary antibody was added for one of the five following proteins: MDR1 (1:4000, ab170904, Abcam, Cambridge, MA), MRP2 (1:200, ALX-801-037-C125, Enzo Life Sciences, Farmingdale, NY),

MRP1, (1:200, ALX-801-007-C125, Enzo), BCRP (1:1000, ab3380, Abcam), and GAPDH (1:2000, sc-25778, Santa Cruz Biotechnology, Dallas, TX). Membranes were incubated in primary antibody for 1-3 hours, then rinsed with TBS-T and incubated in secondary antibody (anti-rabbit, 1:2000, ab16284, Abcam; anti-mouse, 1:10000, ab112458 Abcam; anti-goat, 1:5000, sc2020, Santa Cruz) for 1-2 hours, then rinsed again with TBS-T. Development occurred using Clarity ECL reagents (Bio-Rad, Hercules, CA) with a Chemi-Doc XRS+ Imager (Bio-Rad). All developments were performed using a 5 min exposure, and densitometry relative to GAPDH was calculated using ImageLab 5.2.1 (Bio-Rad). MDR1 and GAPDH were analyzed during the same exposure, then each membrane was stripped and re-probed for MRP2 and BCRP, then MRP1, with all densitometry being compared to the initial 5 min GAPDH exposure. A combination of 15µg each of mouse brain extract, liver extract, and T98G cell lysate (Santa Cruz) was used as the positive control sample.

Quantitative Targeted Absolute Proteomics (QTAP)

Protein isolation and quantitation occurred as described above, with between 10 and 50µg being used for this analysis. Methods for protein digestion and proteomic analysis have been described in detail elsewhere[140,141], but briefly, proteins were dried down and reconstituted in 50mM ammonium bicarbonate buffer with 40mM DTT, 10% sodium deoxycholate (Sigma-Aldrich), and 10µL β-casein (0.1µg/µL). Samples were reduced for 40min at 60°C, then 135mM iodoacetamide (Sigma-Aldrich) was added and samples were incubated for ~30min at room temperature in the dark. 1 pmol stable isotope labeled (SIL) peptide standards (Theracode JPT Inc., Acton, MA) for each transporter of interest (Table 3.1) were added to each sample along with 25µL Trypsin (0.1µg/µL) (Promega, Madison, WI). Samples were digested for at least 18 hours at 37°C after which point the digestion was stopped with 10% trifluoroacetic acid (Sigma-

Aldrich). Samples underwent solid phase extraction using Strata-X 33µm polymeric reversed phase extraction cartridges (Phenomonex, Torrance, CA), then were dried down and reconstituted in modified Mobile Phase (98% formic acid 0.1%, 2% acetonitrile) and transferred to silinized inserts for injection.

Analysis was performed using a nanoACQUITY system (Waters, Milford, MA) coupled to a QTRAP 5500 mass spectrometer (AB SCIEX, Framingham, MA) equipped with Nanospray III source. An injection amount of ~0.2-1µg of total membrane microsomal protein was loaded onto a C18 trap column (180µm x 20mm, 5µm particle size, Waters). Positive ion mode was used for MS analysis with ion spray voltage of 4000. Target scan time was set at 1.5sec with a scheduled MRM detection window of 90 seconds and a 3 millisecond pause time between MRMs. Analyst 1.5 (AB SCIEX) was used for MS control, and MRM analysis was performed using MultiQuant 2.0 (AB SCIEX). Peaks were smoothed prior to integration and area ratios of unlabeled/SIL peptides were determined using the sum of MRMs monitored. The lower limit of detection for the peptides was ~0.2pmol/mg protein.

Immunohistochemistry

Tissues were sliced frozen at 10µm thickness using a cryostat (Leica Biosystems, Wetzlar, Germany) and thaw mounted onto glass microscope slides. The frozen slides were then stained with primary antibody for MDR1 (1:50; Abcam), MRP2 (1:50, Kamiya Biomedical, Seattle, WA), MRP1 (1:100, Santa Cruz), MRP4 (1:20, Abcam) or BCRP (1:50; Santa Cruz) for 15-60 minutes followed by pH antigen retrieval (Leica). DAB (3,3'-diaminobenzidine) was used as a substrate-chromagen for detection. All staining was performed on a Leica Bond automated tissue stainer (Leica). Mouse and NHP liver tissues were used as a positive control for all antibodies, and negative staining was performed using secondary antibody only. Samples were visually evaluated for transporter localization.

ImageJ software (www.imagej.net) was used to quantify observed transporter staining, as extensive staining for several transporter precluded traditional counting of positive cells. Raw images of scanned slides loaded into ImageJ. The IHC toolbox was used to threshold the image to show only positive staining. The thresholded image was then converted to 8-bit greyscale. The image adjust tool was used to maximize the intensity of positive staining, then the image was converted to black and white. The selection tool was used to measure the total area of positive staining (white), then the selection was inverted to measure the total area of negative staining (black). The ratio of positive (white) to negative (black) staining was used as the quantitative endpoint.

Human Transporter Analysis

The humanization process for both mouse models results in extensive reconstitution of human lymphocytes.[109,142] As drug transporters that affect ARV flux have been shown to be present on the surface of human lymphocytes, and these transporters may contribute to ARV disposition in the GI tract, an analysis of human gene and protein expression was completed in parallel to mouse expression in samples from both humanized mouse models. For gene expression, cDNA preamplification and qPCR was performed with human-specific Gene Expression Assays (Appendix 3.1). Western blot analysis used human specific primary antibodies on the same membranes to assess human protein expression. For QTAP, human proteotypic peptides were optimized in addition to those used for quantitation of mouse proteins. Non-humanized mouse samples were used as negative controls to confirm the specificity of both the Gene Expression Assays and antibodies.

Antiretroviral Plasma and Tissue Concentrations

Plasma samples were extracted by protein precipitation with methanol containing stable, isotopically-labeled internal standards. Samples were vortexed and centrifuged, then the supernatant was diluted with water prior to LC-MS/MS analysis. A Shimadzu high-performance liquid chromatography system with a Waters Atlantis T3 (50mm x 2mm, 5µm particle size) HPLC column was used for separation, and an AB SCIEX API 5000 mass spectrometer (AB SCIEX, Foster City, CA, USA) equipped with a turbo spray interface was used as the detector. The lower limit of quantitation was 1ng/mL for each analyte. The precision and accuracy of the calibration standards and QC samples were within the acceptable range of 15%.

Tissue ARV concentrations were also quantified by LC-MS/MS. Briefly, tissue samples were placed in a tube (Precellys 2mL Hard Tissue Metal Beads Kit) containing 1mL of ice cold 70:30 acetonitrile-water. Samples were homogenized using a Precellys 24 benchtop homogenizer. A portion of the homogenate was then mixed with methanol containing stable, isotopically labeled internal standards. Following centrifugation, the supernatant was evaporated to dryness and reconstituted with water (for TFV/FTC analysis) or 25:75 methanol:water (for ATZ/EFV/MVC/RAL analysis) . LC-MS analysis was performed using the same system as described above except the HPLC separation for ATZ/EFV/MVC/RAL was performed using an Agilent Pursuit XRs Diphenyl (50mm x 2mm, 5µm particle size) column. The lower limits of quantitation for the tissue analysis were 0.002 ng/mL (FTC and MVC), 0.005ng/mL (ATZ, EFV, and RAL), and 0.01ng/mL (TFV). Tissue concentrations were ultimately converted into ng/g tissue units for comparison to plasma.

Statistical Analysis

For both gene and protein expression, comparisons between dosing cohorts were made using one-way Kruskal-Wallis ANOVA on ranks, which was also used to make comparisons

between species and anatomic compartments. Dunn's post-test was used for pairwise multiple comparisons when significant differences ($p<0.05$) were detected. LC-MS concentrations were normalized to paired plasma concentrations to generated tissue:plasma ratios (TPRs) for reporting. Pearson correlation was used to determine the relationship between gene expression and protein expression by each method for all combined samples.

To determine which transporter evaluation method best predicted tissue ARV penetration, univariate regression analysis was performed using log-transformed TPR values as the dependent variable. Transporter expression values (as measured by qPCR, Western blot, QTAP, or IHC) for the efflux transporters were included as independent variables. Those variables achieving $p<0.05$ in the univariate analysis were included in a multivariable analysis using stepwise linear regression to identify combinations of variables significantly predicting TPR. R^2 values from each resulting model were compared across methods to determine which method best predicted tissue penetration for each drug. Descriptive statistics and between-group comparisons were conducted using SigmaPlot 13.0 (Systat Software Inc., San Jose, CA), and the univariate and multivariable analyses were performed using SAS 9.3 (Cary, NC); $p<0.05$ was considered significant.

Results

Human Engraftment and Viral Load in Animal Models

The extent of human engraftment of total lymphocytes (CD45+), total T cells (CD3+), and HIV target cells (CD4+) in both humanized mouse models is shown in Figure 3.1a. At baseline, CD45+ and CD4+ engraftment was similar between the two models and is consistent with what has previously been observed (>50% engraftment),[108,143] and human CD3+ cell percentage was 3-fold lower in the hu-HSC-Rag model compared to the BLT model. At week 4

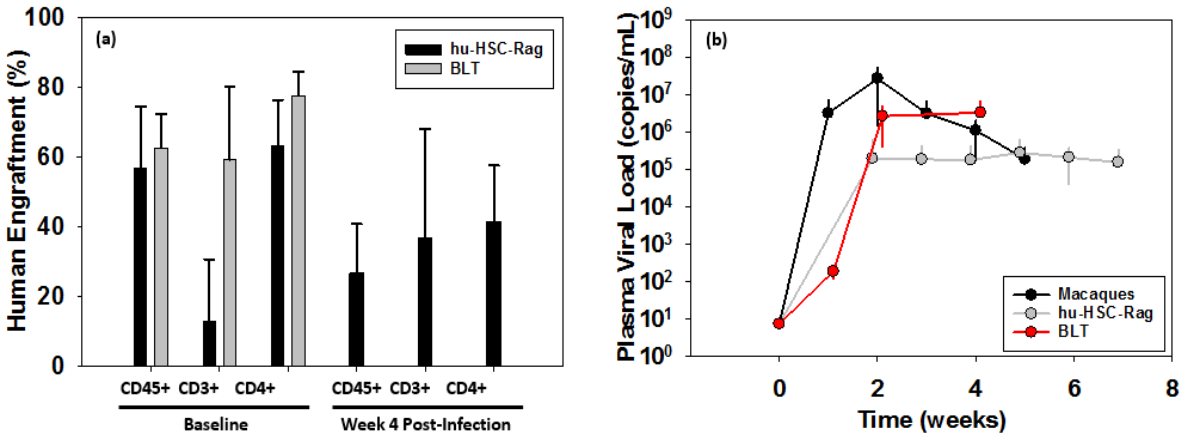

Figure 3.1: Extent of Human Engraftment and Viral Load Among Animal Models Human lymphocyte populations were quantified for the hu-HSC-Rag (black) and BLT (gray) mouse models at baseline and week 4 post-infection (A). Plasma viral loads for both humanized mouse (gray and red) and macaque models (black) are shown over time in (B). Data shown are mean and standard deviation.

post-infection, there was a 2.5-fold decrease in the total lymphocyte population in hu-HSC-RAG (week 4 data was not available for the BLT mice) likely driven by drops in human CD4+ T cells. Figure 3.1b shows the plasma viral load from both mouse models as well as the NHP model over the course of infection. Peak viral loads were observed at week 2 post inoculation and ranged from 10^5 copies/mL in the hu-HSC-Rag to 10^7 copies/mL in NHPs. Plasma viremia was sustained over the course of infection.

Transporter Gene Expression in Humanized Mouse Intestine

Evaluable rectum and ileum tissues were available from all mice that completed dosing. Comparisons between individual dosing cohorts for the ileum and rectum are shown in Appendix 3.2 and 3.3, respectively. These comparisons demonstrate the agreement between uninfected and infected mice and show a significant 2.5-3 log increase in *ABCC4* expression in the hu-HSC-Rag mice versus BLT mice (Appendix 3.2d and 3.3d) which was observed in both the ileum and rectum. There was also a trend for lower *ABCB1* expression in the ileum and rectum of BLT mice, but this did not reach statistical significance (Appendix 3.2c and 3.3c). ARV dosing did not significantly modulate gene expression for any transporter with the exception of *ABCC2* in the ileum, for which gene expression was nearly 3-fold higher in the non-dosed control mice (Appendix 3.2b) compared to all other mice evaluated.

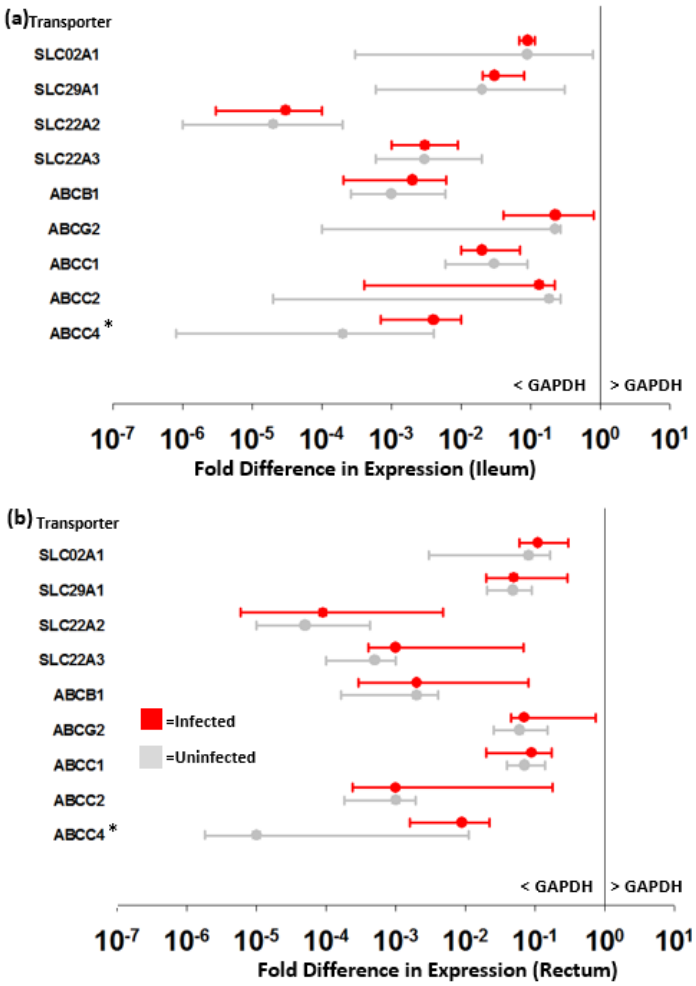

Figure 3.2: Mouse Transporter Gene Expression in Humanized Mouse Gut Combined transporter expression from all humanized mice (all hu-HSC-Rag and BLT) is shown relative to GAPDH for infected and uninfected animals in the ileum (a) and rectum (b). Data shown are median and range. * represents $p<0.05$.

Because there were no significant differences observed between individual dosing cohorts, these data were combined to assess total gene expression (Figure 3.2**)**. In the ileum (Figure 3.2a),

transporter expression ranged from 10^{-6} to 1-fold of GAPDH expression, with detectable gene expression in every sample. These expression levels were consistent with the rectum (Figure 3.2b), with similar trends between transporters. Importantly, gene expression was generally consistent between uninfected and infected mice with the exception of *ABCC4*, which had significantly higher expression in infected mice versus uninfected mice ($p<0.05$).

Interspecies Comparison of Transporter Gene Expression

Pooled ileum and rectum data from mice and macaques were compared in Figure 3.3, which shows inconsistent agreement between compartments and between species. Among the efflux transporters, *ABCC2* (Figure 3.3b) showed agreement between species in both the absolute level of expression (10^{-1} fold GAPDH in the ileum) and expression between compartments (3-log increase in ileum vs rectum). *ABCB1* demonstrated a significant 2-fold increase in expression in macaques vs mice (Figure 3.3c), while *ABCC1* and *ABCG2* did not differ significantly between species or tissue site. The significant differences in *ABCC4* expression between uninfected and infected mice are again demonstrated here (Figure 3.3d), but otherwise no significant differences were observed. The uptake transporters *SLCO2A1* and *SLC29A1* did

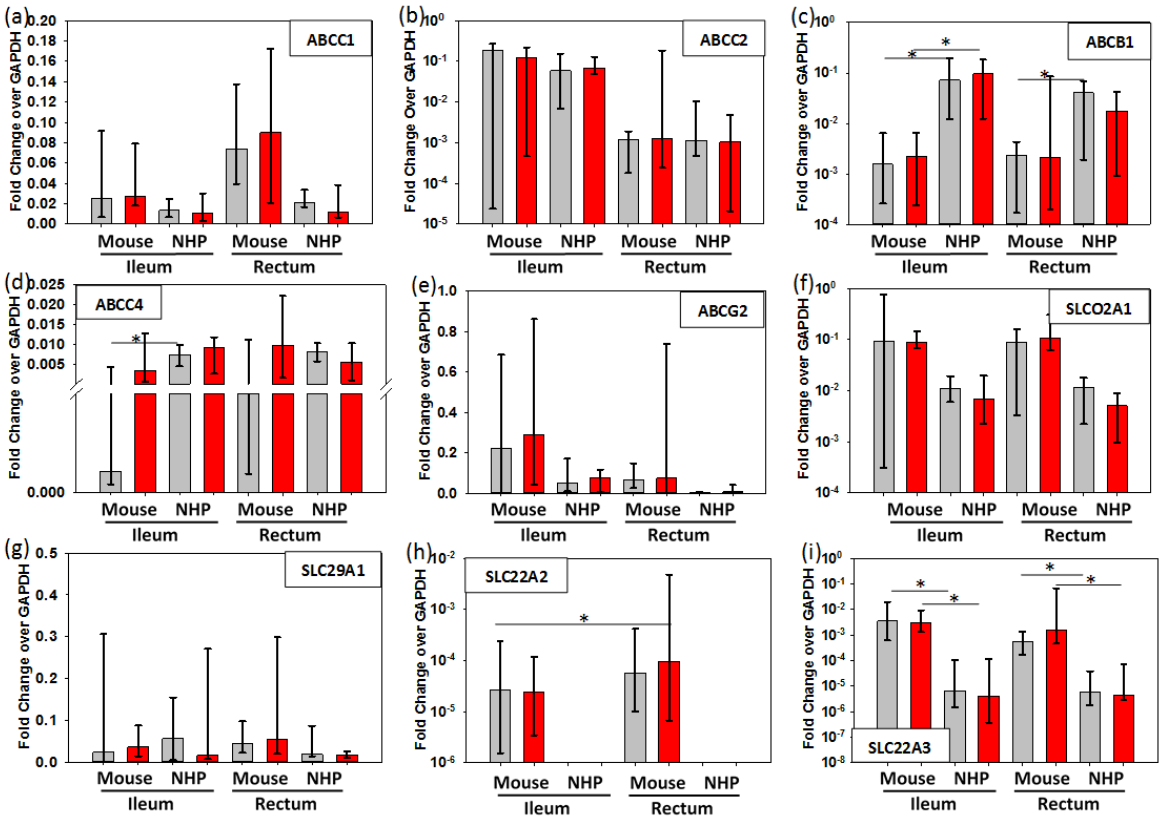

Figure 3.3: Multispecies Comparison of Transporter Gene Expression Gene expression is represented as fold change of GAPDH for uninfected (gray) and infected (red) animals from multiple dosing cohorts. Data shown are median and range. SLC22A2 was observed in mouse tissues only. NHP=non-human primate. * represents $p<0.05$

not differ between species, but *SLC22A2* was increased 0.5-fold in mouse rectum versus ileum and was not detected at all in macaque tissues (Figure 3.3h). Conversely, *SLC22A3* was 2-3 logs more highly expressed in mice ileum and rectum compared to macaques (Figure 3.3i).

Interspecies Comparison of Transporter Protein Expression by Western Blot Analysis

Figure 3.4 showcases transporter protein expression as measured by Western blot, with representative blots shown in 3.4a-e. Densitometry data from all mouse samples are shown in Figure 3.4f and 3.4g, which demonstrates large variability in protein expression, ranging from

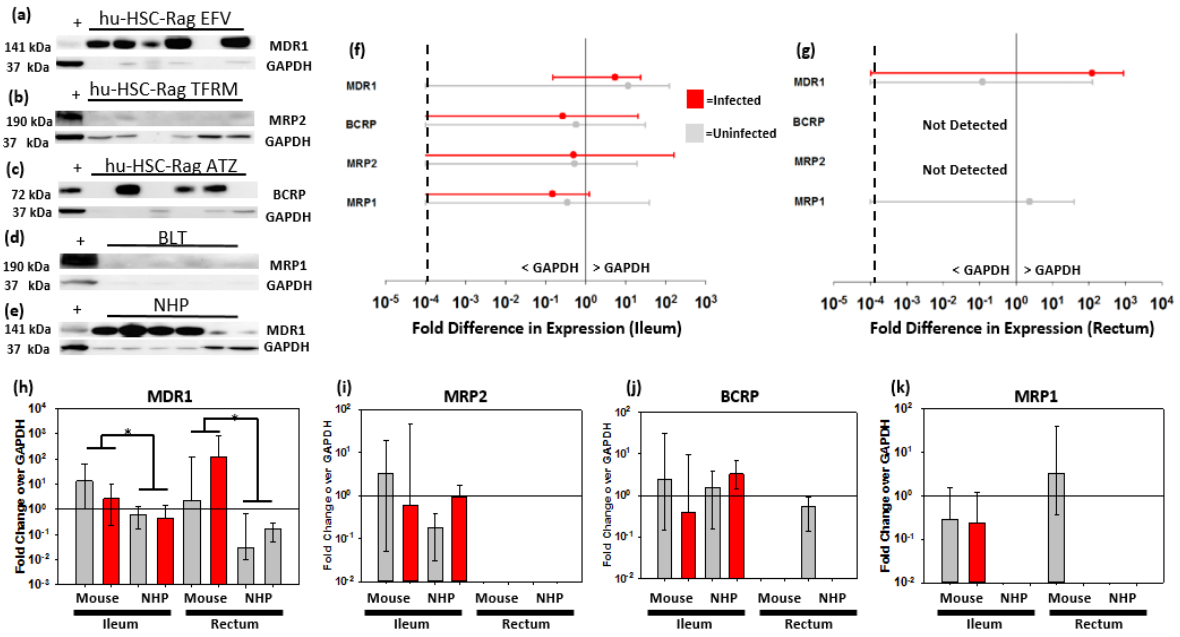

Figure 3.4: Transporter Protein Expression Humanized Mice Ileum and Rectum Representative Western blots for four efflux transporters from the ileum of each humanized animal cohort (a-e). + represents the positive control sample. Samples with no detectable GAPDH were not included in subsequent analyses. Densitometry data from each blot was quantified for each transporter in mice (f[ileum]&g[rectum]), where protein expression is represented as a fold change over GAPDH for uninfected (gray) and infected (red) animals. Zero values were imputed at 10^{-4} (dashed line) for graphing purposes. Comparison of all mice and macaques is shown in h-k, where data are median and range. Solid line represents equal protein expression to GAPDH. * represents $p<0.05$

0.2 fold GAPDH in some MRP1 samples to >100 fold GAPDH for MDR1. Densitometry analysis of individual mouse dosing cohorts is shown in Appendix 3.4, and did not indicate significant differences between dosing cohorts or mouse models. Figure 3.4h-k compares mouse and NHP Western blot data. Relative protein expression trends were similar between mice and macaques for MRP1, MRP2, and BCRP. Interestingly, MDR1 protein expression showed a

significant opposite trend compared to the *ABCB1* gene expression between species, with relative MDR1 protein expression 1-2 logs higher than macaques in both the ileum and rectum.

Interspecies Comparison of Transporter Protein Expression by Targeted Quantitative Proteomic Analysis

Proteomics analysis of absolute transporter protein concentrations for individual mouse dosing cohorts is shown in Appendix 3.5 and 3.6, where there was good agreement between dosing cohorts with no significant differences observed between infected and uninfected animals. Ileac and rectal QTAP data from all cohorts of mice were combined and compared to those generated in macaques (Figure 3.5). MDR1 protein concentrations were 2 logs higher in the mouse ileum compared to macaques (Figure 3.5c), which is the opposite of observed *ABCB1* gene expression trends. Further, the significant differences in *ABCC4* expression between infected and uninfected mice were not replicated in the protein analysis (Figure 3.5d). The 3-log

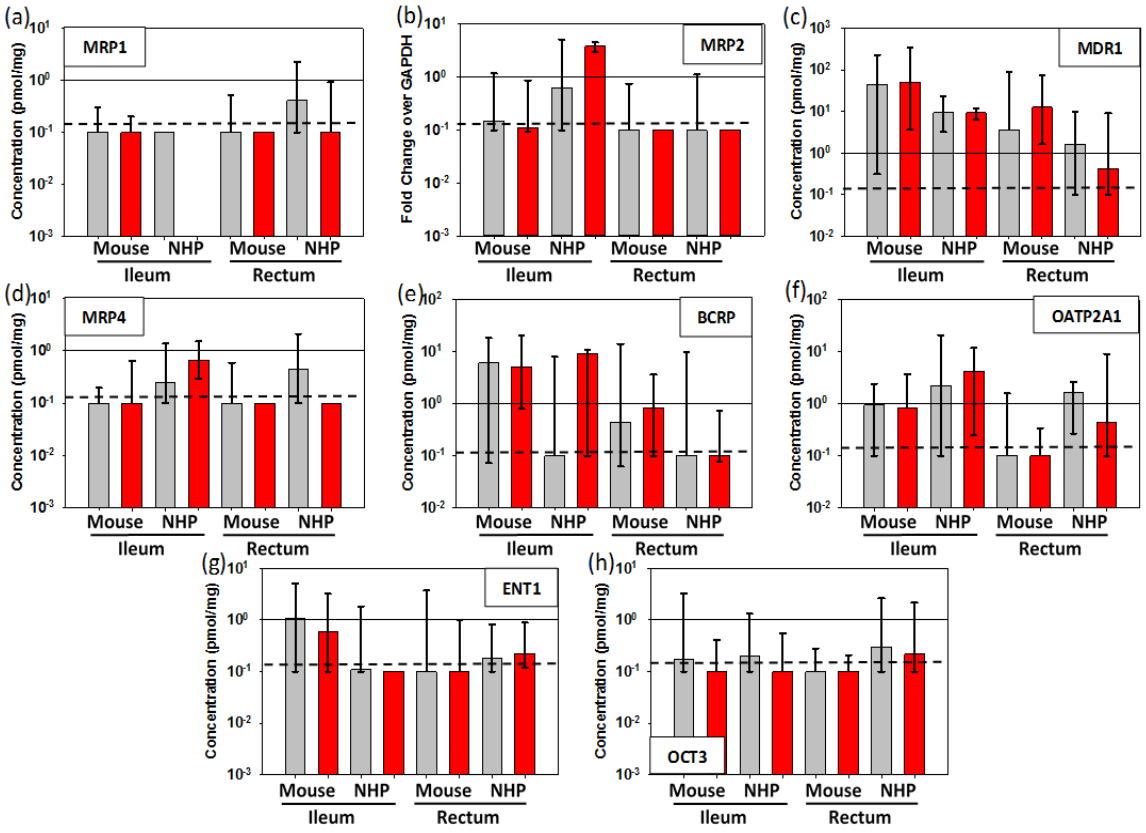

Figure 3.5: Multispecies Comparison of Transporter Protein Expression by QTAP Absolute protein concentrations are represented as pmol/mg protein for uninfected (gray) and infected (red) animals from multiple dosing cohorts. Solid lines represent 1pmol/mg; dashed lines represent the lower limit of quantitation. Data shown are median and range. * represents $p<0.05$

increase in *SLC22A3* gene expression in mice over macaques was also not replicated here (Figure 3.5h). There were also several significant differences in protein concentrations that were not present in the qPCR analysis. *SLCO2A1*, for example, was not significantly different between species in gene expression, however a significant increase in OATP2A1 concentrations was observed in macaques compared to mice (Figure 3.5f).

Transporter Localization in the Ileum and Rectum

IHC staining revealed distinct localization of several drug transporters within the GI tract (representative images in Figure 3.6). In both the ileum and rectum, MDR1 was found to localize on the luminal surface of the gut mucosa in tissues from all three animal models, and was readily expressed. Conversely, MRP2 was not detected in any tissue from any animal, though protein

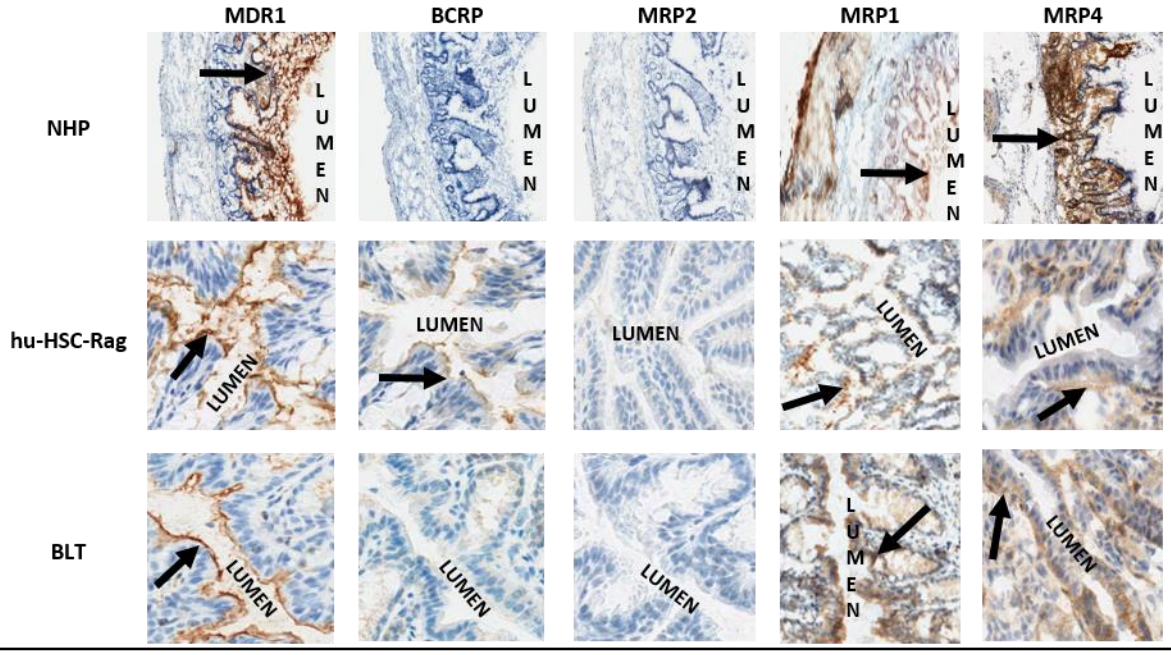

Figure 3.6: Efflux Transporter Localization Within the Macaque and Mouse Gut. Immunohistochemical staining for MDR1, BCRP, MRP2, MRP1 and MRP4 in NHP, hu-HSC-Rag mice, and BLT mice. Positive cells (brown staining) are indicated with black arrows. Lumen is labelled in each image.

was sporadically detected with Western blot (Figure 3.4) and QTAP (Figure 3.5). BCRP was detected in the ileum of both mouse models, and showed a similar localization profile to MDR1. Interestingly, BCRP expression in the rectum of these animals was much lower, with only a few positive-staining cells detected, and was not detected at all in the macaque tissues despite low levels of detection in the macaque ileum by QTAP. MRP1 localized to the luminal surface in a similar fashion to MDR1 and was expressed in all tissues. MRP4 was localized to the lamina

propria in all three species, with extensive positive staining on the basolateral surface of mucosal cells.

Human Transporter Expression in Humanized Mice

Figure 3.7 provides an overview of human transporter gene expression as it relates to mouse gene expression in the same tissues. Human gene expression was observed for more than half of the transporters evaluated. Expression was in general 1-5 logs lower than the mouse genes, with the notable exceptions of *ABCB1* and *ABCC4*, which in some samples was 2 logs higher than mouse expression. Trends were similar between ileum and rectum, with no significant differences detected between infected and uninfected animals. Human genes were not detected in any sample for *ABCC2*, *SLC22A2*, or *SLC22A3*. The Gene Expression Assay for human *SLCO2A1* was found to be cross-reactive to mouse genes and was therefore not included in the analysis. An analysis of the

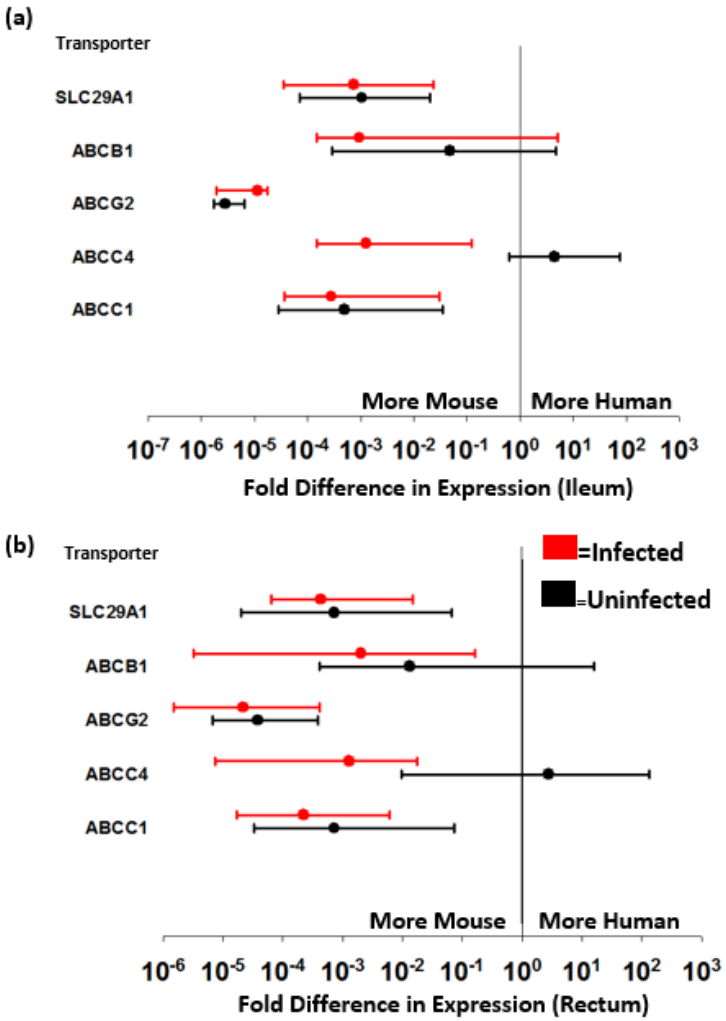

Figure 3.7: Human Transporter Gene Expression in Humanized Mouse Gut Combined transporter expression from all humanized mice (all hu-HSC-Rag and BLT) is shown relative to mice for infected and uninfected animals in the ileum (a) and rectum (b). Data shown are median and range. SLC22A2 and SLC22A3 were not observed in any animal, and the SLCO2A1 primers were found to be cross reactive and thus were not included.

relationship between the extent of humanization and the amount of human transporter gene expression did not show any significant relationship (data not shown). Western blot analysis using human-specific antibodies showed detectable bands for MDR1 only, which had fold-GAPDH values that were within 50% of mouse protein expression (data not shown). However, QTAP analysis using human-specific SILs did not detect any MDR1 in any humanized mouse sample, nor did it detect human protein from any other transporter (data not shown). To demonstrate that earlier interspecies comparisons for *ABCB1* and *ABCC4* were not confounded by a lack of accounting for human gene expression, we re-analyzed these data after accounting for the contribution of human gene expression of these transporters (Appendix 3.7). Our *ABCB1* results were not significantly altered, however median *ABCC4* expression in the uninfected mouse rectum greatly increased ($p<0.01$) over corresponding data in NHPs.

Antiretroviral Tissue Penetration

Tissue:plasma ratios for each ARV investigated in both the ileum and rectum are shown in Table 3.2 for all three animal cohorts. No significant differences were seen between infected and uninfected animals so these data were combined for analysis.

Table 3.2: Tissue:Plasma Ratios for Evaluated Antiretrovirals in Intestinal Tissue

	Ileum			Rectum		
Drug	**Mice**		**All Macaques**	**Mice**		**All Macaques**
	BLT	**hu-HSC-Rag**		**BLT**	**hu-HSC-Rag**	
TFV	12 (1,28)	17 (0,56)	13 (3,58)	52 (1,448)	160 (0,628)	32 (2,145)
FTC	2 (0.3,5)	2 (0,16)	23 (5,133)	4 (1,717)	0.6 (0,2)	76 (9,496)
RAL	1 (0.4,3)	3 (1,26)	32 (2,49)	0.7 (0.2,279)	3 (2,4)	753 (137,1163)
EFV		0.7 (0,509)	6 (4,42)		13 (0,156)	9 (0.1,328)
MVC	24 (5,131)	9 (0.9,31)	135 (8,422)	29 (5,81)	6 (1,18)	385 (17,2831)
ATZ	12 (0.1,87)	25 (0.2,749)	2709 (9,30000)	11 (0.2,1239)	15 (0.6,183)	8763 (0.1,19812)

*data shown are median and range

In mice, quantifiable concentrations of ARVs were detected in most plasma samples, ranging from 65% detection for MVC to 100% detection for TFV and FTC. Tissue concentrations were detected more frequently, ranging from 79% detection for RAL to 100% detection for TFV and FTC. Among the ARVs evaluated, TFV showed the highest penetration into both the ileum and rectum. TFV penetration was similar between BLT and hu-HSC-Rag mice in the ileum, but was increased by 3-fold in the hu-HSC-Rag rectum vs BLTs (160 vs 52). FTC, RAL, and ATZ TPRs were not significantly different between mouse models or compartments, while EFV achieved 18-fold higher TPR values in the hu-HSC-Rag rectum versus the ileum. MVC penetration was similar between the ileum and rectum, but was 3-fold and 5-fold higher in BLTs versus hu-HSC-Rag mice in these respective compartments.

The NHP samples had detectable ARV concentrations in >85% of samples for every ARV evaluated in both plasma and tissue. TPRs in NHP tissues were significantly increased ($p<0.05$) over both mouse models for FTC, RAL, MVC, and ATZ, ranging from 9-fold (MVC

ileum) to 150-fold (ATZ ileum) higher in NHPs. TFV penetration between animal models was not significantly different. EFV penetration was 8.5-fold higher in the NHP vs. mouse ileum ($p<0.05$), but this difference was not observed in the rectum. MVC and ATZ achieved the highest exposure of any drugs in both species, and median TPR values were increased by 3-fold in the rectum versus the ileum for both of these drugs. These large ratios were driven by high tissue exposure rather than low plasma concentrations, which were consistent with previously published data in non-human primates.

Methodology Comparison for Drug Transporter Evaluations

To determine whether or not the three methodologies used here to evaluate drug transporter expression agree with one another, correlation matrices were generated for the four efflux transporters evaluated by all three methods using combined data from all animals (Figure 3.8). Correlation coefficients were low for all comparisons, ranging from 0.01 (MRP2 QTAP vs Western) to 0.42 (MRP1 qPCR vs Western) and showcasing the lack of

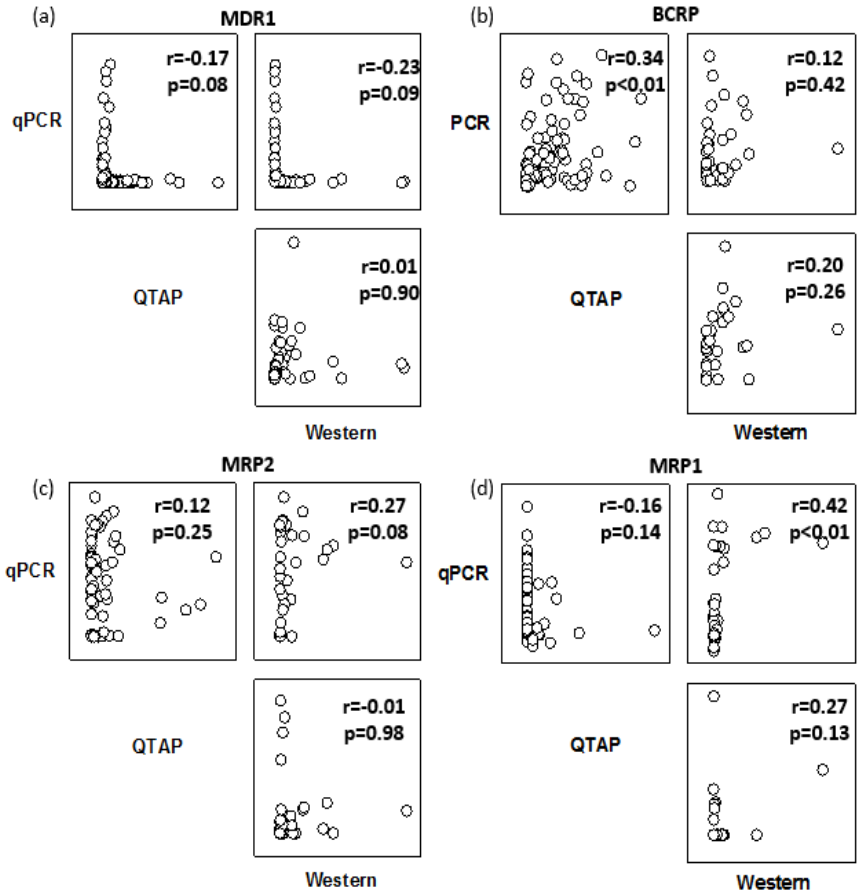

Figure 3.8: Lack of Agreement Between Transporter Evaluation Methods Correlation matrices are shown for the four efflux transporters evaluated by all three methods.

agreement between techniques. Comparison of qPCR and QTAP for BCRP showed the strongest correlation, and reaches statistical significance ($r=0.34$, $p<0.01$), however the large amount of variability in the data does not provide convincing evidence that these methods are in high agreement.

Results from the multivariable analysis are shown in Table 3.3. Predictive ability was generally low, with R^2 values ranging from 0.09 (TFV TPR predicted by qPCR) to 0.51 (FTC TPR predicted by WB). qPCR data was able to generate significantly predictive regression models for each drug evaluated, though the resulting R^2 values tended to be lower than those generated by WB. QTAP data generated significant models for TFV, FTC, and RAL only, and R^2 values were lower than qPCR or WB in every case. IHC quantitation poorly predicted TPR values and did not offer improvement over qPCR or QTAP. There was little agreement between methods regarding which specific efflux transporters were found to significantly contribute to each model, though BCRP and MRP1 expression were the most commonly implicated transporters.

Table 3.3: Multivariable Regression Analysis of Drug Transporter Expression Methods on TPR

Drug	Method	MDR1	BCRP	MRP2	MRP1	MRP4	R^2
TFV	qPCR	-	-	**0.01**	-	-	0.09
	WB	-	**0.01**	-	0.05	-	0.38
	QTAP	-	**0.01**	-	-	-	0.11
	IHC	-	-	-	-	-	n/a
FTC	qPCR	-	**0.007**	-	**0.008**	-	0.41
	WB	-	**0.01**	-	**0.002**	-	0.51
	QTAP	**0.04**	-	0.05	-	-	0.15
	IHC	-	-	-	-	-	n/a
RAL	qPCR	0.56	**0.002**	-	**0.002**	-	0.43
	WB	-	**0.03**	-	**0.01**	-	0.51
	QTAP	-	-	-	0.58	**0.008**	0.16
	IHC	-	-	-	-	-	n/a
EFV	qPCR	-	**0.004**	-	0.07	-	0.39
	WB	-	0.12	-	-	-	0.22
	QTAP	-	-	-	-	-	n/a
	IHC	-	-	-	-	-	n/a
ATZ	qPCR	-	-	-	-	0.06	0.17
	WB	-	-	-	-	-	n/a
	QTAP	-	-	-	-	-	n/a
	IHC	-	-	-	-	-	n/a
MVC	qPCR	-	-	-	**0.002**	-	0.23
	WB	-	-	-	-	-	n/a
	QTAP	-	-	-	-	-	n/a
	IHC	-	-	-	-	-	n/a

Discussion

This is the first study to comprehensively compare drug transporter expression in the GI tract across animal models, and has demonstrated several novel findings with important implications for drug development and HIV eradication research. Transporter gene expression in mice was shown to be similar regardless of drug regimen and mouse model. There were, however, a few notable exceptions. *ABCB1* expression tended to be lower in the BLT mice than

in hu-HSC-Rag animals. Though this difference did not reach statistical significance due to the high variability of these data, it may be the case that GI exposure of MDR1 substrates (including most ARVs) may be increased in the BLT model. This is supported by the LC-MS data generated here, where MVC and RAL (two MDR1 substrates) were undetectable in the hu-HSC-Rag animals but readily detected in BLT mice (Table 3.1). Conversely, TFV and ATZ concentrations showed the opposite trend despite also being MDR1 substrates.

Additionally, we observed significant multiple log increases in *ABCC4* expression in infected mice, which was found in both the ileum and rectum and was consistent between the drug regimens and mouse models (Figure 3.2). Given that MRP4 is known to transport TFV,[61] higher levels of *ABCC4* expression and MRP4 efflux activity during infection may mean that TFV exposure is reduced in tissues with high amounts of HIV replication, contributing to the propagation of tissue reservoirs. These changes also have implications for the development of novel ARVs that are also MRP4 substrates. For example, the observed tissue exposure of an investigational agent may depend solely on whether or not the animals used were infected or not, potentially changing the course of a drug's development. Though we did not observe these same differences in MRP4 protein expression with QTAP or Western blot, overall detection of this protein was low and it may be that lower detection limits would have yielded more conclusive results. TFV tissue concentrations evaluated here by LC-MS were not significantly different between infected and uninfected animals after adjustment for plasma concentrations, casting doubt on whether or not the observed differences in gene expression have any clinical implication. Lack of agreement between mRNA expression and protein expression and function (discussed in more detail below) or the effect of numerous drug transporters acting in concert may help explain this disconnect.

When gene and protein expression data were pooled to investigate differences between anatomic compartments and between species, several important differences were observed. The multiple log differences observed between mice and macaques for *ABCB1*/MDR1 and *ABCC4*/MRP4 indicate ARV PK data generated in one model may not easily be extrapolated to the other. Given that several of these transporters have been shown to efflux numerous ARVs, the species used in investigations of ARV disposition into tissues, whether for prevention or eradication, is a critically important variable. RAL, for example, has been shown to reach rectal concentrations that are 35-fold greater than plasma in macaques.[144] We have also recently shown that RAL distributes readily throughout the macaque rectum, but that distribution in humanized mouse rectum is lacking.[76] In this study, RAL NHP ileum and rectum concentrations were increased over mice by 16- and 376-fold, respectively. Given that RAL is known to be effluxed by MDR1, it may be the case that RAL distributes into the intestinal mucosa in both species, but is effluxed back into the intestinal lumen by MDR1 to a greater extent in mice versus macaques, helping to explain the decreased tissue concentrations in this model. The distinct differences observed here provide support that transporter expression may also differ between animal models and humans.

When compared to data generated by others using human tissues, the animal data generated here shows several striking differences. De Rosa et al evaluated the gene and protein expression of five efflux transporters in the sigmoid colon of 16 HIV negative and 9 HIV positive men.[100] The authors found the highest level of gene expression for *ABCC2* (0.76-fold vs cyclophilin) and the lowest expression level for *ABCG2* (0.17-fold). We observed comparatively lower expression levels in both mice and NHPs, with a maximum median expression level of 0.5 (*ABCG2* in infected mice), though we normalized to a different housekeeping gene. Protein

expression by Western blot in their study showed relative expression ranging from 40-100-fold higher than the loading control (actin), again higher than what we observed. Of note, we failed to observe any MRP2 and little BCRP from the rectum of both animal species despite expression in human colon of 60-70-fold that of loading control. Further, analysis of human data showed a significant downregulation of *ABCB1* and *ABCC2* genes in HIV infection, and significant alterations in protein expression during cART, neither of which were observed here. Studies of human tissue done by our group (described in Chapter IV) provide additional insight on interspecies differences and minimize inter-lab variability effects that may be confounding these comparisons.

Not only does the current study provide important information on transporter expression between animal models, we also are the first to formally compare methodologies for measuring transporter expression in tissues relevant for HIV research. The extent of agreement between methods was generally poor, with *ABCG2*/BCRP showing the only significant relationship. There are several possible explanations for this lack of correlation, including the fact that, compared to the robust qPCR data, protein expression was highly variable and was not observed in all samples. Conditions for these experiments have been optimized by our lab, however lot-to-lot antibody variability and lack of an accepted standard for quantifying densitometry data are persistent challenges with the Western blot technique.[145] Further, mRNA inhibition by native micro-RNAs or post-translational protein modifications are known to affect the relationship between gene and protein expression and may be influencing the observed results. Additionally, differential rates of mRNA degradation between GAPDH and transporters may falsely lower observed expression despite correction for this housekeeping gene.

The lack of agreement between qPCR and Western blot data even after correction for GAPDH expression is concerning, as there is currently no accepted standard in the field for measurement of transporter expression. Several groups have published data generated using both methods[100,65], however the utility of Western blot data is limited due to narrow dynamic range and often possible antibody cross reactivity. Further, relative gene expression data should be interpreted with caution, as the high sensitivity may lead to false positives. Using DNA standards, we have determined that 8-10,000 copies of GAPDH were present in each mouse sample, with 60-100,000 GAPDH copies present in each NHP sample (data not shown). Based on these values, relative transporter expression values of 10^{-4} or greater represent biologically-plausible expression of these genes in our samples, however lower relative expression values may simply mean that the gene is not expressed at all.

Proteomics analysis of the same tissues showed much more robust data compared to those generated by Western blot in terms of overall frequency of detection (80% for QTAP vs 71% for WB). However even these data showed little agreement when compared to qPCR data. The transporters with statistically significant relationships between the methods (BCRP and MRP1) did not demonstrate a significant predictive ability, with R^2 values of 0.34 and 0.42, respectively. Despite the lack of agreement with qPCR data, QTAP tended to agree with transporter localization data determined by IHC, where MDR1 and BCRP were the most highly expressed throughout the ileum and rectum, with decreased expression of MRP1 and almost no expression of MRP2. The ability of QTAP to provide robust, downstream protein expression data with high sensitivity and specificity for multiple transporters from a single sample make this an appealing technology. The lack of agreement between QTAP and WB is inconsistent with previous reports showing good correlation between these methods[146]. However, those results

have been generated using recombinant enzymes, which do not represent the complex biological tissue matrices studied here. To our knowledge, ours is the first study to compare these data using tissue homogenates. While this technology requires specialized equipment and expertise its use has become more widespread in recent years.[147–149]

Despite these advantages, the multivariable regression analysis found that QTAP data did not provide a significant increase in predicting observed TPR values over data derived from other techniques (Table 3.3). Further, the efflux transporters identified as significantly predicting TPR were not consistent between methods. The biologic plausibility of the observed results is also variable. For example, BCRP expression measured by WB showed a moderate predictive capacity (R^2= 0.38) for the TPR of TFV, a BCRP substrate. MRP1 was found to significantly affect the TPR of FTC using qPCR and WB data (R^2=0.41 and 0.51, respectively), supporting studies that show FTC as an MRP1 substrate. Conversely, there are several instances where significant prediction was unexpectedly not found given existing substrate data (e.g. MDR1 for RAL, MRP4 for TFV). These results may be explained in part by the large amount of undetectable samples for Western blot and QTAP, which may have reduced the ability to detect significant relationships. Further, the possibility of drug-drug interactions affected tissue ARV exposure, particularly in the NHPs receiving EFV, must be considered.

The negative results of this regression analysis may indicate that drug transporters alone do not govern ARV tissue concentrations in a significant way, but must be measured in the context of additional variables such as drug metabolizing enzyme expression or drug PK properties, which were not examined here. It is possible that consideration of these variables in tissue accumulation would have improved the predictive ability of the model. Given the high sensitivity and low variability of qPCR data compared to other methods, it is surprising that these

models did not identify expected transporters, however qPCR was able to identify at least one significant variable for every drug. The fact that gene expression is not always reflected by protein expression could be seen as an issue with the qPCR technique.

One of the most notable findings of this analysis is the characterization of human drug transporter expression in the tissues of both humanized mouse models. The extent of peripheral immune humanization observed here was consistent with previous studies using these models[108], but this is the first study to quantify human transporter expression in these animals. The detection of some human transporter gene expression should not be surprising given that many of these transporters are expressed on the surface of human lymphocytes, which are abundant in the humanized mouse GI tract, particularly in the ileum. We observed human gene expression from nearly every transporter evaluated, and found that *ABCB1* and *ABCC4* were expressed at an extent equal to or greater than mouse transporters in tissues from five mice (Figure 3.7). This implies some amount of underestimation of the size of the total transporter pool, and when human transporter isoforms were accounted for (Appendix 3.8), *ABCC4* results significantly changed. However, *ABCB1* results remained consistent and the use of species-specific antibodies and SILs for Western blot and QTAP, respectively, preserved the validity of our protein results.

This finding is particularly relevant to intracellular ARV exposure in the context of infection. As the majority of ARVs have intracellular sites of action, drug transporters on the surface of lymphocytes (e.g. ENT1, MRP1, MPR4, BCRP)[150] are equally important to those regulating overall exposure in the tissue. Human lymphocytes are the only cells infected in these chimeric mice, and the contribution of human transporters on the surface of these cells to the overall transporter population cannot be ignored. Though species differences in the specificity of

these transporters for the ARV substrates studied here have yet to be quantified, protein sequence homology is high compared to mice (78-88%), and it is reasonable to expect that ARVs utilize transporters from both origins. Evaluations that quantify transporters from only one species or the other may underestimate the effect of some transporters for ARV disposition, as we have demonstrated here. Future studies of drug transporters and/or drug metabolizing enzymes in these mouse models should include the analysis of both mouse and human-derived proteins.

As the body of evidence for persistent HIV replication within tissue reservoirs continues to grow, so does the need to define and quantify the factors influencing ARV disposition within these tissues. Targeting new or existing ARV therapies to these sites will require a knowledge of the specific variables that favor increased exposure at the site of action. To that end, this analysis is the first to formally compare drug transporter expression between commonly used animal models, and to assess the effect of HIV infection on transporter expression. We also demonstrated that the methods commonly used to evaluate transporter expression have little agreement with each other, and that robust downstream measures may have the most utility. Finally, we are the first to quantify the contribution of human transporters to the overall transporter pool in the GI tissue of these humanized mouse models. These data can inform the development of future therapies targeted toward HIV reservoirs and, when coupled with within-tissue ARV distribution data, represent an important step toward HIV eradication.

Chapter IV: Clinical Assessment of Antiretroviral GALT Distribution and Drug Transporter Expression with Interspecies Comparisons to Inform Drug Development

Summary

Inadequate antiretroviral (ARV) exposure within gut-associated lymphoid tissue (GALT) may contribute to HIV persistence, but traditional LC-MS techniques cannot fully address this hypothesis. Mass spectrometry imaging (MSI) shows heterogeneous ARV distribution in GALT in animal models, which may be affected by drug transporters. However, application of these findings are limited without comparing these data to humans. Here, we assess ARV localization and drug transporter expression in HIV-infected subjects and make novel inter-species comparisons. Ileum and rectum biopsies (n=10 each) were collected from five HIV-infected females receiving combination ARVs (Truvada® + raltegravir (RAL), efavirenz (EFV), atazanavir (ATZ), or maraviroc (MVC)). Co-localization analysis of ARVs (measured by MSI) and T cells (measured by immunofluorescence) was performed in Matlab using Pearson correlation (r). Drug transporter protein concentration was measured from replicate biopsies by LC-MS/MS proteomics. Human data were compared to our previously generated animal data in non-human primates (n=12) and humanized mice (n=49) using ANOVA on ranks. ARV localization was heterogeneous within tissue and across therapeutic classes. After correction for heme signatures, MVC and EFV showed the best ARV-T cell co-localization, which was 5-fold higher in the rectum versus ileum, and not significantly different ($p>0.05$) from data in primates or mice. HIV RNA localization was anti-correlated to the distribution of all ARVs except MVC

and ATZ and was consistent with animal data. Human drug transporter concentration was in better agreement with mice (1 to 9-fold difference) versus primates (1 to 21-fold difference), with 4-fold lower P-gp expression in primates. We show that ARV distribution within biopsies is heterogeneous and may not co-localize with HIV target cells. This is consistent with animal data and may implicate ARV tissue exposure in the propagation of HIV GALT replication. Human drug transporter concentrations agreed with humanized mice better than primates, suggesting that the former may be a better animal model for developing novel ARV therapies targeted at GALT, particularly for P-gp substrates.

Introduction

Despite advancements in treatment and prevention strategies, HIV continues to present an enormous global health burden, and remains a top ten cause of death worldwide.[151] The inability to cure this disease is a direct consequence of HIV persistence in cellular and tissue reservoirs despite treatment with combination antiretrovirals (ARVs).[5,7,14] Although the latent cellular reservoir remains the primary obstacle to HIV eradication, ongoing replication in certain tissue sites, including gut-associated lymphoid tissue (GALT), may represent an additional barrier to cure.[10–13] The consequences of HIV persistence in GALT (described in Chapter I) are distinct from other tissue reservoirs and make this site a priority for understanding the mechanisms underlying this persistence (e.g. reduced ARV exposure).

The generation of PK/PD relationships at the site of action is critical to optimizing therapy for HIV eradication, and must be performed before testing interventions in late-phase development. Several studies have attempted to circumvent this process by simply intensifying existing ARV regimens to reduce the reservoir size, with limited success.[54,55] Given that these studies have been unsuccessful to date, and the fact that viral rebound upon treatment cessation is observed in nearly all patients, it is reasonable to assume that novel therapies will need to be developed that target tissue reservoirs specifically. A novel small molecule that achieves increased exposure at the site of action and subsequently reduces or eliminates HIV replication in tissues would be an important step toward eradication.

The development of any novel therapy will require initial characterization in pre-clinical models of HIV infection. In addition to traditional safety and efficacy measures, it is critical to define the exposure-response relationship in tissues to maximize the likelihood of clinical success. The mixed success of pre-exposure prophylaxis (PrEP) trials in the HIV prevention field

is due, in part, to the lack of pre-clinical PK/PD to inform Phase III trial design.[51,152] Several variables required to define this relationship, such as ARV distribution within tissues and drug transporter expression and localization, were described in Chapters II and III of this dissertation, respectively. Significant differences were found between animal models (i.e. 1.7-log increase in TFV-CD3+ T-cell co-localization in NHPs vs mice, 2-fold decrease in MDR1 expression in BLT vs hu-HSC-Rag mice), but the utility of these data are limited without appropriate comparison to human tissues.

The use of pre-clinical data to predict human PK/PD is complicated by a paucity of data directly comparing animals to humans, despite evidence that factors influencing drug disposition may be substantially altered between species. For example, drug metabolizing enzymes such as the CYP2C family can be as much as 12-fold higher in rats versus humans.[102] Further, the gene and protein expression of drug transporters quantified in Chapter III does not agree with existing data from human subjects (e.g. lower gene and protein expression of *ABCG2*/BCRP and *ABCC2*/MRP2 in animals compared to humans[100]). In order to prevent inappropriate extrapolation of data from one species to another, formal interspecies comparisons must be performed.

In this study, we characterize ARV distribution within several putative viral reservoirs from HIV positive subjects, and measure drug transporter expression and localization from these same sites. We compare these data to those generated using similar methods in humanized mice and non-human primates to determine which pre-clinical species best predicts results from humans. These data address whether or not current therapies achieve adequate exposure at the site of action, and identify specific variables to target or avoid to maximize efficacy. By directly

comparing animals to humans, we can also inform the development of inter-species scaling factors to streamline the development of targeted therapies for HIV eradication.

Methods

Trial Design

This was a single-center, open label, observational study of ARV localization within GALT (terminal ileum & rectum), vaginal, and cervical tissues (for future analysis) in the setting of undetectable plasma HIV. This study enrolled 5 of a planned 22 HIV positive women between 18 and 65 years of age with intact gastrointestinal and genital tracts, who had an undetectable viral load within 3 months preceding the study. Participants were recruited from the infectious disease clinic at UNC Hospitals on the basis of receiving one of the study regimens as part of their ongoing HIV care. The primary objective of the study was to quantify the distribution of ARVs in the GALT of HIV positive women receiving one of four ARV regimens and identify tissue compartments in which ARV exposure is lacking or concentrated.

Participants were excluded if they had any clinically significant comorbidities or abnormal screening laboratory tests; untreated sexually transmitted infections (rectal or vaginal chlamydia or gonorrhea, syphilis, trichomonas); were pregnant or lactating; had an abnormal Pap smear result within the previous 36 months or previous hysterectomy or cervical resection; or tested positive for any drugs of abuse that would complicate sedation. Additional exclusion criteria included receiving CYP3A4 inducers or inhibitors (other than those contained in their HIV regimens) in the previous 6 months; receiving any investigational drug in the last 4 months; history of inflammatory bowel conditions (IBD, Crohn's); or not using an approved method of contraception (systemic hormonal contraception, IUD, bilateral tubal ligation, vasectomized

male partner, condom plus spermicide, female-only sex partners, or 3 months of abstinence before enrollment). A complete list of inclusion and exclusion criteria is listed in Appendix 4.1.

After participant education, informed consent, and screening for study eligibility, participants were assigned to the treatment arm associated with the HIV regimen they were receiving (Figure 4.1). Within 42 days of screening, participants were admitted to the UNC HealthCare Clinical Trials Research Center (CTRC) for a 36-hour inpatient pharmacokinetic

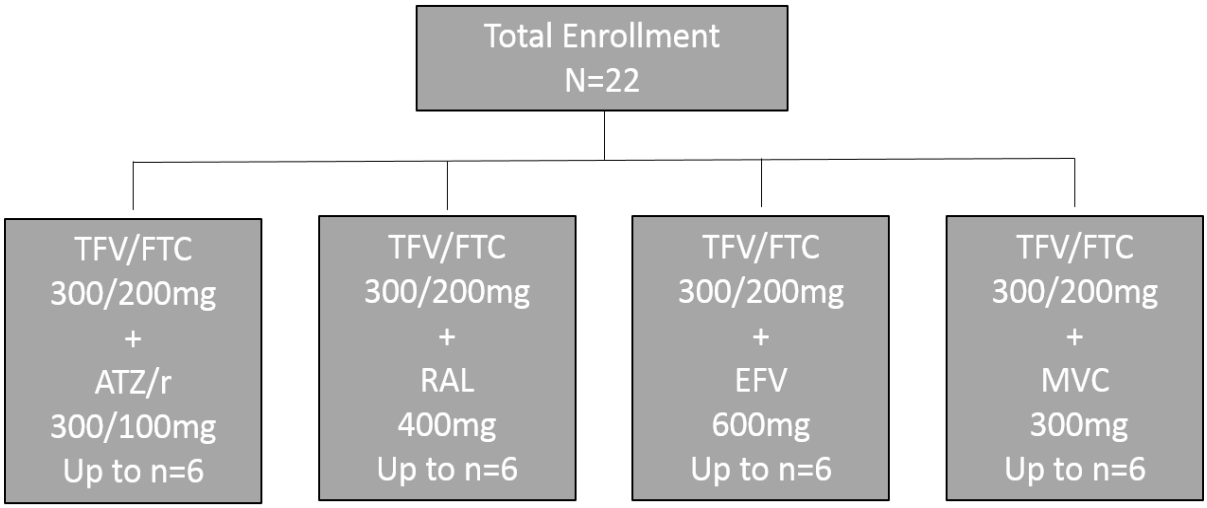

Figure 4.1: Treatment Arms Evaluated Subjects were analyzed by treatment arm according to their current cART regimen.

visit (Figure 4.2). For the 7 days prior to admission, participants were asked to follow a strict low-fiber diet in preparation for a colonoscopy. Once admitted, participants were given only clear liquids until 4 hours prior to the colonoscopy. On day 1 of the visit (within 3-4 hours of admission), each participant provided 2 biopsies each from the cervix and vaginal wall and a paired blood sample. After genital tract biopsies were taken, participants were given an oral laxative (two 5mg bisacodyl tablets) followed by a colonic preparation with a PEG solution

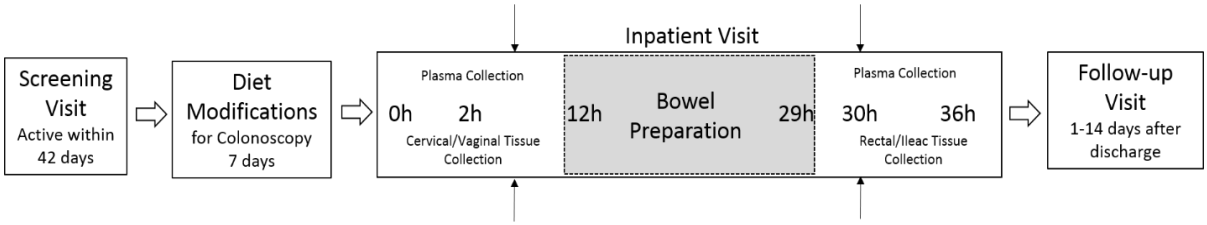

Figure 4.2: Study Design Schematic After screening, subjects underwent a 36 hour inpatient visit where tissues were collected (represented by black arrows on Day 1 and 2

(Golytely). The preparation was divided into 2 separate 2-hour blocks; the first beginning 18 hours before the scheduled procedure, and the second half beginning 6 hours pre-procedure. Participants were NPO for the immediate pre-colonoscopy period. Before the procedure, a single paired blood sample was taken. During the procedure, 10 biopsies each were taken from the terminal ileum and rectum. After the colonoscopy procedure, subjects were monitored for 6 hours and then discharged home, with follow-up visits within 14 days of discharge.

Safety assessments were conducted on each day of the inpatient visit and during follow-up. Adverse events were evaluated using a standard questionnaire, with grading according to the DAIDS adverse events grading table.[153] Women were screened for pregnancy at each visit. This study was conducted using Good Clinical Practice procedures and was approved by the UNC Institutional Review Board. All participants provided written informed consent before study procedures were performed.

Sample Collection and Analysis

Cervical and vaginal biopsies were collected using sterilized Tischler forceps (Cooper Surgical, Trumbull, CT). Ileac and rectal biopsies were collected during colonoscopy with Radial Jaw 4 large capacity biopsy forceps (Boston Scientific, Boston, MA). All tissues were immediately snap frozen on dry ice, then placed in aluminum foil pouches and stored at -80˚C until analysis. Whole blood was collected in 3mL EDTA tubes and centrifuged at 3000rpm for 10 minutes at 4˚C. Plasma was aliquoted into a 2mL cryovial and stored at -80˚C until analysis.

LC-MS

Plasma and tissue samples were analyzed as described in Chapter III. Briefly, plasma samples were extracted by protein precipitation with methanol containing stable, isotopically-labeled internal standards. Samples were vortexed and centrifuged, then the supernatant was diluted with water prior to LC-MS/MS analysis. Tissue samples were placed in a tube (Precellys 2mL Hard Tissue Metal Beads Kit) containing 1mL of ice cold 70:30 acetonitrile-water, homogenized, then mixed with methanol containing stable, isotopically labeled internal standards. Following centrifugation, the supernatant was evaporated to dryness and reconstituted with water (for TFV/FTC analysis) or 25:75 methanol:water (for ATZ/EFV/MVC/RAL analysis). A Shimadzu high-performance liquid chromatography system with a Waters Atlantis T3 (50mm x 2mm, 5µm particle size) HPLC column was used for separation, and an AB SCIEX API 5000 mass spectrometer (AB SCIEX, Foster City, CA, USA) equipped with a turbo spray interface was used as the detector. The lower limit of quantitation was 1ng/mL for plasma, and 0.002 ng/mL (FTC and MVC), 0.005ng/mL (ATZ, EFV, and RAL), and 0.01ng/mL (TFV) for tissue samples.

Tissue Imaging

Tissue biopsies underwent IR-MALDESI (for detailed methods, see Chapter II), with one additional step during sample processing. Due to the small size of the tissue biopsies, samples were embedded in groups of 4 tissues in a 50:50 gelatin carboxymethylcellulose gel block, which was snap frozen and stored at -80°C (in an identical fashion to the mouse tissues described in Chapter II). Briefly, tissues were sliced frozen at 10µm thickness using a cryostat (Leica Biosystems, Wetzlar, Germany) and thaw mounted onto glass microscope slides. Thaw mounted tissues were placed into the source chamber and maintained at -10˚C while an ice layer was

deposited. Tissues were ablated with two pulses of a mid-IR laser (IR-Opolette 2371, Opotek, Carlsbad, CA) with a 100um spot-to-spot distance, ionized, and analyzed using a Thermo Fisher Scientific Q Exactive mass spectrometer (Bremen, Germany). Because the detection of certain analytes (e.g. TFV, EFV) was found to be increased by probing for negative ions, polarity-switching was used during these experiments using 5mM ammonium acetate in 50:50 methanol water as the electrospray solvent. Raw data were converted to the imZML format for analysis with MSiReader, interrogating both positive and negative ions.

IHC, IF, and ISH were performed as described in Chapter II using identical reagents and antibodies. Image co-localization proceeded using MatLab vR2015 (Mathworks, Natick, MA). Pixel intensity matrices for each ARV of interest, plus cholesterol and heme, were imported into MatLab along with downsampled IHC/IF/ISH images. Cholesterol and heme masks were applied as described in Chapter II, then images were co-registered. Co-localization of each ARV and biologic variable of interest (CD3, HIV RNA, MDR1, etc.) was performed using Pearson correlation to quantify distributional overlap.

Drug Transporter Analysis

With the remaining ileac and rectal tissue, drug transporter gene and protein expression were measured by qPCR, WB, and LC-MS proteomics as described in Chapter III. Drug transporters evaluated were identical to those described in Chapter III (Table 3.1). For qPCR analysis, 200ng of extracted RNA were reverse transcribed to cDNA, then pre-amplified and diluted to ensure adequate volume for qPCR. 40 PCR cycles were performed on a QuantStudio 6 (Life Technologies) using human-specific gene expression assays (Appendix 3.1). Raw C_T values were calculated based on a threshold value of 0.2, and expression for all transporters was normalized to the housekeeping gene GAPDH using the $2^{-\Delta CT}$ method.[139]

Protein extraction for Western blot and QTAP analysis occurred similarly to the methods described in detail in Chapter III. Briefly, whole tissue biopsies were homogenized in 1.3mL hypotonic buffer containing 150uL of Complete Protease Inhibitor Solution (Sigma-Aldrich, St. Louis, MO), and underwent differential centrifugation to isolate protein. Protein concentrations were quantified using the BCA protein assay (Pierce, Rockford, IL). For WB, up to 10µg of protein was loaded onto a 4-12% electrophoresis gel (NuPage) and run for 110 minutes at 180V. Transfer onto a PVDF membrane (NuPage) occurred over 90 minutes at 30V. After blocking in 5% milk, membranes were incubated in primary antibody for 1-3 hours, then rinsed and incubated in secondary antibody for 1-2 hours. Development occurred using Clarity ECL reagents (Bio-Rad, Hercules, CA) with a Chemi-Doc XRS+ Imager (Bio-Rad), and densitometry relative to GAPDH was calculated using ImageLab 5.2.1 (Bio-Rad). A combination of 15µg each of mouse brain extract, liver extract, and T98G cell lysate was used as the positive control sample.

For proteomics, protein extracts were reconstituted in 50mM ammonium bicarbonate buffer with 40mM DTT, 10% sodium deoxycholate (Sigma-Aldrich), and 10µL β-casein (0.1µg/µL). Samples were reduced for 40min at 60°C, then incubated for ~30min in the dark with 135mM iodoacetamide (Sigma-Aldrich). 1 pmol stable isotope labeled (SIL) peptide standards (Theracode JPT Inc., Acton, MA) for each transporter of interest (Table 3.1[61,154,155]) were added to each sample along with 25µL Trypsin (0.1µg/µL) (Promega, Madison, WI). Digestion occurred for at least 18 hours at 37°C and was stopped with 10% trifluoroacetic acid (Sigma-Aldrich). Samples underwent solid phase extraction using Strata-X 33µm polymeric reversed phase extraction cartridges (Phenomonex, Torrance, CA). Analysis was performed using a nanoACQUITY system (Waters, Milford, MA) coupled to a QTRAP 5500 mass

spectrometer (AB SCIEX, Framingham, MA) equipped with Nanospray III source. An injection amount of ~0.2-1µg of total membrane microsomal protein was loaded onto a C18 trap column (180µm x 20mm, 5µm particle size, Waters). Analyst 1.5 (AB SCIEX) was used for MS control, and MRM analysis was performed using MultiQuant 2.0 (AB SCIEX). Peaks were smoothed prior to integration and area ratios of unlabeled/SIL peptides were determined using the sum of MRMs monitored. The lower limit of detection for the peptides was ~0.2pmol/mg protein.

Statistical Analysis

Descriptive statistics (median, min-max) were generated for the concentration of each ARV in each tissue site as determined by LC-MS and MSI. Tissue concentrations were divided by the plasma concentration of each ARV, corresponding to the time when the tissue sample was taken to correct for variability in plasma exposure between individuals (i.e. tissue/plasma ratio,TPR). To perform inter-compartmental comparisons, plasma-corrected ARV concentrations in tissue were compared between rectal and ileal tissue using an exact Wilcoxon signed-rank test. To compare ARV localization and drug transporter gene and protein expression between species, the human data generated here was plotted against the pooled data from mice and non-human primates (as there were no significant differences observed between infected and uninfected animals). One-way Kruskal-Wallis ANOVA on ranks was used for inter-species comparisons; $p<0.05$ was considered significant.

Results

Subject Demographics and Adverse Events

As of February 10th, 2017 a total of 5 women have completed the study, with summary demographics shown in Table 4.1. Participants had a mean age of 52 and a mean BMI of 37.2, and 4 of 5 were African-American. Menopause status was evenly distributed (2 pre-, 3 post). All 5 participants had been HIV-positive for >5 years (mean 18 years) and had been on their current

regimen for a mean of 8 years. Participants had well-controlled HIV infection as evidenced by undetectable plasma viremia and high CD4 counts (mean 786 cells/mm^3). A single adverse event (Grade I headache) was observed.

Table 4.1: Subject Demographics

	EFV (n=1)	**RAL (n=1)**	**ATZ (n=2)**	**MVC (n=1)**
Age (years)	55	49	50 (47, 53)	56
Race				
Caucasian			1	
African-American	1	1	1	1
Menopause Status				
Pre	1		1	
Post		1	1	1
BMI (kg/m2)	39.1	44.8	37.7 (35.6, 39.8)	26.7
CD4 (cells/mm3)	782	753	862 (651, 1074)	672
Time on Current Regimen (years)	7	5	9.5 (8, 11)	8
Time Since Diagnosis (years)	26	6	20.5 (17, 24)	18

*data shown are median and range

ARV Localization in Gastrointestinal Tissues

Table 4.2 shows the results of LC-MS analysis on these tissues. Pooled TPR values for all ARVs in the ileum and rectum are shown in Figure 4.3, where a significant 3-fold increase in

Table 4.2: Tissue Penetration Ratios

ARV	ILEUM	RECTUM
TFV (n=5)	131 (78, 297)	46 (14, 52)
FTC (n=5)	8 (6,12)	4 (1, 8)
RAL (n=1)	189	242
EFV (n=1)	5	6
MVC (n=1)	74	31
ATZ (n=1)	55	43

median ARV penetration into the ileum is observed. To show that this difference is not driven by a single ARV, individual values from both compartments are shown in Figure 4.3b. With the exception of RAL, all ARVs had higher penetration into the ileum versus the rectum, with TFV showing the greatest difference (3-fold higher penetration into the ileum).

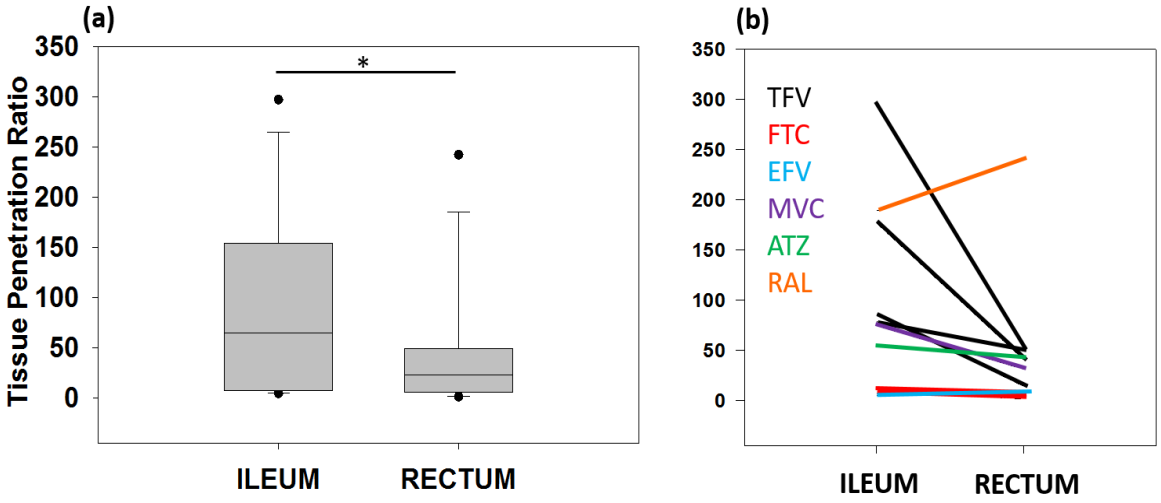

Figure 4.3: ARV Penetration into Human Gut Biopsies Pooled ARV penetration ratios into the ileum and rectum (a). Individual plots for each ARV between these two compartments (b).

Representative images of ARV localization as determined by MSI are shown in Figure 4.4. Despite detectable concentrations of TFV and FTC and in the plasma and tissue by LC-MS, these two drugs were only sporadically detected in these samples by MSI, even before heme correction (Figure 4.4b&c). In contrast, the remaining ARV in each regimen (EFV, RAL, ATZ, MVC) were detected in every ileum and rectum sample and showed broad distribution throughout the mucosa and submucosa of biopsy sample (Figure 4.4d). Heme was extensively distributed in many tissue slices (Figure 4.4e), resulting in large decreases in

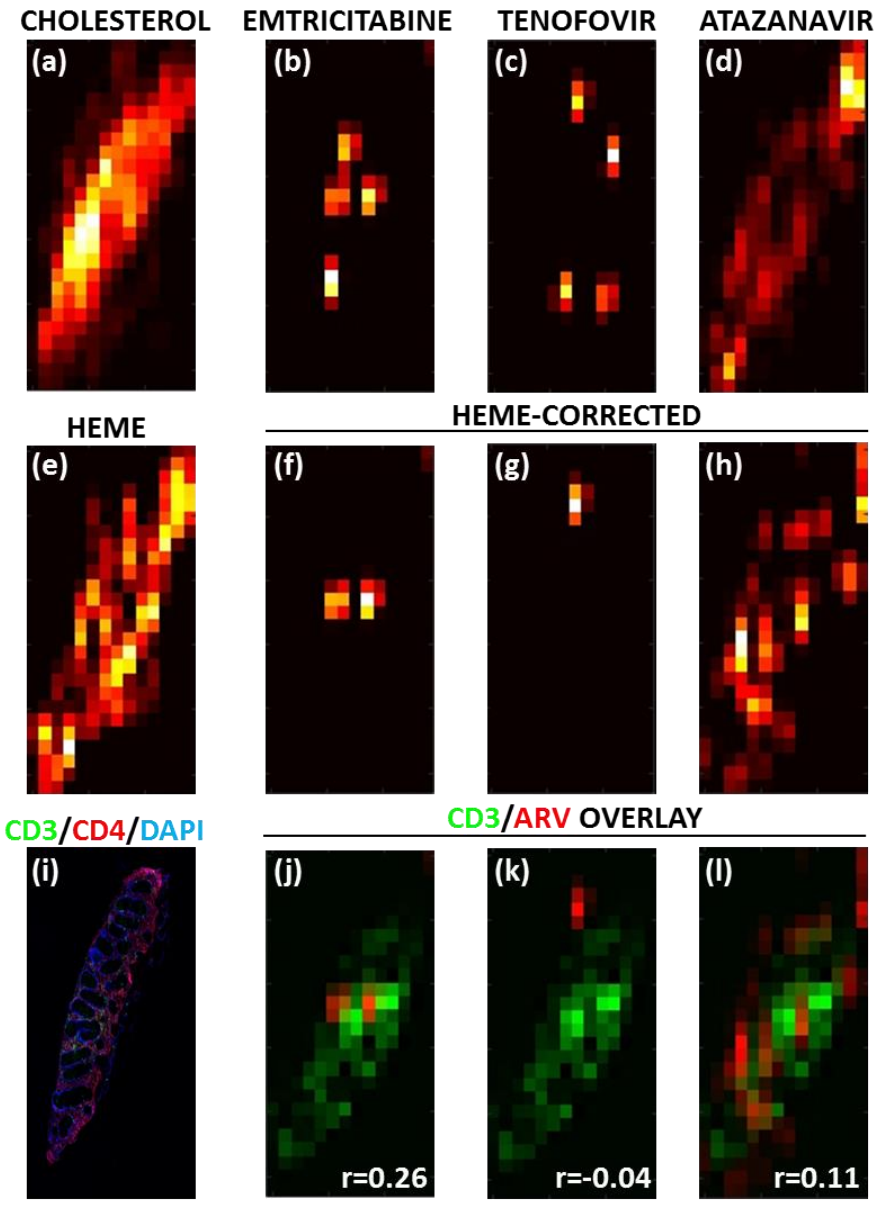

Figure 4.4: ARV Localization in Human Gut Biopsies Representative images of ARV localization in a rectal biopsy from an HIV+ subject. a-d show raw MSI images. Heme distribution (e) was corrected for in f-h. ARV image overlay with IF stain (i) is shown in j-l, with CD3 in green and the ARV in red.

ARV response after heme correction (Figure 4.4f-h). As a result, co-localization with CD3+ T cells by IF (Figure 4.4j-l) was low. T-cell co-localization was 2-5 fold higher in the rectum versus the ileum, with EFV and MVC showing the best co-localization overall.

Figure 4.5 compares ARV-T cell co-localization from human biopsies to data generated in similar tissues from humanized mice and NHPs (Chapter II). In the ileum (Figure 4.5a), human data was in better agreement with co-localization values generated in humanized mice versus NHPs for every ARV except MVC and EFV. MVC correlations in hu-HSC-Rag mice were 5-fold higher than humans, though this was not significantly different. Median EFV co-localization was higher in NHPs than any other species, but ranged from -0.04 to 0.28. In the rectum (Figure 4.5b), NHP

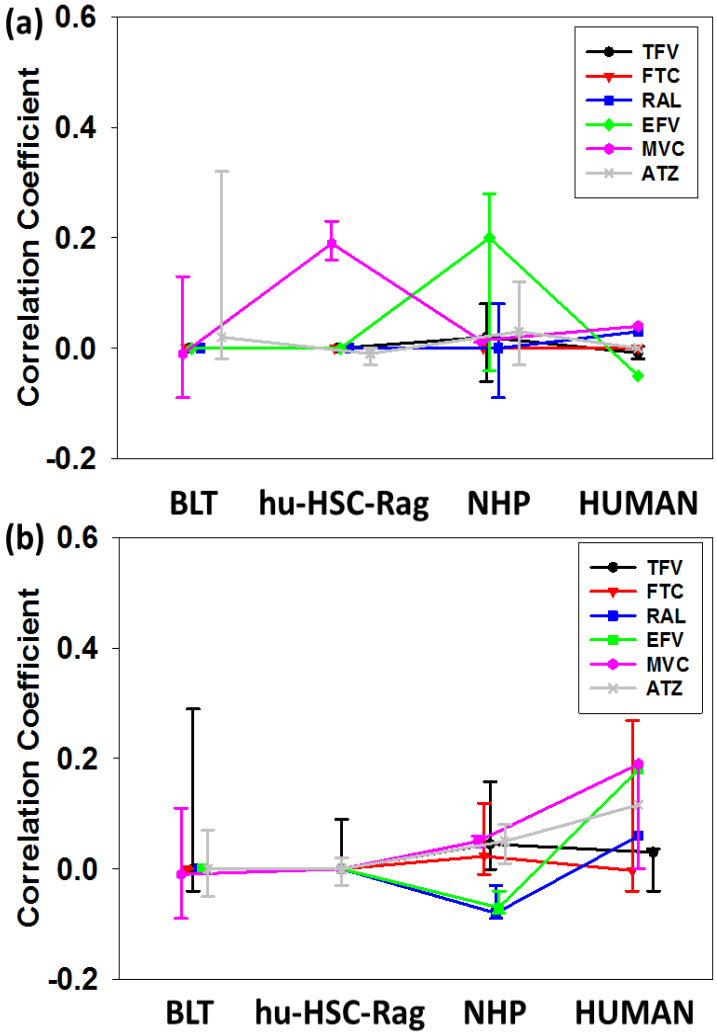

Figure 4.5: Interspecies comparison of ARV-CD3+ T cell Correlation Median (dot) and range (whiskers) correlation coefficients for each animal model and humans are shown for the ileum (a) and rectum (b). Some data points are offset to ease interpretation.

MVC and EFV co-localization was much lower, with EFV and RAL trending toward anti-correlation with CD3+ T cells. In humans, MVC and EFV correlation was 4 and 3-fold higher than mice or NHPs, respectively, though ultimately no inter-species differences were statistically significant.

HIV RNA Localization and Co-registration with ARVs

HIV RNA was detected in all ileum samples, but was only detected in the rectum of two subjects. A representative image of HIV RNA and ARV co-localization is shown in Figure 4.6. Similar to the NHP and mice tissues, RNA was detected in discreet tissue areas that corresponded to CD3+ T cell localization. When overlayed with heme-corrected ARV images, it was found that HIV RNA was localized to

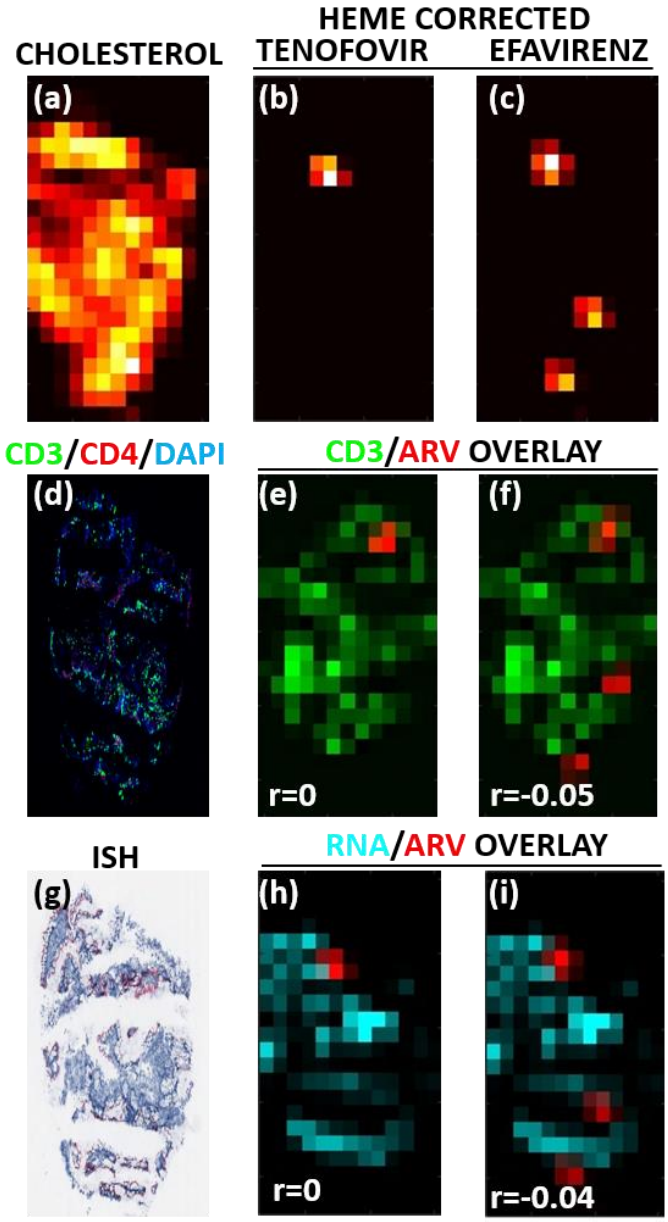

Figure 4.6: ARV-HIV RNA Co-localization in Human Gut Biopsies Representative images from the ileum of a single HIV+ subject. Raw IR-MALDESI images are shown in a-c. IF image showing CD3+ T cell distribution (green; d) were overlayed with ARV images in e & f. Raw ISH image is shown in g, with positive staining in red. Co-localization of ARV images (red) and HIV RNA (cyan) are shown in h & i, with corresponding correlation coefficients.

areas of low ARV signal (Figure 4.6h & j), and corresponding correlation coefficients indicated anti-correlation of these variables. This was true for every ARV with the exception of MVC and ATZ, which showed positive correlation with HIV RNA (r=0.07 and 0.05, respectively), though these values are very low.

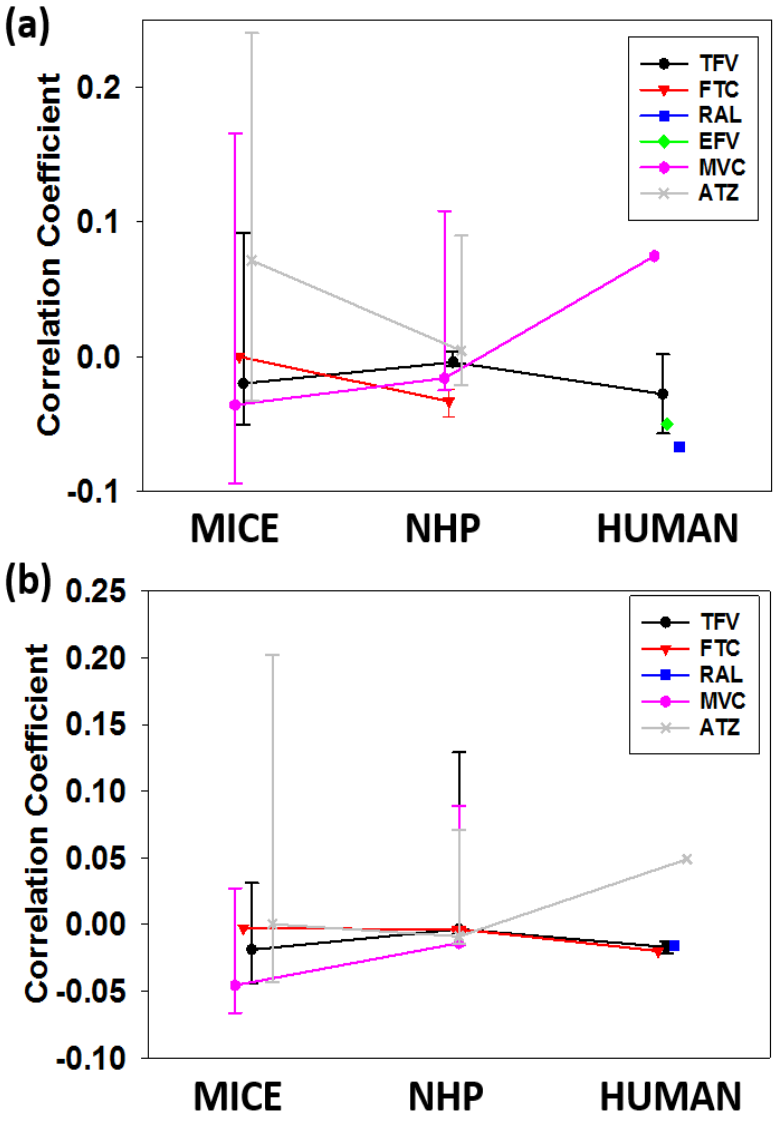

Figure 4.7: Interspecies comparison of ARV-HIV RNA Correlation Median (dot) and range (whiskers) correlation coefficients for each animal model and humans are shown for the ileum (a) and rectum (b). Some data points are offset to ease interpretation.

Figure 4.7 compares ARV-HIV RNA co-localization values in humans to those generated in NHPs and mice (reported in Chapter II). Because 30% of mouse samples did not have detectable HIV RNA, the two humanized mouse models were combined for analysis. There were no statistically significant differences between species in either the ileum or the rectum. Median coefficients for all models trended toward anti-correlation, though maximum values were as high as 0.26. ATZ tended to co-localize best with HIV RNA in animals, and this was consistent with

human data, where ATZ in the rectum also showed a positive correlation. In contrast, TFV showed the strongest anti-correlation with HIV RNA in mice, NHPs, and humans.

ARV Co-localization with Drug Transporters

Figure 4.8 shows representative images of ARV co-localization with several drug efflux transporters. Similar to the trends observed in the animal models, MDR1 showed the largest disparity in co-localization between ARVs, with r values ranging from -0.05 with TFV to 0.21

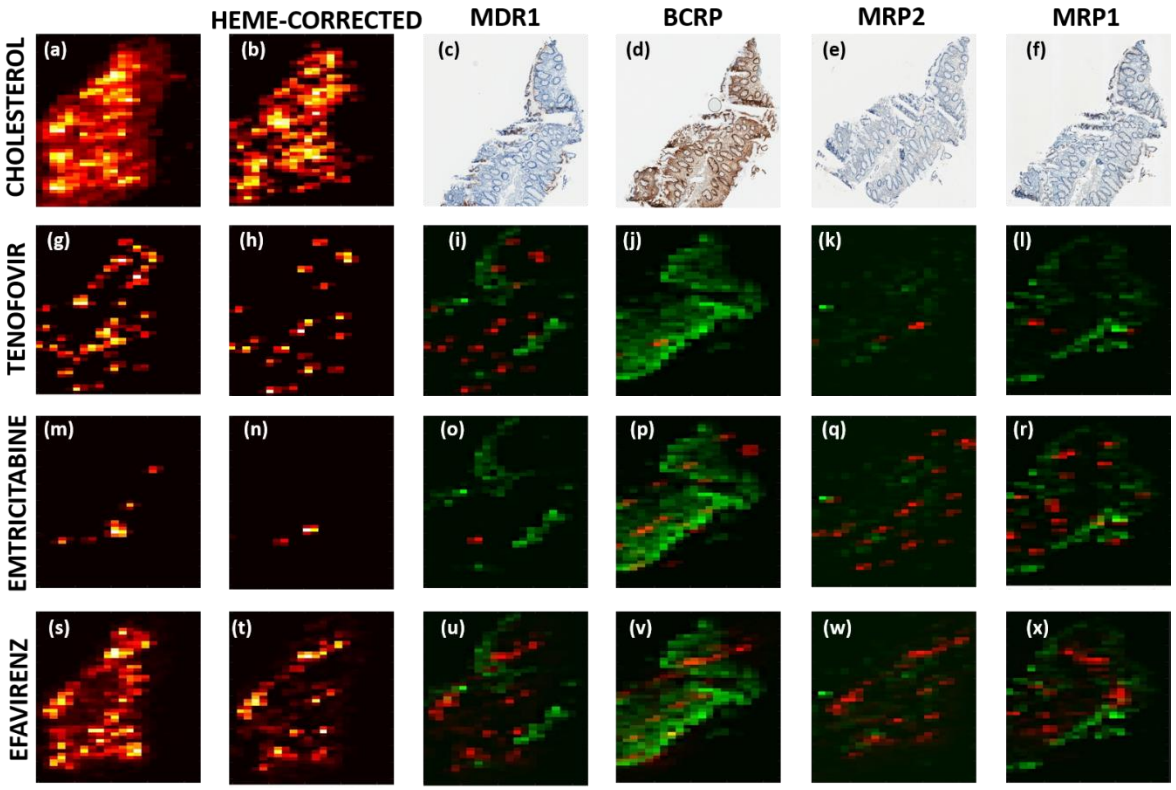

Figure 4.8: Efflux Transporter Localization and Effect on ARV Distribution Representative images from a single ileum sample. Raw MSI (a,g,m,s) and heme-corrected (b,h,n,t) images are shown from a single subject. Overlays for MDR1, BCRP, MRP2, and MRP1 are shown with ARV in red and transporter in green.

with MVC (Appendix 4.2). Again, MRP2 was not readily detected in these tissues despite previous studies showing its expression in the gut.[99,100] BCRP and MRP1 staining were more

apparent, but not differential between ARVs, with similar co-localization values for each of the drugs evaluated.

A quantitative comparison of transporter co-localization between tissues is shown in Figure 4.9. Unlike results in animals (Chapter II), ARV-transporter co-localization tended to be higher in the rectum than the ileum when data were pooled. This was especially true for BCRP and MRP2, which showed 5-fold and 17-fold higher co-localization in the rectum versus ileum, respectively (p=0.02). While MDR1 and MRP1 showed similar trends, these differences were not statistically significant.

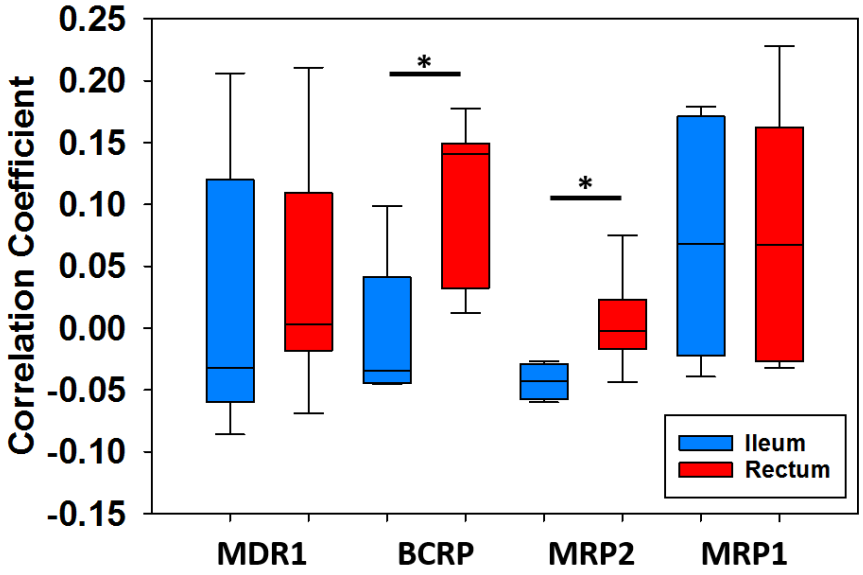

Figure 4.9: Efflux Transporter Co-localization Across Compartments
Correlation coefficients for pooled ARV-transporters in the ileum (blue) and rectum (red). Solid lines represent medians, box ends represent IQR, and whiskers range. * denotes p<0.05

Interspecies Comparison: Transporter Gene Expression

Drug transporter gene expression from human samples is compared to pooled animal data in Figure 4.10, which shows variable agreement between species. Among the efflux transporters, human *ABCB1* expression (Figure 4.10a) was in better agreement with NHP data (8-fold difference) than humanized mouse data (2.6-log increase in humans; p<0.001) in both the ileum

and the rectum. Conversely, mouse *ABCG2* expression was closer to observed human data than NHP expression, which was 4-fold lower than humans in the ileum (Figure 4.10d; p=0.01). *ABCC2*, *ABCC1*, and *ABCC4* expression were similar between humans and animals. Human uptake transporter expression was in better agreement with mouse data, showing multi-log increases in the expression of *SLC22A3* over NHPs in the ileum and rectum (Figures 4.10f and 4.10h; p<0.001).

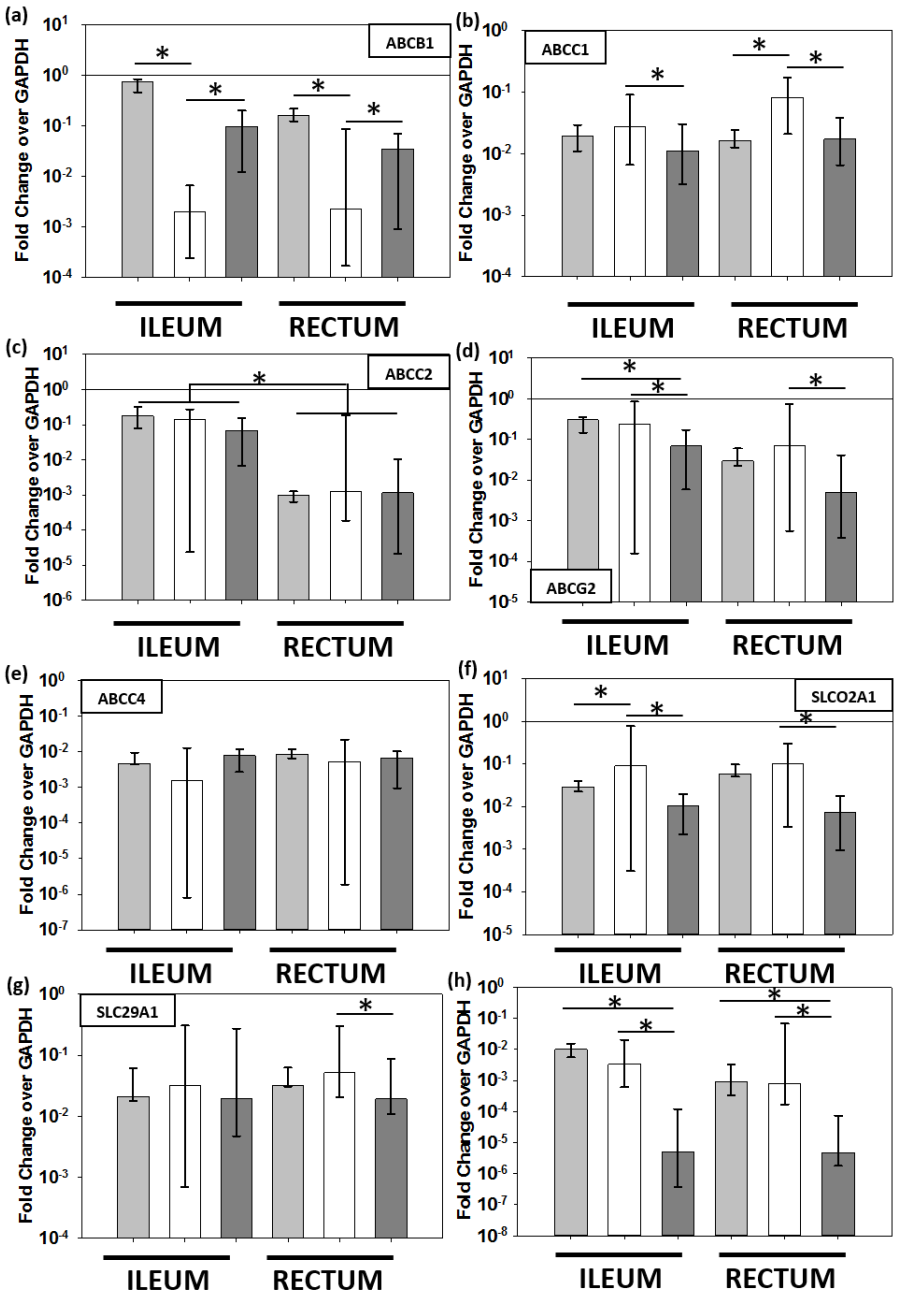

Figure 4.10: Interspecies comparison of Transporter Gene Expression Median (box) and range (whiskers) of gene expression in humans (light gray), mice (white), and NHPs (dark gray) in the ileum and rectum.

Interspecies Comparison: Transporter Protein Expression

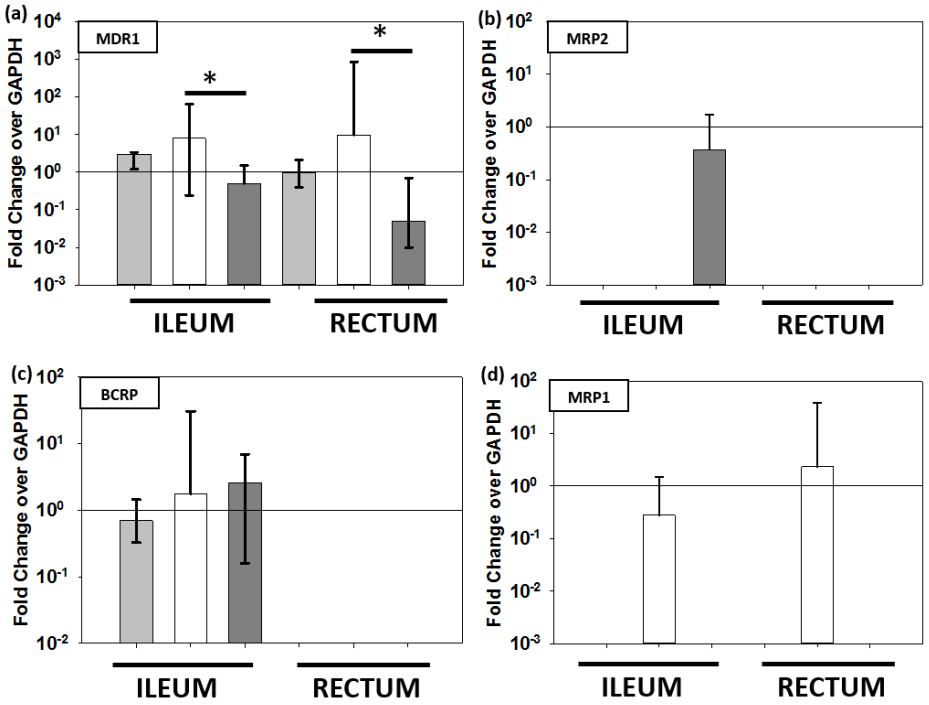

Figure 4.11: Interspecies comparison of Transporter Protein Expression by Western Blot Median (box) and range (whiskers) of protein expression in humans (light gray), mice (white), and NHPs (dark gray) in the ileum and rectum.

Figure 4.11 shows an inter-species comparison of efflux transporter protein expression as measured by Western blot. Interestingly, protein expression of MDR1 (Figure 4.11a) showed the opposite trend of *ABCB1* gene expression results, with human data in better agreement with humanized mice data (2-10 fold difference) over NHPs (6-19 fold difference). The protein expression of BCRP (Figure 4.11C) was not significantly different between species in the ileum, and was undetectable in all species in the rectum. MRP2 (Figure 4.11B) MRP1 (Figure 4.11D) were only detected by WB in NHPs and humanized mice, respectively, despite detection in human and mouse control tissues (data not shown).

QTAP results between species are shown in Figure 4.12. At the protein level, transporter concentrations were generally consistent between species, with several important exceptions. Human MDR1 concentrations were similar to humanized mouse concentrations in both the ileum and rectum, and were 5-fold higher than NHP MDR1, though this was not

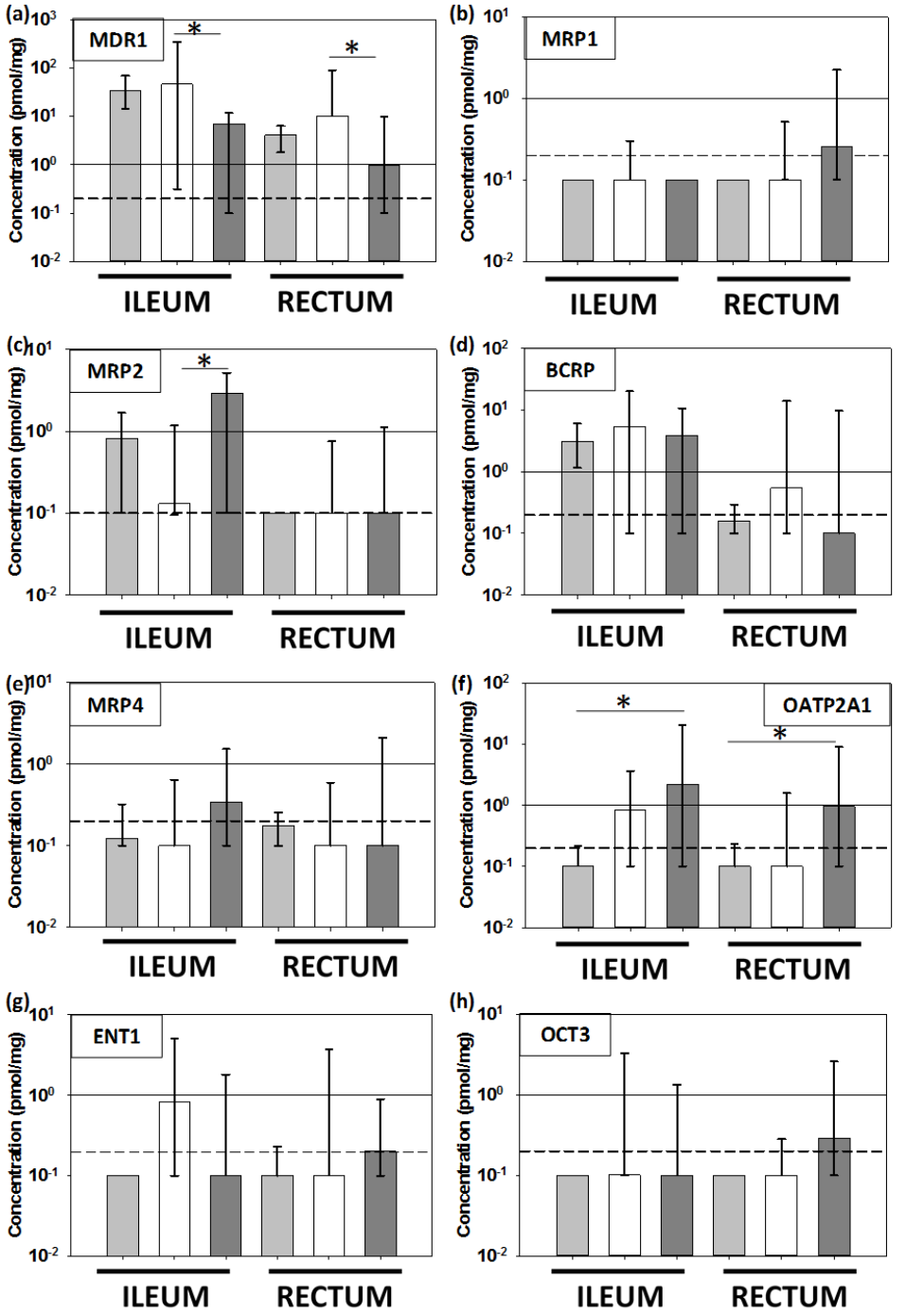

Figure 4.12: Interspecies comparison of Transporter Protein Expression by Proteomics Median (box) and range (whiskers) of gene expression in humans (light gray), mice (white), and NHPs (dark gray) in the ileum and rectum.

statistically significant. As previously reported in Chapter III, MRP2 concentrations were 1.5-logs higher in the NHP versus humanized mouse ileum (Figure 4.12c). Median human MRP2 concentrations fell in between mice and NHPs, and was not significantly different from either species. Among the uptake transporters, only OATP2A1 showed a statistically significant difference between species, with NHP concentrations 1-log higher than humans in the ileum and rectum (Figure 4.12f).

Discussion

The preliminary analyses conducted here provide new insight into ARV distribution in the human GI tract, and reveal interspecies differences that may be important in the development of novel ARVs targeted to these tissues. A particular strength of this study was the use of MSI technology to visualize ARV tissue distribution, which provides detailed data not possible by traditional LC-MS. TPR values observed here were consistent with previous studies of these drugs in GI tissues.[69,156,157] Importantly, plasma concentrations were also consistent with previously reported steady-state values[69,156,157], demonstrating that the use of bowel preparation prior to colonoscopy did not significantly alter drug absorption or local PK in gut tissues. The use of plasma-corrected tissue concentrations to understand tissue distribution and has been the gold-standard for ARV tissue pharmacology to this point, but we show here how limited these data can be.

Initial evaluations of these biopsy samples appeared to show extensive ARV distribution with no evidence of localization (Figure 4.4d). After correcting for the large amount of heme present in each sample, however, ARV detection sharply decreased and T-cell co-localization values declined as a result. The extensive heme present in these biopsy samples (which was not present in whole NHP tissues; Chapter II) is likely a function of the biopsy procedure and the large amount of vasculature present in the gut mucosa, both of which are unavoidable when

collecting human tissues. However, the sharp contrast in results before and after heme correction not only shows the importance of this step when analyzing biopsy samples by IR-MALDESI, but also showcases the advantage of this technology over LC-MS. ARV concentrations generated in tissue homogenates are unable to distinguish between drug within cells/extracellular space and drug in blood, whether contained in the microvasculature or from contamination secondary to tissue procurement. This is an especially important distinction in the setting of HIV eradication, where drug localization within tissue reservoirs may have a direct effect on residual HIV replication.

The importance of drug localization is highlighted by the low correlation between the ARVs investigated here and CD3+ T cell distribution. Similar to the results discussed in Chapter II, inadequate exposure in this cell population may lead to reservoir propagation. This hypothesis was directly tested in the ISH experiments, which show HIV RNA expression occurring preferentially in areas of low or no ARV exposure, with subsequently low co-localization between these two measures (Figure 4.6). Not only does this support data generated previously in human gut and lymph nodes[29,56], but shows that novel ARVs will need to be developed in order to totally eradicate residual replication at this site. An important distinction from the animal experiments is that these human subjects had been on their current regimen for at least 5 years with undetectable plasma viral loads, yet HIV RNA was still detected in many of their tissues. Though much of this HIV RNA is defective and does not represent replication-competent virus[105], this analysis shows that current therapies are insufficient to clear infected cells from this site.

Evaluation of the effect of drug transporters on the disposition of these drugs did not reveal any significant relationships. Though transporters (particularly MDR1 and BCRP) were

readily detected on the epithelial surface of most samples, but we did not observe any examples of ARV sequestration and co-localization with a specific transporter. This is in direct contrast to results from NHPs (Chapter II), where it appeared that the MDR1 substrate RAL was sequestered to the mucosa with relatively high co-localization with this transporter. Similarly, the apparent differential influence of MDR1 on TFV and FTC distribution was not observed here. This may be partially explained by the small sample size in this study, and it is possible that we would have observed similar results with samples from a larger population. It is unlikely that these conflicting results represent a true difference in transporter effects, as these human and macaque transporters have high sequence homology (>80%), though it may be the case that these drugs have lower affinity for human transporters versus NHPs.

This study was also the first to make direct, prospective interspecies comparisons between humans, NHPs, and humanized mice using similar methodology. ARV co-localization with CD3+ T cells in humans was not significantly different from any pre-clinical model, with low correlation coefficients across the board. Consistent with these results were the ISH data, which showed detectable HIV RNA in every species, which was not co-localized with any ARV. These results are consistent with the fact that that HIV latency[137] and persistent replication on cART[138] have both been observed in humanized mice and NHPs, and suggest that lack of ARV localization in GALT is consistent across species. EFV and MVC showed the largest difference, particularly in NHPs versus humans or humanized mice, and it may be that these drugs achieve better exposure in NHPs, though the observed differences were not statistically significant.

As in Chapter III, we observed little agreement between methodologies to evaluate drug transporter expression and localization, with interspecies comparisons of gene and protein expression giving variable and inconsistent results. Results were especially disparate for

ABCB1/MDR1 and *SLCO2A1*/OATP2A1, for which gene expression suggested that NHPs more closely represented human transporter expression, and QTAP results suggesting the opposite. As discussed in Chapter III, the downstream nature of QTAP over qPCR and the fact that QTAP more closely mimics IHC results suggest that QTAP is a more appropriate measure of expression. This is supported by the fact that TPR values for MDR1 substrates (TFV, RAL) humans were lower than what was observed in NHPs, consistent with more efflux by MDR1. Given that many ARVs are MDR1 substrates, these results have important implications for the development of novel ARVs. For example, results of pre-clinical studies of a novel MDR1 substrate ARV may depend on the species utilized, as studies performed in NHPs may show higher exposure in GALT than what would be achieved in humans, as was observed here.

The close agreement between humans and humanized mice for co-localization measures (with CD3 T cells, transporters, and HIV RNA) and drug transporter protein expression suggest that extrapolation of results generated using this pre-clinical model to predict human data is appropriate. While much of the NHP data was not significantly different from either humans or humanized mice, the large increases in CD3+ T cell co-localization with TFV and MVC in NHPs, and the multi-log differences in protein expression of MDR1 and OATP2A1, show that results generated in this model may not accurately predict human data. However, the presence of detectable HIV RNA in areas of low ARV exposure in NHPs provides strong support for observed results in humanized mice and humans. Additional advantages to the humanized mouse model are the lower cost, higher availability, and use of non-chimeric HIV strains for infection (though infection status did not appear to significantly affect ARV tissue distribution; see Chapter II). One caveat to these advantages is the need to quantify the effect of both human and

mouse drug transporters or drug metabolizing enzymes when considering local ARV PK, as discussed in Chapter III.

The interpretation of these results is limited by the small sample size of this study, which resulted in an n=1 for all ARVs except TFV and FTC. Since the inception of these experiments, many novel ARVs have been introduced to market and have quickly been adopted by practitioners, which greatly reduced the number of eligible patients for this study. Although we were able to make direct comparisons between humans and animals by studying identical ARV regimens, it may be that newer small molecule ARVs behave differently in GALT, especially given that at least one novel formulation (tenofovir alafenamide fumurate (TAF)) was developed to exploit PK differences.[158] Additionally, our view of GALT in these humans was limited to the small biopsy samples we collected here. IF analysis showed that mucosal tissue was captured in each biopsy sample, but this is a very limited viewpoint compared to complete tissue cross-sections that were available with humanized mice and NHPs. These biopsies may not be representative of the entire ileum or rectum, or even the entire mucosa, thus results should be interpreted with appropriate caution.

Despite these limitations, these data are the first to formally compare pre-clinical and clinical data of this kind within a single set of experiments. This type of study is critical for reducing inter-lab variability that has made inter-species comparisons difficult in the past. We show that, as in our pre-clinical studies, HIV RNA continues to be expressed in areas of low ARV exposure in the ileum and rectum. We also show that human co-localization and transporter expression data best agrees with those generated from humanized mice versus NHPs. By placing the human data in the context of pre-clinical models, we can inform the development of novel ARVs targeted at GALT.

Chapter V: Impact and Future Directions

Challenges to Characterizing Antiretroviral Exposure in GALT

The data generated in this dissertation are the first of their kind, and address many of the current limitations of using clinical pharmacology to target tissue HIV reservoirs. As discussed in Chapter I, HIV persistence in GALT has substantial clinical consequences and presents unique challenges to eliminating replication.[106] The inability to determine whether or not suboptimal ARV penetration results in ongoing viral replication using traditional LC-MS, the lack of established best practices for evaluating the factors influencing ARV tissue disposition, and the scarcity of interspecies comparisons of these factors hinder the development of targeted therapies for HIV eradication.

In Chapter II, we provide confirmation of our earlier work showing that distribution throughout GI tissues is not homogenous for many ARVs, and show that HIV RNA expression occurs preferentially in areas of lower ARV exposure, providing strong support for the hypothesis that optimizing ARV exposure to these sites may reduce or eliminate ongoing replication. We also show that distribution may be influenced by drug transporter localization, and that this effect can be differential between the ileum and rectum. Importantly, these data would not have been possible using traditional LC-MS techniques, suggesting that MSI-based technologies should be further utilized for evaluation of small molecule tissue disposition. This is especially true for tissues with a high amount of blood contamination, as our imaging results in mice show that correction for this variable greatly reduces ARV signal from tissues. When

leveraged with other imaging modalities (e.g. IHC, ISH, etc.), MSI can be a powerful tool to generate PK/PD relationships in specific tissue sites. These data will not only clarify the mechanisms behind HIV persistence in GALT, but will inform the design of novel therapies with increased GALT exposure.

The primary limitation of this aim is the lack of cellular resolution in tissues. The 100 micron resolution of the IR-MALDESI images necessitated the down-sampling of high-resolution IHC and ISH images to allow for co-localization. Because of this, we are unable to determine ARV concentrations within individual cells, or between cell populations. General co-localization with CD3+ T cells provides a crude estimate of exposure at the site of action, but limits the ability to generate site-specific target concentrations for efficacy. Additionally, the use of HIV RNA as a PD endpoint is an overestimation of true replication, as it has been shown that much of this RNA is defective and unable to produce viral proteins.[105] Thus, the gene expression endpoint provides a "worst-case scenario" for ongoing replication and should be interpreted with appropriate caution. Finally, we observe ARV distribution in a single slice from a single point in time, and did not collect tissues across a dosing interval. It is possible that, although the animals were dosed to steady-state, ARV localization varies with plasma concentrations, or that localization is inconsistent even in small portions (microns-millimeters) of the GI tract. Future evaluations of ARV tissue distribution using IR-MALDESI are warranted, but should include multiple slices from a single tissue site as well as tissues from multiple points along a dosing interval.

Chapter III summarizes a comprehensive comparison of methods for evaluating drug transporter expression, and defines for the first time expression differences between preclinical models of HIV infection. The relevance of drug transporters for ARV disposition in GALT is

supported by the findings in Chapter II, as well as previous work by us and others implicating transporters as significant variables for ARV tissue penetration.[52,98,100] The lack of agreement between gene and protein expression observed in all animal models is compelling, as there is currently no standard for reporting this type of data. Although we were unable to conclusively show the superiority of one method over another in predictive tissue ARV penetration, the quantitative downstream protein data generated by QTAP may provide the best measures moving forward. Observed expression differences between species for transporters like P-gp or BCRP will be important in selecting appropriate animal models for the development of novel ARVs which are utilized by these proteins. The outcomes of this aim demonstrate that careful consideration should be given to the method and model used to evaluate transporter expression, and provide important interspecies comparisons to inform drug development.

Quantifying transporter gene and protein expression and localization using four methods was challenging in a single piece of tissue. This was particularly true in mice, where in many cases <10mg of tissue material was available for analysis, resulting in limited protein available for WB and QTAP analysis. It may be the case that increasing protein would have resulted in fewer BLQ/BLD values (particularly among WB results) and provided stronger agreement between these techniques, which has previously been reported.[146] An additional obstacle in this aim was the inability of any method to reliably predict tissue penetration makes it difficult to advise the field on best practices for transporter evaluations. The extensive staining for transporters like P-gp and BCRP precluded traditional IHC quantitation, forcing us to evaluate positive staining as a function of tissue area. This may explain why IHC results were the least predictive measure in the regression model despite being the most downstream and relevant transporter measurement. In the future, emphasis should be placed on maximizing protein yield

for WB and QTAP, and optimizing IHC staining to allow for traditional quantitation methods. Moreover, we show that the contribution of human transporter isotopes to the total transporter population in humanized mice must be considered, as interspecies comparisons of *ABCC4* were significantly altered after accounting for human genes.

In addition to drug transporters, there are many other factors that influence small molecule penetration into tissues.[51] Characteristics such as protein binding, drug-metabolizing enzymes, blood perfusion, and physicochemical properties (e.g. molecular size, lipophilicity, ionization state) were not addressed in this study but likely play a role in ARV distribution within the gut. However, the ARVs chosen for evaluation span a large range of values for many of these variables and can provide a qualitative starting point for future analysis. For example, differences in EFV and RAL localization in NHP tissues (illustrated in Figure 2.5 and 2.9) may be explained by the lipophilic nature of EFV, which could allow it to penetrate further into tissues versus RAL. Quantitative measures of these variables and incorporation into our regression analysis may provide improved predictive capacity. Previous attempts to incorporate these features into a global QSAR model to predict female genital tract penetration were only modestly successful; however, the use of a stepwise linear regression model may represent a more focused approach to identifying additional variables for GALT exposure.

The clinical study performed in Chapter IV provided insight into how well data from preclinical models translates to humans. The ARV distribution and HIV RNA results observed supported observations from Chapter II and show that humanized mice data more closely mimicked human results for most ARVs. The lack of agreement between transporter expression measures confirms the importance of choosing the appropriate method; however, we show again that humanized mice transporter protein expression was more similar to that in humans. Given

that the data shown in Chapters II and III indicate that some transporters (e.g. P-gp, BCRP) play a larger role in ARV disposition than others (e.g. MRP1, OCT3), the 4-fold differences in MDR1 protein expression between mice/human and NHPs are particularly important. Understanding the relationship between animal and human transporter expression and ARV distribution patterns will streamline the developed of targeted ARVs and prevent the inappropriate extrapolation of data from one species to another.

We were severely limited in our ability to recruit eligible subjects for this study, primarily because the ARV regimens we used in the animal models were rapidly replaced with newer regimens in clinical practice over the course of the study. Although we were able to generate data for each of the ARVs investigated, the small sample size of five subjects (n=1 for most ARVs) precluded performing any robust statistical analysis or reliable interspecies scaling for variables like mucosal accumulation or T-cell co-localization. A related limitation is the potential lack of relevance for clinical practice, as most treatment naïve HIV patients are being started on newer regimens. Though we cannot necessarily extrapolate the distribution of these drugs to newer agents from the same class (e.g. RAL to DTG), it is not unreasonable to assume that the species differences observed here, particularly for drug transporter expression, would hold true for similar drugs. Expanding the inclusion criteria of the study to allow for newer regimens would allow us to test these assumptions directly, and provide additional clinical relevance.

Opportunities for Targeted Therapies

The development of novel therapies that achieve optimal GALT exposure will require full characterization of ARV exposure at this site. Though the work in this dissertation provides an experimental foundation for this work, there are many opportunities to hone our

understanding of the PK/PD relationship in this tissue. As MSI technology improves, increased spatial resolution will become available and allow for ARV quantitation at a cellular level. Single-cell data can supplement the work performed here to understand the relationship between ARV exposure in the intracellular versus extracellular environment, and whether or not there are certain cell populations that have reduced exposure. Additionally, more rigorous analyses should be performed on multiple tissue slices from a single anatomic site in order to understand how ARV exposure in GALT changes along the length of the ileum or rectum. These evaluations should also include tissues taken at multiple times along the dosing interval to determine what, if any, changes occur secondary to plasma exposure at steady-state.

Importantly, alternative PD surrogates and cell types should be explored in addition to HIV RNA expression. In particular, a marker of HIV replication that is able to be detected by IR-MALDESI (thus overcoming the limitations of RNAscope) would be enormously helpful when co-localizing ARV-virus distribution. Proteins produced during the HIV life cycle (e.g. Nef, Gag, Env) represent a promising set of potential PD endpoints, as they are more likely to represent true HIV replication over RNA. Unfortunately, the size of even the smallest of these proteins is outside of our current analysis window (200-800m/z) and we would thus be unable to detect whole protein by IR-MALDESI. However, peptide fragments from these proteins can be found on the surface of antigen-presenting cells as a result of lysosomal degradation.[159,160] If a small, conserved peptide sequence that can be adequately ionized and analyzed by IR-MALDESI is identified, our estimate of viral localization can be refined. As a candidate peptide sequence that meets these criteria has yet to be identified, alternative approaches to measuring downstream viral expression can be useful. The viral capsid protein p24 is often utilized as a surrogate for HIV protein expression, and IHC protocols staining for this marker have already been optimized.

Not only would p24 staining provide a more relevant marker of infection, we could also compare the distribution this antigen to RNA as an additional validation step. Additionally, understanding ARV distribution into more specific T cell subsets can also help narrow down targets for optimized exposure. A comprehensive assessment of ARV disposition in GALT will help to clarify the mechanisms of persistence and define targets for optimized therapy.

Finally, a statistically robust method to isolate ARV signal from cells and tissues should be developed and implemented. As discussed in Chapter II, subtracting ARV signal on the basis of heme distribution alone likely underestimates actual ARV exposure in tissues. Further, though cholesterol is a useful biomarker to isolate "on-tissue" ARV response, cholesterol contained within the blood plasma (though small in comparison to the amount in tissues) may confound results. A method that takes into account the relative contribution of each of these biomarkers to refine correlation between variables would be useful. Specifically, applying a statistical method that can interpolate tissue-specific signal based on heme and/or cholesterol response within a single voxel will reduce the over-correction secondary to our current methods.

Perhaps the most straightforward approach to this interpolation is to estimate the amount of drug present within each heme-containing voxel based on the known plasma concentration of each drug. For example, in an animal with a MVC plasma concentration of 50ng/mL and an estimated blood volume of 10μL/voxel, we can estimate that in voxels containing both heme and MVC signal, approximately 50pg of MVC is contained in blood. This value can then be subtracted from the total amount in the voxel to provide a more reasonable concentration estimate. The limitations of this approach include the fact that it is susceptible to error propagation from upstream measurements of plasma concentration as well as error in the

estimates of blood volume in a given voxel. This error propagation can be accounted for using bootstrapping techniques, but the limitation remains.

Alternatively, rather than specify a specific value to subtract from each voxel, our current "all-or-nothing" approach can be modified to account for variation in heme signal. By building a continuum of cutoff values we can correct for the fact that some voxels show more heme signal than others. For instance, in voxels containing both heme and ARV where heme signal is above a theoretical "high" threshold, ARV signal from that voxel would be reduced by 50%. In cases where heme shows a "moderate" intensity, ARV signal would be reduced by 30%. In this way, we can account for the fact that greater ARV intensity would be expected in voxels with greater heme signal, and mask each ARV in a consistent way. By applying these modified correction algorithms, we can better understand true ARV exposure at the site of action.

The work performed here and elsewhere[98,100] suggests that drug transporters are an important variable in defining ARV exposure in GALT. We performed a rigorous analysis of nine efflux and uptake transporters for the purposes of generating method and interspecies comparisons, and attempted to use expression data from all of these proteins in combination to predict ARV exposure (Chapter III). However, a more step-wise approach to identifying specific transporters to target or avoid in order to increase ARV tissue exposure would provide precision evidence to be used in drug development. This can be accomplished initially through the use of transporter knockout mice, which have already been used to implicate P-gp and BCRP as important transporters for CNS penetration.[62] A similar approach using IR-MALDESI to assess the impact of knocked-out transporters on ARV GALT distribution would be feasible and provide more precise data. Another approach would be to co-administer ARVs with transporter-specific inhibitors to assess whether increased GALT exposure can be accomplished in a more

clinically feasible setting, and whether this increased exposure has any effect on HIV replication. The ultimate goal of this work would be to identify specific transporters to target or avoid to maximize GALT penetration and reduce or eliminate replication. Once these have been identified, novel therapies can be developed to exploit these effects in a similar fashion to ritonavir use as a CYP3A4 inhibitor to increase plasma exposure of protease inhibitors.

The development of any novel ARV or ARV formulation will require testing in preclinical species before use in humans. The data generated in Chapter IV show that the agreement between animal models and humans depends on the variable being evaluated. As mentioned previously, although the present study evaluated ARV distribution across three species, the regimens used are no longer clinically relevant. Because any novel therapy is more likely to have properties related to new versus old ARVs, it is important to define these relationships using more modern drugs (e.g. DTG vs RAL, TAF vs TDF, etc.). Therefore, ongoing or future studies in humans should be performed that include these newer regimens. Additionally, once a sufficient sample size for each ARV has been achieved, interspecies scaling factors should be developed for both distributional variables (mucosal accumulation, HIV co-localization) as well as transporter expression (gene and protein). Once scaling factors are developed, they can be applied in the development process to inform go/no-go decision making. An ideal scenario would be generating a series of characteristics that are known to favor GALT exposure (similar to "Lipinksi's rule of five") that would allow for easy extrapolation of animal data to humans to predict efficacy. Taken together, these strategies will build on the work performed here to inform efforts to eliminate HIV replication in GALT.

Implications for Eradication Research

This aims of this dissertation addressed a relatively narrow field of research questions, focusing on depth over breadth. However, the implications of the data generated here are far-reaching and will inform the wider field of HIV eradication research. The results summarized in Chapter II provide strong support for the hypothesis that ongoing HIV replication occurs in tissues, and is secondary to reduced ARV exposure. This is an important finding, as previous studies provided only indirect evidence of this relationship.[56] This finding provides much needed insight into the interplay between active replication and latency, which remains the primary obstacle to cure. The relative contribution of each of these mechanisms to total HIV persistence remains undefined, but this work suggests that complete HIV eradication will require elimination of both latent virus and ongoing replication in tissue reservoirs.

To that end, the methods and concepts addressed here can easily be applied to the latency-reversing agents (LRAs), many of which are small molecules. As discussed in Chapter I, the success of an LRA is dependent on it reaching adequate concentration at the site of action, which includes lymphoid tissues. The pharmacologic principles governing ARV disposition and active HIV replication also apply to LRAs and latently-infected cells. Current methods for assessing the efficacy of LRAs, such as the quantitative viral outgrowth assay (QVOA), are difficult to perform and likely underestimate the true size of the reservoir[161], making evaluations of LRA efficacy difficult and variable.[105,162] The ability to perform PK/PD assessments at the tissue or cellular level from LRA-dosed animals would provide an additional avenue for eradication research. We have already demonstrated our ability to detect and quantify LRAs in tissue using IR-MALDESI[78], and evaluations are underway to assess the efficacy of these agents at inducing viral gene expression.

There are many putative HIV reservoirs outside of the GALT[10–13] that remain unstudied. GALT was chosen for this dissertation based on the clinical consequences of persistence at this site, as well as the relative ease of collecting human tissue for interspecies comparisons. We have already shown in preliminary experiments that ARV distribution is heterogeneous in tissues such as the lymph node[163], but homogenous in others like the testes.[75] Whether or not these trends hold true for every ARV, or whether viral gene expression will continue to occur preferentially in areas of low ARV exposure in each of these tissues will need to be determined. It should be noted that variables such as sample preparation, IR-MALDESI conditions, cell types, or PD endpoints will need to be tissue-specific to generate the most useful data. However, these data form a sound experimental framework upon which to build future studies. Finally, the interspecies work described in Chapter IV can be used to inform the development of non-ARV agents including LRAs, several of which are known to be utilized by or affect the expression of drug transporters.[164]

Conclusion

This dissertation describes an innovative use of clinical pharmacology to characterize ARV disposition in a putative HIV reservoir. We use a novel technology to visualize ARV distribution in tissues, perform a multi-modal analysis of the factors influencing observed distribution, and determine how well the results from pre-clinical models predict similar data from human subjects. These data provide theoretical and practical frameworks to inform the HIV field, and have the potential to streamline the development of novel therapies for HIV eradication.

APPENDIX 2.1: EFFLUX TRANSPORTER CO-LOCALIZATION VALUES

	Drug	Ileum			Rectum		
		Mice		All Macaques	Mice		All Macaques
		BLT	hu-HSC-Rag		BLT	hu-HSC-Rag	
MDR1	TFV	-	-	0 (-0.05,0.19)	0.14 (0.01,0.43)	0.10 (-0.05,0.19)	0 (-0.05,0.06)
	FTC	-	-	0 (-0.05,0.12)	-	-	0.02 (0,0.05)
	RAL	-	-	0.29 (-0.02,0.34)	-	-	0.18 (0.01,0.20)
	EFV		-	0.04 (-0.06,0.29)		-	0.16 (0.01,0.28)
	MVC	0.01 (-0.09,0.24)	0.13 (0.02,0.24)	0.11 (0.04,0.14)	0.14 (0,0.35)	-	0.06 (0,0.29)
	ATZ	0.03 (-0.09,0.23)	0.23 (0.10,0.36)	0.16 (0.04,0.19)	0.12 (-0.03,0.54)	0.28 (n=1)	0.05 (0,0.22)
BCRP	TFV	-	-	0 (-0.01,0.03)	0.11 (-0.07,0.39)	0.05 (-0.05,0.16)	0.01 (-0.08,0.04)
	FTC	-	-	0 (-0.01,0)	-	-	0 (-0.01,0.05)
	RAL	-	-	0 (-0.03,0.03)	-	-	0.07 (0,0.21)
	EFV		-	0 (-0.02,0.04)		-	0.07 (0,0.31)
	MVC	0.10 (-0.04,0.34)	0.02 (-0.08,0.13)	0 (-0.01,0.02)	0.11 (-0.12,0.35)	-	0.02 (0.02,0.02)
	ATZ	0.08 (-0.06,0.13)	0.05 (0,0.11)	0 (-0.01,0)	0.02 (-0.05,0.55)	0.33 (n=1)	0 (0,0)
MRP2	TFV	-	-	0 (-0.03,0.16)	-	-	0 (0,0.04)
	FTC	-	-	0 (-0.01,0.08)	-	-	0.01 (0,0.02)
	RAL	-	-	-0.02 (-0.06,0.21)	-	-	0.02 (0.02,0.03)
	EFV		-	0 (-0.06,0.07)		-	0.02 (0.01,0.03)
	MVC	-	-	0 (0,0)	-	-	-0.03 (-0.03,-0.03)
	ATZ	-	-	0 (-0.01,0)	-	-	0 (0,0)
MRP1	TFV	-	-	0 (-0.04,0.04)	0.02 (-0.04,0.36)	0.02 (-0.01,0.13)	0.08 (-0.02,0.18)
	FTC	-	-	0.01 (-0.05,0.06)	-	-	0.02 (-0.01,0.08)
	RAL	-	-	-0.02 (-0.03,0)	-	-	0.17 (0,0.27)
	EFV		-	0.01 (0,0.14)		-	0.14 (0,0.25)
	MVC	0.06 (-0.04,0.32)	0.05 (-0.02,0.13)	0.04 (0.04,0.04)	-0.01 (-0.05,0.15)	-	0.28 (0.28,0.28)
	ATZ	0.02 (0,0.04)	0.17 (0,0.34)	0.04 (0.03,0.05)	0.02 (-0.08,0.50)	0.03 (n=1)	0.28 (0.28,0.28)

APPENDIX 3.1: GENE EXPRESSION ASSAYS USED FOR EACH SPECIES

Gene Name	Species	Catalog Number
ABCB1	Mouse	Mm00440736_m1
ABCC1	Mouse	Mm00456156_m1
ABCC2	Mouse	Mm00496899_m1
ABCC4	Mouse	Mm01226381_m1
ABCG2	Mouse	Mm00496364_m1
SLCO2A1	Mouse	Mm00459638_m1
SLC29A1	Mouse	Mm01270577_m1
SLC22A2	Mouse	Mm00457295_m1
SLC22A3	Mouse	Mm00488294_m1
GAPDH	Mouse	Mm99999915_g1
ABCB1	Macaque	Rh02788239_m1
ABCC1	Macaque	Hs01561502_m1
ABCC2	Macaque	Rh02788077_m1
ABCC4	Macaque	Rh02858818_m1
ABCG2	Macaque	Rh02788848_m1
SLCO2A1	Macaque	Rh02858210_m1
SLC29A1	Macaque	Rh02794207_m1
SLC22A2	Macaque	Hs01010723_m1
SLC22A3	Macaque	Hs01009568_m1
GAPDH	Macaque	Rh02621745_g1
ABCB1	Human	Hs00184500_m1
ABCC1	Human	Hs01561502_m1
ABCC2	Human	Hs00166123_m1
ABCC4	Human	Hs00988717_m1
ABCG2	Human	Hs01053790_m1
SLCO2A1	Human	Hs00194554_m1
SLC29A1	Human	Hs01085704_g1
SLC22A2	Human	Hs01010723_m1
SLC22A3	Human	Hs01009568_m1
GAPDH	Human	Hs02758991_g1

APPENDIX 3.2: TRANSPORTER GENE EXPRESSION AMONG MOUSE DOSING COHORTS (ILEUM)

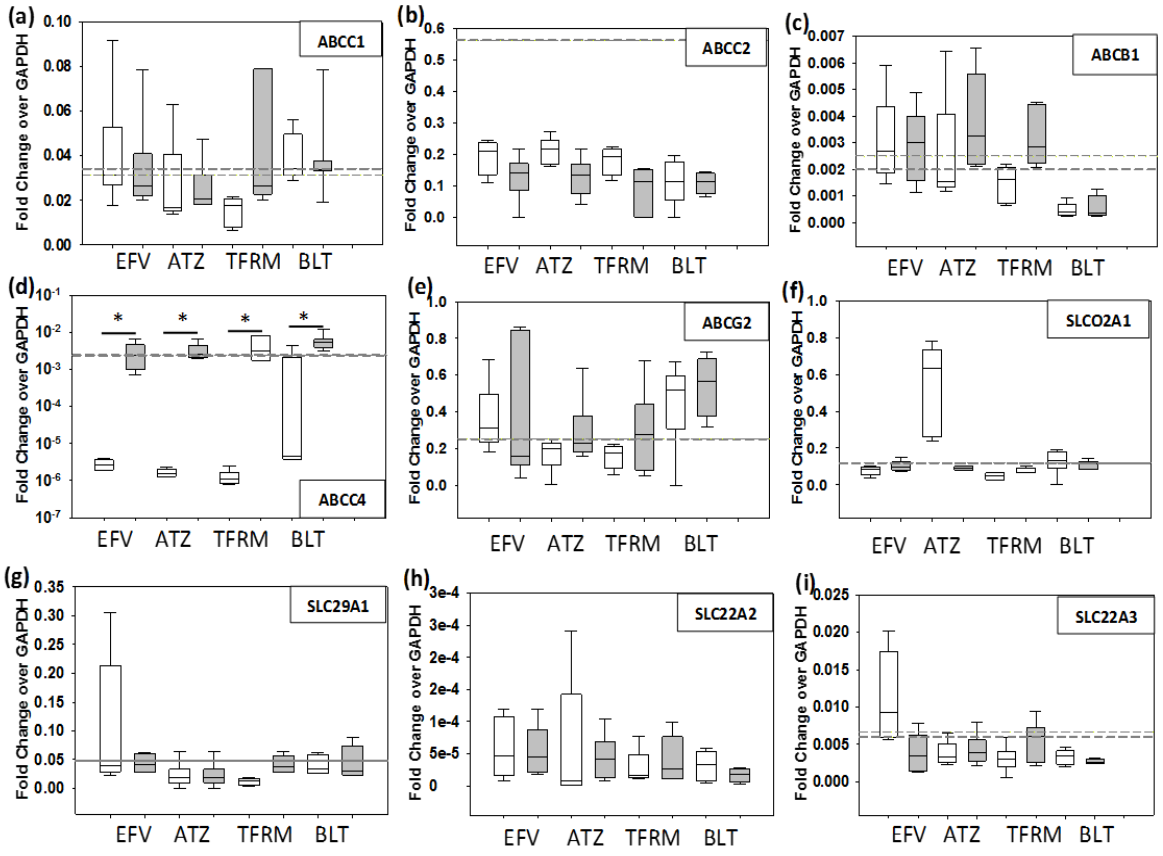

Appendix 3.2: Transporter Gene Expression Among Mouse Dosing Cohorts (Ileum) Gene expression is represented as fold change of GAPDH for uninfected (white) and infected (gray) animals from multiple dosing cohorts. Data shown are median (line) and interquartile range (box) with range (whiskers). Dashed lines are the values for the non-dosed control animals (n=2). EFV=hu-HSC-Rag dosed with EFV; ATZ=hu-HSC-Rag mice dosed with ATZ; TFRM=hu-HSC-Rag mice dosed with TFV, FTC, RAL, MVC; BLT= all BLT mice. N=6 for all groups. * represents $p<0.05$

APPENDIX 3.3: TRANSPORTER GENE EXPRESSION AMONG MOUSE DOSING COHORTS (RECTUM)

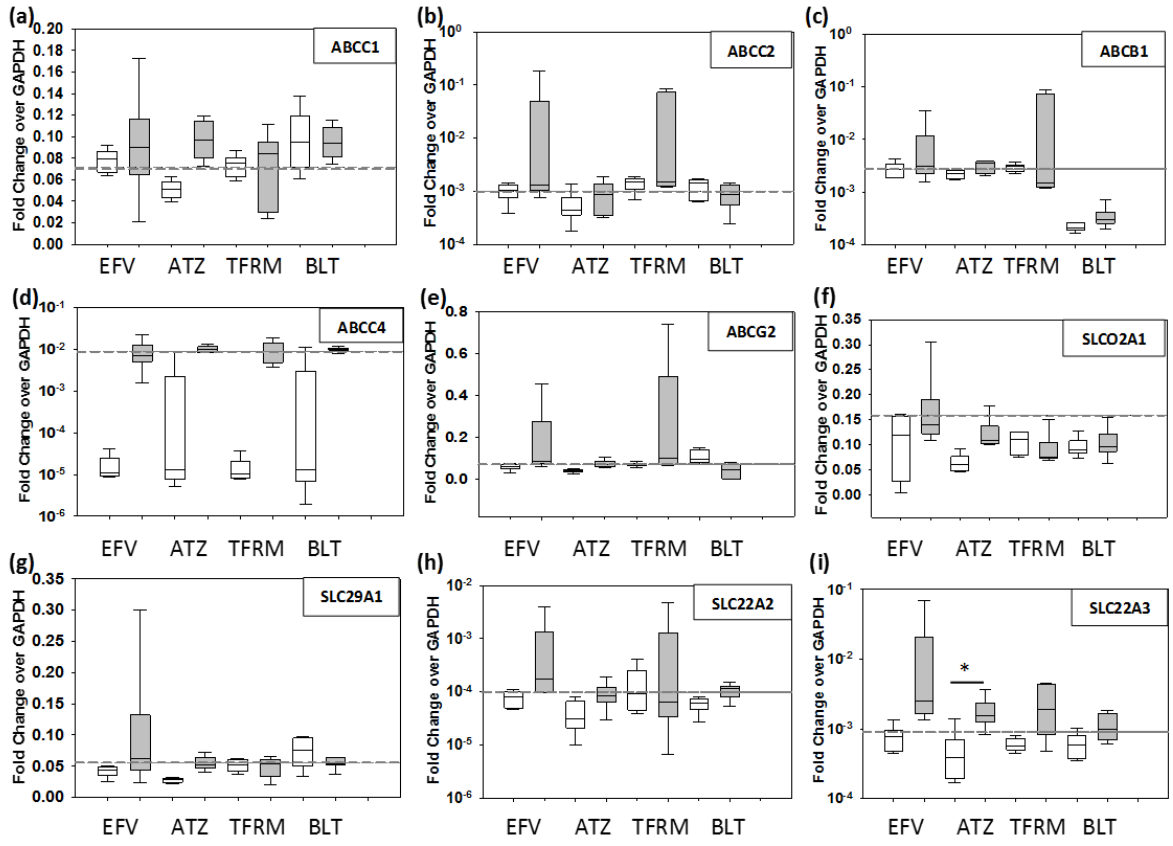

Appendix 3.3: Transporter Gene Expression Among Mouse Dosing Cohorts (Rectum) Gene expression is represented as fold change of GAPDH for uninfected (white) and infected (gray) animals from multiple dosing cohorts. Data shown are median (line) and interquartile range (box) with range (whiskers). Dashed lines are the values for the non-dosed control animals (n=2). EFV=hu-HSC-Rag dosed with EFV; ATZ=hu-HSC-Rag mice dosed with ATZ; TFRM=hu-HSC-Rag mice dosed with TFV, FTC, RAL, MVC; BLT= all BLT mice. N=6 for all groups. * represents $p<0.05$

APPENDIX 3.4: TRANSPORTER PROTEIN EXPRESSION BY WESTERN BLOT AMONG MOUSE DOSING COHORTS

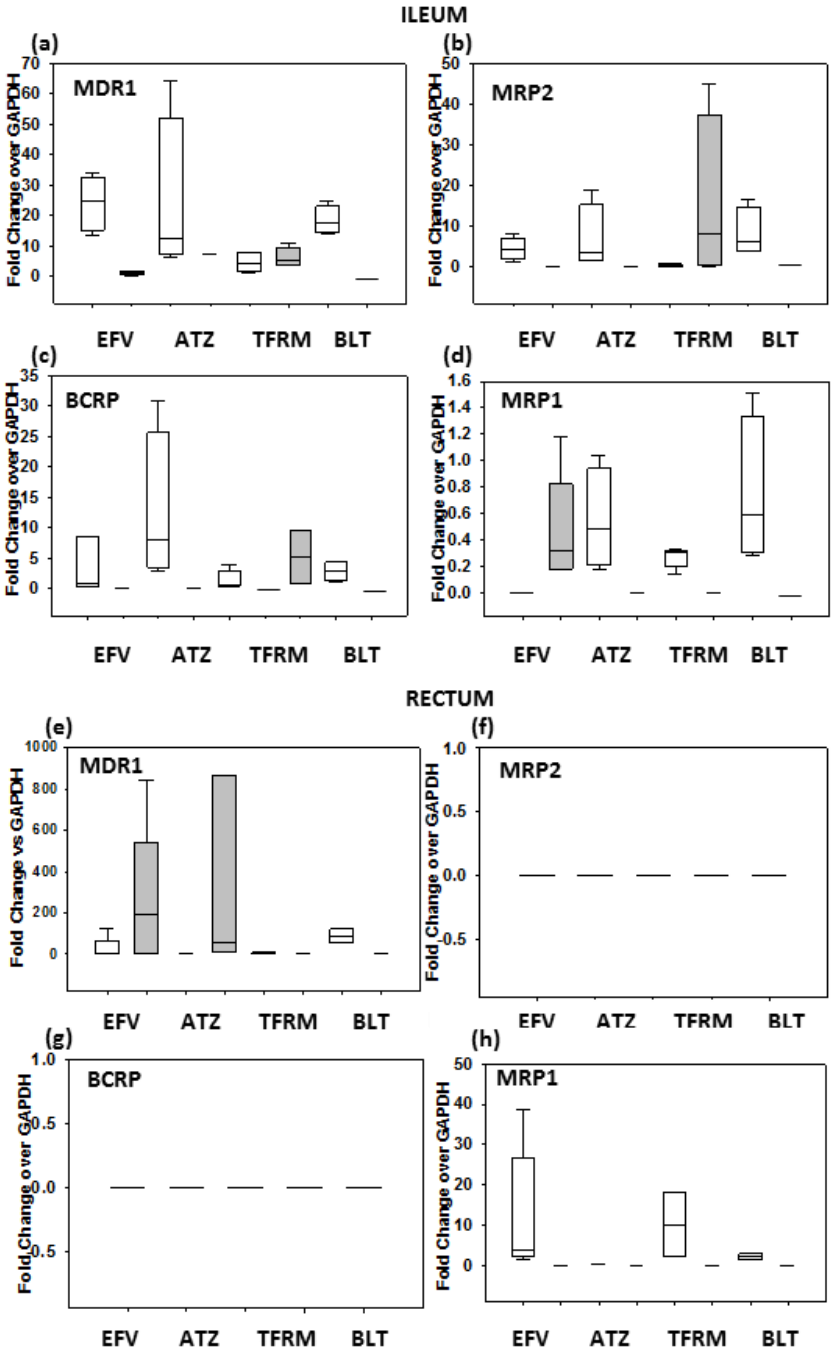

Appendix 3.4: Transporter Protein Expression by Western blot Among Mouse Dosing Cohorts. Densitometry data from each blot was quantified for each transporter in a-h, where protein expression is represented as a fold change over GAPDH for uninfected (white) and infected (gray) animals. Data shown are median (line) and interquartile range (box) with range (whiskers). EFV=hu-HSC-Rag dosed with EFV; ATZ=hu-HSC-Rag mice dosed with ATZ; TFRM=hu-HSC-Rag mice dosed with TFV, FTC, RAL, MVC; BLT= all BLT mice. N=6 for all groups.

APPENDIX 3.5: TRANSPORTER PROTEIN EXPRESSION BY PROTEOMICS AMONG MOUSE DOSING COHORTS (ILEUM)

Appendix 3.5: Transporter Protein Exprssion by Proteomics Among Mouse Dosing Cohorts (Ileum)

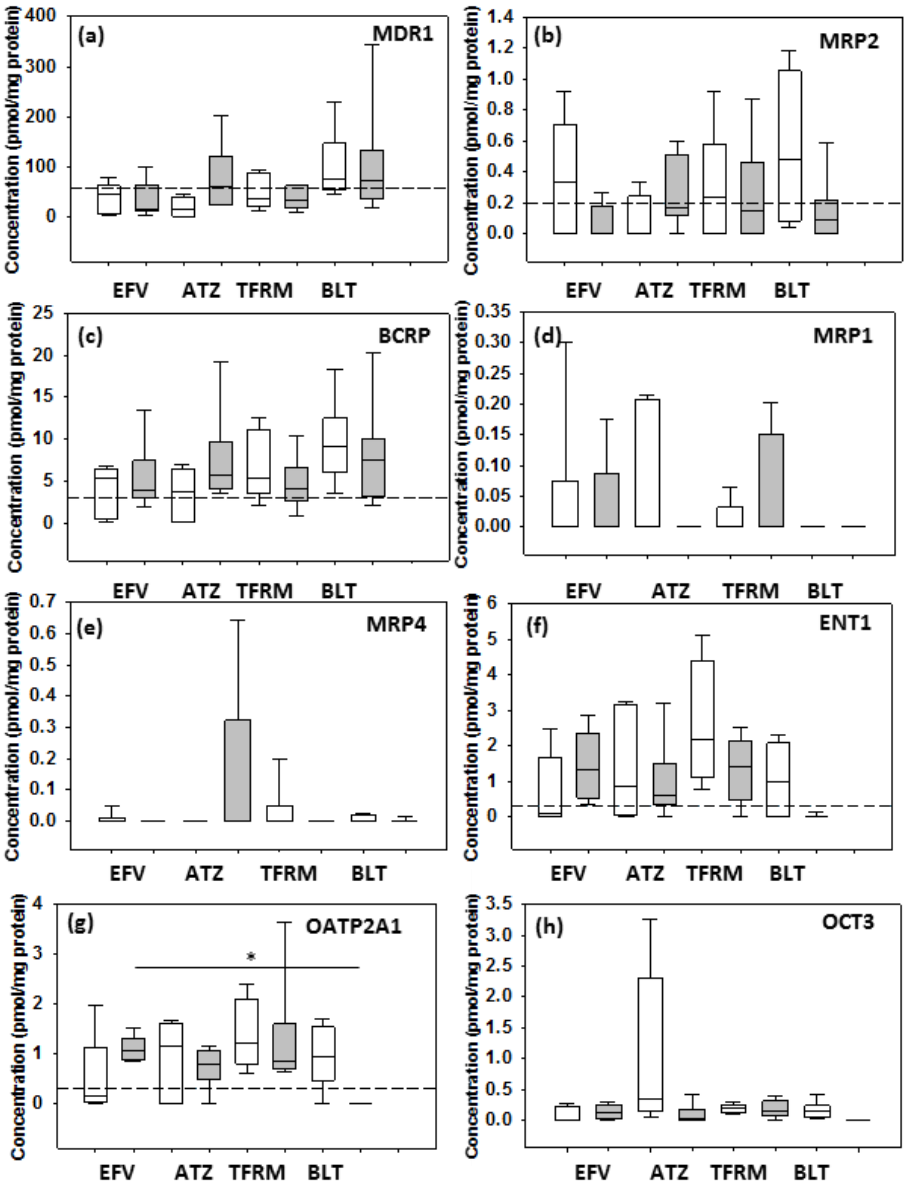

Protein concentrations are presented as pmol/mg total protein for each cohort of uninfected (white) and infected (gray) mice. Values for non-dosed control animals (n=2), when detectable, are shown as dashed lines. EFV=hu-HSC-Rag dosed with EFV; ATZ=hu-HSC-Rag mice dosed with ATZ; TFRM=hu-HSC-Rag mice dosed with TFV, FTC, RAL, MVC; BLT= all BLT mice. N=6 for all groups.* represents $p<0.05$

APPENDIX 3.6: TRANSPORTER PROTEIN EXPRESSION BY PROTEOMICS AMONG MOUSE DOSING COHORTS (RECTUM)

Appendix 3.6: Transporter Protein Expression by Proteomics Among Mouse Dosing Cohorts (Rectum)

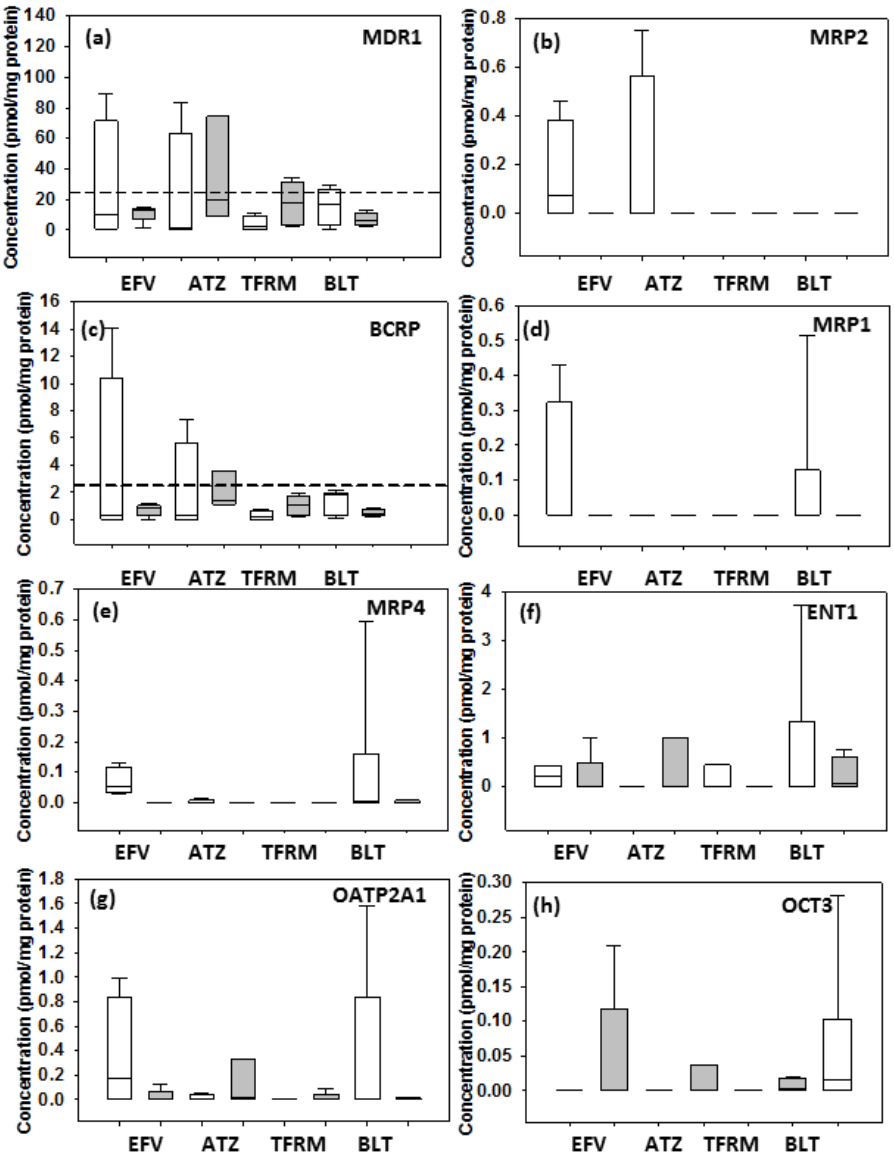

Protein concentrations are presented as pmol/mg total protein for each cohort of uninfected (white) and infected (gray) mice. Values for non-dosed control animals (n=2), when detectable, are shown as dashed lines. EFV=hu-HSC-Rag dosed with EFV; ATZ=hu-HSC-Rag mice dosed with ATZ; TFRM=hu-HSC-Rag mice dosed with TFV, FTC, RAL, MVC; BLT= all BLT mice. N=6 for all groups.* represents $p<0.05$

APPENDIX 3.7: HUMAN CONTRIBUTION TO TOTAL TRANSPORTER POOL

Appendix 3.7: Human Contribution To Total Transporter Pool Original gene expression values for each mouse were multiplied by the fold change value for human expression for the transporters *ABCB1* (a) and *ABCC4* (b). The resulting value was added back to the original expression value to account for the contribution of human gene expression. For example, an original mouse expression value of 0.03 was multiplied by 2.5 (as it was found that human gene expression was 2.5-fold higher than mouse gene expression). The result of 0.075 was added back to 0.03 to get 0.105, which represents total gene expression for this transporter.

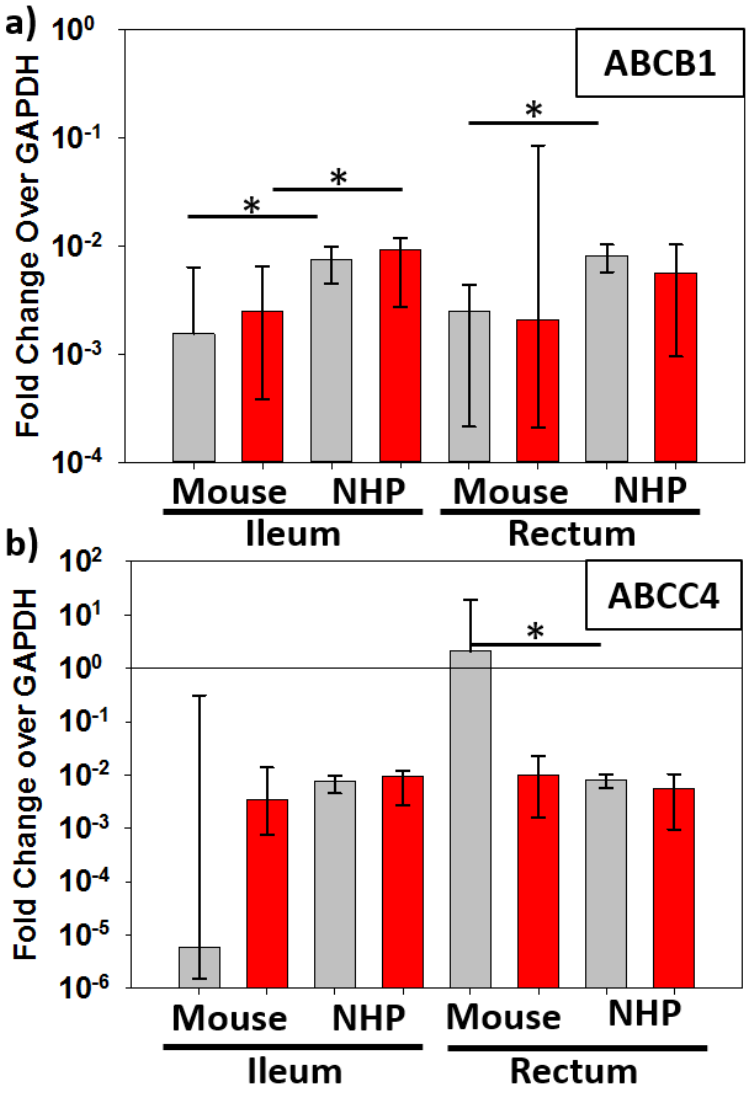

Gene expression is represented as fold change of GAPDH for uninfected (gray) and infected (red) animals from multiple dosing cohorts. Data shown are median and range. NHP=non-human primate. * represents $p<0.05$

APPENDIX 3.8: LINEARITY OF PEPTIDE DETECTION IN PROTEOMIC ASSAY

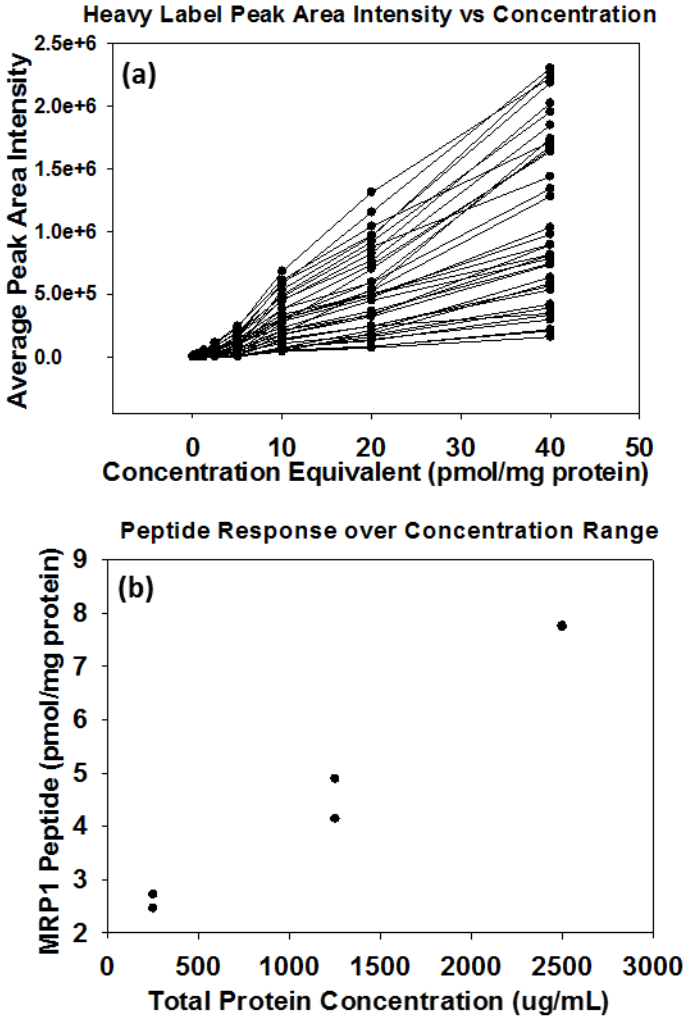

Appendix 3.8: Linearity of Peptide Detection in Proteomics Assay Five-fold dilution of SILs (a) resulted in linear peak area intensities across dilution range. (b) 3-fold dilution of a representative peptide of known starting concentration (MRP1 from cell lysate standard) resulted in linear quantitation across dilution range.

APPENDIX 4.1: COMPLETE INCLUSION/EXCLUSION CRITERIA

Inclusion Criteria:

1. Healthy HIV-positive female subjects between the ages of 18 and 65years, inclusive on the date of screening, with an intact gastrointestinal tract, uterus, and cervix. Healthy is defined as no clinically relevant abnormalities that would interfere with the interpretation of results, or pose unnecessary risk onto volunteers due to study procedures.
2. All subjects must have an undetectable viral load (<40copies/mL) at the time of screening or a documented undetectable viral load within the preceding 3 months of screening.
3. All subjects must be receiving one of the study regimens as part of their regular HIV care for at least 6 months preceding the date of enrollment.
4. Subjects must not have a history of GI disease (e.g. Crohn's disease, irritable bowel syndrome, ulcerative colitis, diverticulitis, colon cancer) or have a history of GI surgery.
5. All subjects must have a negative serum pregnancy test at screening and negative urine pregnancy tests on days of sampling and should be using at least one of the following methods of contraception from the screening visit through 72 hours prior to inpatient admission (at which time the women will be asked to remain abstinent until after their follow-up visit):
    a. Systemic hormonal contraceptive (oral, depot, transdermal or implant)
    b. IUD placed at least 1 month prior to study enrollment
    c. Bilateral tubal ligation (Sterilization)
    d. Vasectomized male partners
    e. Condom + Spermicide

f. *Unless engaged in sexual activity with female only sex partners or abstinent for at least 3 months prior with no intention of becoming sexually active during the study period. Any history of recent or present concomitant male sex partners will be addressed and ruled out in the context of screening participants for eligibility for the protocol

6. Body Mass Index (BMI) of approximately 18 to 37 kg/m2; and a total body weight > 45 kg (99 lbs).
7. Evidence of a personally signed and dated informed consent document indicating that the subject has been informed of all pertinent aspects of the trial.
8. Willing and able to comply with scheduled visits, treatment plan, laboratory tests, and other trial procedures.
9. Subject must have documentation of a normal pap smear within 36 months of the screening visit, no procedures for abnormal cervical/vaginal pathology in the last six months, at least one prior gynecological visit as part of subject's routine medical history.
10. Not receiving any known CYP3A4 inducers (rifampin, carbamazepine, St. John's wort) or inhibitors (ketoconazole, non-DHP calcium channel blockers, macrolide antibiotics) other than those contained in their HIV regimen for at least 6 months prior to enrollment.
11. Subject must be willing to abstain from sexual intercourse, douching, and all intravaginal and intrarectal objects and products for at least 72 hours prior to enrollment until study completion.
12. Subject must be Hepatitis B surface antigen negative as documented on screening labs.
13. Subject must not be actively involved in the conception process.
14. Subject must be able to swallow pills and have no allergies to any component of the study

products (i.e. bowel preparation regimen)

Exclusion Criteria

1. Evidence or history of clinically significant hematological, renal, endocrine, pulmonary, gastrointestinal, cardiovascular, hepatic, psychiatric, neurologic, or allergic disease (including documented drug allergies, but excluding untreated, asymptomatic, seasonal allergies at time of dosing).
2. Subjects with a history of hysterectomy or cervical resection that would preclude obtaining a cervical biopsy.
3. Subjects who are pregnant, possibly pregnant or lactating.
4. Subjects with a presence of abnormal vaginal discharge bleeding at screening.
5. History of febrile illness within five days prior to enrollment.
6. A positive urine drug screen for illicit substances (e.g. cocaine, methamphetamines) that would increase risk associated with sedation.
7. Active Hepatitis B infection as determined by positive Hepatitis B surface antigen (HBsAg).
8. An untreated-positive test for syphilis, gonorrhea, Chlamydia, or trichomonas at screening, Tests for these STIs will be performed on samples from both the vaginal and rectal orifices.
9. Any laboratory chemistry or hematology result Grade 3 or greater according to the DAIDS Laboratory Grading Tables
10. Treatment with an investigational drug within 4 months preceding the first dose of trial medication.
11. History of regular alcohol consumption exceeding 14 drinks (1 drink = 5 ounces (150 mL) of wine or 12 ounces (360 mL) of beer or 1.5 ounces (45 mL) of spirits) per week.

12. Participation in a clinical trial involving vaginal or rectal biopsies within 6 months preceding enrollment.
13. Blood donation of approximately 1 pint (500 mL) within 56 days prior to dosing.
14. History of sensitivity to heparin or heparin-induced thrombocytopenia.
15. Allergy to lidocaine or Monsel's solution.
16. Allergy to latex.
17. Abnormal pap smear in the past 36 months
18. Any degree of ectopy or abnormality evident during the pelvic exam at screening.
19. Any condition which, in the opinion of the investigator, is likely to interfere with follow-up or ability to take the bowel preparation appropriately.
20. Unwilling or unable to comply with the dietary and concomitant drug restrictions in regard to study drug administration as outlined in the study procedures and prohibited medications sections.

APPENDIX 4.2: HUMAN EFFFLUX TRANSPORTER CO-LOCALIZATION VALUES

ARV	TRANSPORTER	ILEUM	RECTUM
TFV (n=5)	MDR1	-0.05 (-0.08, -0.03)	0 (-0.02, 0.21)
	BCRP	-0.04 (-0.05, -0.03)	0.06 (0.03, 0.14)
	MRP2	-0.03 (-0.03, -0.03)	0 (-0.01, 0.03)
	MRP1	0 (0, 0)	-0.03 (-0.03, 0.11)
FTC (n=5)	MDR1	-	0 (-0.01, 0.02)
	BCRP	-	0.14 (0.03, 0.15)
	MRP2	-	-0.01 (-0.02, -0.01)
	MRP1	-	0.09 (-0.01, 0.17)
RAL (n=1)	MDR1	-0.03	-0.07
	BCRP	-0.04	0.15
	MRP2	-0.05	0
	MRP1	0.18	0.23
EFV (n=1)	MDR1	0.03	0.02
	BCRP	-0.02	0.18
	MRP2	-0.06	0.08
	MRP1	-0.03	0.07
MVC (n=1)	MDR1	0.21	-
	BCRP	0.09	-
	MRP2	-0.03	-
	MRP1	0.16	-
ATZ (n=2)	MDR1	-	0.19
	BCRP	-	0.01
	MRP2	-	-0.05
	MRP1	-	0.04

APPENDIX 5: RELEVANT PREVIOUSLY PUBLISHED WORK AND ABSTRACTS

Mass Spectrometry Imaging Reveals Heterogeneous Efavirenz Distribution within Putative HIV Reservoirs

Corbin G. Thompson[1], Mark T. Bokhart[2], Craig Sykes[1], Lourdes Adamson[3], Yuri Fedoriw[4], Paul Luciw[3], David C. Muddiman[2], Angela DM Kashuba[1], Elias P. Rosen[2]

[1]Division of Pharmacotherapy and Experimental Therapeutics, University of North Carolina at Chapel Hill, Chapel Hill, NC, USA
[2]W.M. Keck FTMS Laboratory for Human Health Research, Department of Chemistry, North Carolina State University, Raleigh, NC, USA
[3]University of California, Davis, CA, USA
[4]School of Medicine, University of North Carolina at Chapel Hill, Chapel Hill, NC, USA

Original Citation: **Thompson CG**, Bokhart MT, Sykes C, Adamson L, Fedoriw Y, Luciw P, Muddiman DC, Kashuba ADM, Rosen EP. Mass Spectrometry Imaging Reveals Heterogeneous Efavirenz Distribution Within Putative HIV Reservoirs. *Antimicrob Agents Chemother* 2015;59(5):2944-2948

HIV replication has been shown to persist in certain anatomic sites, known as active viral reservoirs, despite treatment with highly-active antiretroviral therapy (HAART).[25,129] Understanding the factors that contribute to the formation and propagation of these active viral reservoirs is essential to the design of targeted therapies for HIV eradication. It has been suggested that sub-therapeutic drug concentrations in certain tissues resulting from poor drug penetration may provide a favorable environment for reservoir formation and drug-resistant viral variants.[56] Several groups, including our own, have assessed antiretroviral (ARV) penetration into tissues by directly measuring drug concentrations using liquid chromatography/mass spectrometry (LC-MS) of homogenized whole tissue[123] or isolated mononuclear cells[56,165]. Though these methods can provide useful quantitative data, they do not have the ability to spatially define the distribution of drug within the tissue, as either the entire sample is consumed in the homogenization process or spatial information is lost during cellular isolation. This is a critical limitation of these methodologies, as our preliminary data have shown that ARV distribution across tissue is not uniform.[163]

Mass spectrometry imaging (MSI) offers an alternative strategy for quantifying ARV distribution into tissues and cells that maintains the sensitivity and specificity of LC-MS while preserving the spatial distribution of analytes within tissue. Through step-wise interrogation of discrete sample locations, MSI simultaneously collects information that can be concatenated into images of multiple molecules and their respective metabolites. This attribute is an important advantage for the combinatorial nature of HAART and has already led to the implementation of MSI in the drug development process.[74] One approach to MSI that is particularly well suited to the analysis of small molecules is infrared matrix-assisted laser desorption/electrospray

ionization (IR-MALDESI)[166], which we have previously demonstrated allows detection of ARVs in human tissue.[77,107]

Here, we utilize IR-MALDESI to characterize ARV distribution in 11 non-human primate tissues implicated as viral reservoirs.[26,167–169] Further, we quantify the variability of ARV exposure between tissues and compare this to LC-MS and immunohistochemistry (IHC) data, allowing for absolute quantification of observed ARV signal abundance and identification of the tissue compartments or cellular populations where a drug may be concentrating. These data are the first quantitative images of ARV distribution in a macaque, an important species for studies of HIV/SIV therapy, and show that MSI is a promising approach for evaluating ARV disposition in HIV reservoirs.[170]

One healthy male rhesus macaque (*Macaca mulatta*) was given 7 daily oral doses of 200 mg efavirenz (EFV). This dose of EFV equates to roughly 60 mg/kg and is consistent with standard treatment doses for SIV.[171,172] Prior to necropsy, blood plasma and cerebrospinal fluid were collected. The animal was euthanized by pentobarbital overdose 24 hours after the final dose of EFV, and necropsy was performed by the pathology staff at the California National Primate Research Center. Tissue samples from the GI tract (ileum, colon, rectum), central nervous system (CNS:cerebellum, basal ganglia), lymph nodes (axillary, iliac, mesenteric, inguinal), and spleen were snap frozen on dry ice, and stored at -80°C until analysis.[138] Calibration of IR-MALDESI response to EFV from the dosed tissue was conducted by MSI of tissues from non-dosed ("blank") macaques (BioreclaimationIVT, Baltimore, MD), matching dosed tissue samples where possible, upon which a set of EFV standards were pipetted. Prior to imaging, 10 µm sections of each tissue (dosed and non-dosed) were sliced and thaw mounted on a single glass microscope slide uniformly coated with internal standards and the tissue sections

were spotted with 100 nL of 0-5000 pg EFV before placing the sample slide in the IR-MALDESI imaging source. Serial 10 µm sections were set aside for LC-MS/MS and IHC analysis.

The IR-MALDESI MSI approach for analysis of tissue samples has been described previously.[107,166] Briefly, tissue samples maintained at -10°C in the source chamber were ablated at a spot-to-spot distance of 100 □m by two pulses of an IR laser (IR-Opolette 2371; Opotek, Carlsbad, CA, USA) that resulted in the complete desorption of neutral molecules for a given volume element, or voxel. The desorbed neutral molecules were then ionized by an orthogonal electrospray plume and sampled into a high resolving power Thermo Fisher Scientific Q Exactive (Bremen, Germany) mass spectrometer for synchronized analysis.[107] To generate images from mass spectrometry data, raw data from each voxel was converted to the mzXML format using MSConvert software.[173] These mzXML files were interrogated using MSiReader, a free software developed for processing MSI data, from which measurements such as tissue surface area can be made and images of analyte distribution can be generated.[115]

For LC-MS/MS analysis of efavirenz concentrations, serial 10 µm tissue sections were homogenized in 1 mL of 70:30 acetonitrile:1 mM ammonium phosphate (pH 7.4) using a Precellys 24 tissue homogenizer (Bertin Technologies, Montigny-le-Bretonneux, France). A Shimadzu HPLC system performed chromatographic separation and an AB SCIEX API 5000 mass spectrometer (AB SCIEX, Foster City, CA, USA) equipped with a turbo spray interface was used as the detector. The samples were analyzed with a set of calibration standards (0.02-20ng) and QC samples. Precision and accuracy of the calibration standards and QC samples was within acceptance criteria of 15%. Homogenate LC-MS/MS quantification of EFV for each tissue section was compared to the summed MSI response on a per-mass-tissue basis using the MSI-derived tissue surface area, the known section thickness, and an assumed tissue density of

1.06 g/cm^3. The MSI quantitation and LC-MS/MS analysis were performed by different individuals at separate institutions, and no data were shared before analyses were completed. The LC-MS/MS data underwent quality control by a designated individual not directly involved in this study to ensure accuracy.

To verify tissue quality and assess architecture for comparison to EFV distribution by MSI, serial sections of frozen tissue were sliced at 10 µm thickness, thaw mounted on glass slides, and fixed in 100% ethanol for 10 minutes. After fixation, the tissues were stained with hematoxylin and eosin (H&E) using standard histological techniques. IHC analysis was performed on similarly prepared frozen tissue slices using human primary antibodies for CD3 (clone LN10, Leica Biosystems, Buffalo Grove, IL) followed by staining with secondary antibodies. All stains were performed using the Leica Bond automated tissue stainer (Leica Biosystems). MSI revealed heterogeneous intra-tissue EFV distribution into several anatomic sites. **Figure 1** showcases these findings for representative tissues. When MSI images were compared with IHC staining, interesting spatial distributions were noted. For example, EFV was concentrated in the mucosa and lamina propria of the colon (**1A**), which corresponds to high CD3+ cell density on IHC. However, this distribution was not observed in the ileum (**1B**). The inguinal lymph node showed EFV in some, but not all, primary follicles (**1C**). EFV concentrated in the grey matter of the cerebellum (**1D**), and showed a homogeneous distribution in the spleen, testes, and axillary lymph node (**1E**). The heterogeneity of EFV distribution is quantified in

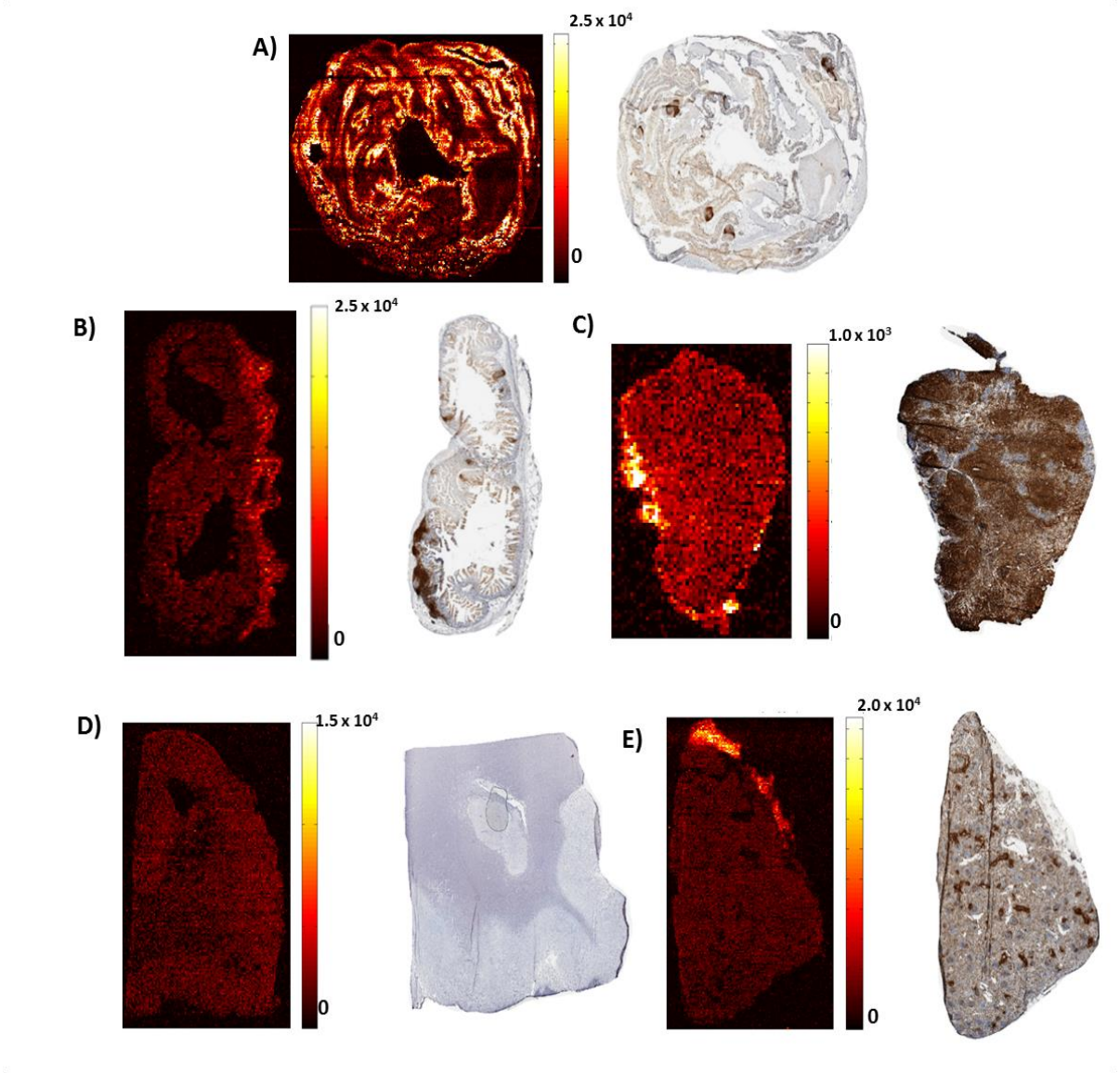

Figure 1: EFV Distribution into Macaque Reservoir Sites Representative MSI images are shown on the left, with adjacent CD3+ cell staining of serial tissue slices for colon (**A**), ileum (**B**), inguinal lymph node (**C**), cerebellum (**D**), and spleen (**E**). MSI signal intensity is shown next to each image on a concentration-dependent scale. The bottom of the scale (0) represents no EFV present, while the top of the scale reflects the highest per-voxel EFV signal observed within each slice. Brighter colors represent higher EFV concentrations.

Table 1 by the dynamic range in MSI response (expressed in the base-10 units of decibels, dB) to each tissue type that can be observed from the images of Figure 1. The dynamic range of EFV response was lower in tissues such as the basal ganglia and lymph nodes reflecting more

homogeneous EFV distribution, whereas tissues such as the colon (37.6 dB) and rectum (26.8 dB) had much larger differences between minimum and maximum concentrations that suggest greater biological differences in drug uptake.

Table 1: Variability of EFV MSI Response Within Dosed Macaque Tissues

Tissue Type	Maximum	Median	Minimum	Dynamic range
	ng/voxel			dB
Cerebrum	1.8E+04	5.0E+03	6.5E+02	14.5
Basal ganglia	1.8E+03	9.2E+02	4.8E+02	5.8
Lymph node: Axillary	3.0E+04	4.2E+03	2.0E+03	11.8
Lymph node: Mesenteric	9.8E+03	2.6E+03	1.1E+03	9.5
Lymph node: Inguinal	2.7E+04	1.6E+03	8.1E+02	15.2
Lymph node: Iliac	4.0E+03	9.3E+02	3.4E+02	10.7
Spleen	4.2E+04	5.1E+03	1.4E+03	14.6
Ileum	1.4E+04	3.7E+03	2.5E+03	7.5
Colon	8.7E+06	1.4E+04	1.5E+03	37.6
Rectum	1.6E+06	1.2E+04	3.4E+03	26.8
Testes	2.7E+03	5.9E+02	3.7E+02	8.6

*EFV concentration within each voxel was quantified using calibration standards and averaged across the entire tissue slice. These averages and the maximum and minimum concentrations for each slice are reported.

**Relative standard deviation was calculated

Inter-tissue EFV quantitation is summarized in **Table 2**. LC-MS/MS analysis demonstrated a 20-fold variability in total tissue EFV exposure, with concentrations ranging from 1.2 □g/g in the testes to 20.8 □g/g in the colon. A similar trend is observed from the MSI quantification, though agreement varies between tissue types. EFV concentrations were found to be in agreement (<30% difference) between MSI and LC-MS/MS for half of the tissues after correction for tissue size. In tissues such as the lymph nodes, concentrations varied by as little as

8%. Tissues of the GI tract demonstrated less agreement between techniques, with variations up to -70%. **Table 2** also compares EFV exposure in tissue and in plasma. EFV achieved high exposure in the CNS, where tissue concentrations were 6.8-7.6 logs higher than in the CSF. EFV exposure was consistent among the lymph nodes, with 1.7-2.2 log increases over plasma observed. In the GI tract, EFV exposure was 3.6 logs higher than plasma in the colon and rectum, and 2.7 logs higher in the ileum.

Table 2: Comparison of EFV Quantitation in Macaque Tissues using MSI and LC-MS/MS

Tissue Type	LC-MS/MS (□g/g tissue)	LC-MS/MS Log Increase Over Plasma or CSF*	MSI (□g/g tissue)	MSI Log Increase Over Plasma or CSF*	Difference** (%)
Cerebellum	6.86	7.6	3.09	6.8	-54.89
Basal ganglia	2.01	6.4	1.67	6.2	-16.80
Lymph node: Axillary	3.91	2.0	3.33	1.8	-14.91
Lymph node: Mesenteric	3.82	2.0	3.12	1.8	-18.48
Lymph node: Inguinal	4.80	2.2	2.86	1.7	-40.38
Lymph node: Iliac	2.82	1.7	3.06	1.7	8.40
Spleen	5.01	2.2	3.61	1.9	-27.83
Ileum	8.41	2.7	3.20	1.8	-61.94
Colon	20.77	3.6	6.12	2.4	-70.54
Rectum	20.69	3.6	8.22	2.7	-60.26
Testes	1.22	0.8	2.91	1.7	138.94
Day 8 Plasma (ng/mL)	541	n/a	n/a	n/a	n/a
Day 8 CSF (ng/mL)	3.30	n/a	n/a	n/a	n/a

*To compare tissue concentrations to plasma or CSF, tissue concentrations (μg/g) were converted to ng/mL assuming a tissue
density of approximately 1g/mL, then divided by the plasma or CSF concentration and converted to log units
**Difference between methods was calculated by subtracting LC-MS/MS concentrations from MSI concentrations, dividing by the
LC-MS/MS concentration and multiplying by 100%

The persistence of HIV replication within anatomic reservoirs necessitates the use of tissue pharmacology to inform the design of effective treatment strategies. This will require knowledge of tissue penetration to sites of action, as underscored by recent findings that the 50-90% reduction of EFV in mononuclear cells isolated from reservoir tissues relative to PBMCs was associated with persistent viral replication in these tissues.[56] This finding, in combination with the fact that EFV receives widespread clinical use as a component of Atripla® (a fixed dose combination of tenofovir, emtricitabine, and efavirenz dosed once daily) and is frequently included in HIV treatment and cure research regimens for macaques, led us to choose EFV for our evaluations.

The observed ARV drug distribution within these putative viral reservoirs reveals important information regarding tissue pharmacology that can inform treatment strategy. The heterogeneous penetration of EFV into the lymphoid follicles suggests that further quantification of effective drug exposure in these tissues is required. Conversely, the abundance of EFV signal in the CD3+ cell populations of the gut is evidence that adequate EFV concentrations are likely reached in this compartment. Both of these findings are consistent with previous studies that have examined EFV tissue concentrations by LC-MS.[165] The EFV distributions observed here would not have been possible with traditional LC-MS of tissue homogenates or isolated mononuclear cells: the heterogeneity of EFV distribution within tissue slices as measured by the dynamic range of response (**Table 1**) is only measurable using MSI. Moreover, our MSI analysis provides evidence that the use of plasma or CSF as a surrogate for tissue concentrations may be inappropriate without detailed quantification of these relationships. The increased CNS tissue concentrations compared to the CSF (**Table 2**) and the concentration of EFV within the grey

matter of the cerebellum (**Figure 1**) agree with brain microdialysis data showing that CNS drug concentrations are higher than CSF concentrations.[174,175]

The variability in the extent of EFV distribution between tissue types suggests that biological processes, more than the cellular populations present, drive the movement of EFV into tissues. The non-homogenous distribution of EFV in tissues such as the colon may be attributable to the physicochemical properties of EFV, or to active transport mechanisms. Our previous work identifying variables affecting ARV exposure in the female genital tract (another putative viral reservoir) found that the efflux transporters MRP1 and MRP4 were associated with ARV penetration into this compartment.[52] While EFV is not a known substrate of these transporters, other drug transporters such as MDR1 or BCRP may affect its disposition and explain the areas of EFV concentration seen here.[176,177]

There are several limitations to this analysis which should be addressed, the most important of which is our limited sample size. As this study was conducted in a single animal, the variability in tissue drug distribution between animals remains unknown and remains to be evaluated. Further, the assessment of EFV distribution shown in Figure 1 is based on individual slices of tissue under steady-state conditions. Repeated sectioning may reveal additional biological variability. Although EFV has a long plasma half-life and relatively flat blood plasma concentration-time curve, EFV exposure over the dosing interval could not be determined due to the fact that sampling was only performed at the end of the dosing interval. Additionally, we were unable to determine the relationship between drug and viral dynamics in this uninfected animal, though we selected tissues with previous evidence supporting persistent HIV infection.[26,167–169] Finally, only CD3 was used for an IHC correlate to drug distribution. Though visualization of the overall T cell compartment is informative, future work will relate

ARV localization to CD4+ T cell distribution, as these cells are the most relevant for HIV infection.

This is the first study to apply MSI to ARV distribution in potential tissue reservoirs for HIV infection. Using IR-MALDESI, we have confirmed that ARV tissue distribution is heterogeneous, and that the distribution of a single ARV can vary greatly between tissues within an individual. By comparing to the gold standard of tissue quantification, LC-MS/MS, our analysis confirms the importance of MSI for drug quantification. Future work will address existing limitations of our approach. For MSI, this will entail a systematic exploration of factors, such as matrix effects or electrospray ionization capacity, which may influence the quantitative agreement with LC-MS for different tissue types and drug exposure. IR-MALDESI is sensitive to a wide variety of endogenous lipids (profiles of which vary between tissue types) that are ablated and analyzed simultaneously with EFV. Any suppression of EFV response as a result of tissue-specific ablation and ionization conditions is intended to be taken into account by performing EFV calibrations on matching or closely related blank tissue types and evaluating IR-MALDESI response to an internal standard. However, a more thorough investigation of these effects must be undertaken to improve analytical agreement. Additionally, lower limits of detection for all antiretrovirals and their active metabolites within a drug regimen must be attained in order to link tissue drug exposure and suppression of viral replication. We will also evaluate ARV distribution in SIV/HIV infected samples to determine the effect of ARV disposition on viral expression. Despite these limitations, these data show that MSI is a critical tool for the disposition of ARVs within putative active HIV reservoirs, which is an important step toward understanding how to eradicate HIV infection.

ABSTRACT PRESENTED AT THE AMERICAN SOCIETY OF CLINICAL PHARMACOLOGY AND THERAPEUTICS 2017 CONFERENCE, WASHINGTON, D.C.

Imaging Antiretroviral Distribution Within Gastrointestinal Tissues Across Pre-Clinical Species: Implications For Hiv Eradication

Corbin G. Thompson, Elias P Rosen, Michelle Mathews, Nicole White, Craig Sykes, Yuri Fedoriw, Paige Charlins, Leila Mulder, Martina Kovarova, Lourdes Adamson, David C Muddiman, Ramesh Akkina, Victor Garcia, Paul Luciw, Angela DM Kashuba

HIV replication within the gut may be propagated by reduced antiretroviral (ARV) exposure. Mass spectrometry imaging (MSI) provides biodistribution data that LC-MS cannot. Here, we use MSI to visualize ARV distribution within gut tissues from two species, and assess colocalization with HIV target cells and drug efflux transporters.

Two humanized mouse (n=49) and one primate (NHP, n=12) models were given combination ARVs. One 10µm slice from frozen ileum and rectum was analyzed by MSI. Serial slices were analyzed for CD3+ T cell and efflux transporter (MDR1, BCRP, MRP1, MRP2) localization by IHC. Colocalization of ARV and IHC imaging was performed in Matlab using Pearson correlation (r).

ARV distribution was heterogeneous (Figure, column 1, NHP ileum) with 2-fold greater mucosal accumulation in NHP vs mice. ARV-T cell correlation ranged from 0.007 to 0.55, was 19-fold higher in NHP vs mice and 11-fold higher in the NHP rectum versus the ileum. Transporter colocalization was highest for MDR1 (range 0.06-0.62) in both species.

Large interspecies differences in ARV distribution were noted. Colocalization suggests efflux transporter expression results in lower ARV exposure in HIV target cells in the ileum, which may contribute to low level HIV replication. These data will inform the development of targeted therapies for HIV eradication.

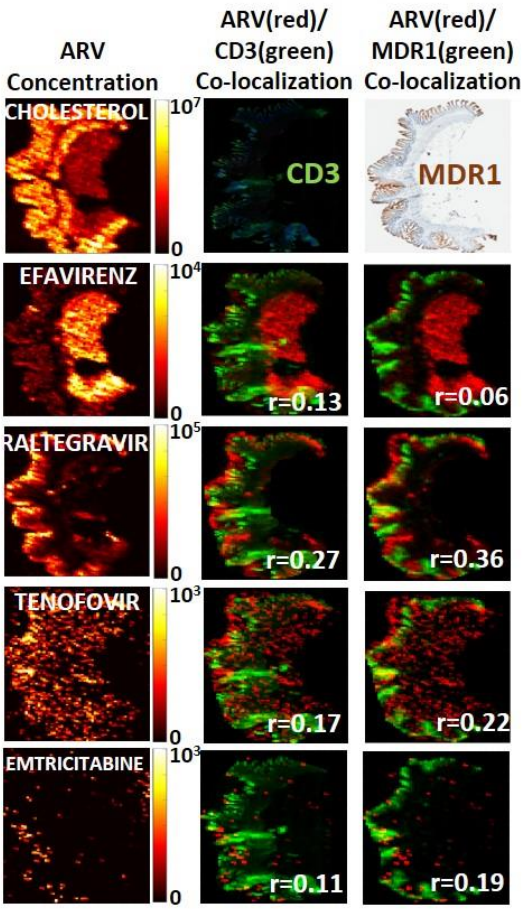

ABSTRACT PRESENTED AT 17TH INTERNATIONAL WORKSHOP ON CLINICAL PHARMACOLOGY OF HIV AND HEPATITIS C THERAPY, WASHINGTON, D.C.

Quantitative Proteomic Analysis of Drug Transporter Expression in the GI Tract of Multiple Animal Models of HIV Infection

Corbin G. Thompson[1], John K. Fallon[1], Paige Charlins[3], Leila Mulder[3], Martina Kovarova[1], Lourdes Adamson[2], Paul Luciw[2], J. Victor Garcia[1], Ramesh Akkina[3], Philip C. Smith[1], and Angela DM Kashuba[1]

[1]University of North Carolina at Chapel Hill, Chapel Hill, NC, USA

[2]University of California, Davis, CA, USA

[3]Colorado State University, Fort Collins, CO, USA

The persistence of HIV in tissue reservoirs such as the GI tract may be reduced or eliminated with optimized exposure of antiretrovirals (ARVs) at the site of action. Drug transporters affect ARV tissue disposition and can be exploited to maximize ARV exposure, but quantitative measures of drug transporter protein expression across preclinical species are not available. In this study, we use proteomics to obtain absolute transporter concentrations and assess agreement with corresponding gene and immunometric protein data. We also examine the effect of HIV infection on transporter expression in the GI tract.

Animals from two humanized mouse (hu-HSC-Rag (n=18); BLT (n=7)) and one primate (rhesus macaque, (NHP, n=3)) models were infected with HIV or SHIV for 4-6 weeks before being

dosed to steady-state with combination ARV treatment. Ileum and rectum were collected at necropsy and analyzed for protein expression of ARV efflux (MDR1, BCRP, MRP1, MRP2, and MRP4) and uptake (ENT1, OATP2A1, OCT3) transporters using quantitative targeted absolute proteomics (QTAP) and Western blot (WB). Transporter mRNA was measured by qPCR. Gene and protein expression were compared against historical data from uninfected animals, and comparisons between anatomic sites and animal models were made using ANOVA on ranks. Agreement between analytical techniques was assessed by linear regression. Data are presented as median concentration.

QTAP analysis showed a 1.7 log increase in MDR1 expression in the ileum of infected mice versus infected macaques (49.9 vs 1.6 pmol/mg protein; $p<0.001$), and significantly higher OATP2A1 concentrations in macaque vs mouse rectum (10.4 vs undetectable pmol/mg protein;$p=0.002$). Transporter concentrations were similar between ileal and rectal tissues with the exception of ENT1, which was significantly higher in mice ileum versus rectum (1.1 vs undetectable pmol/mg protein;$p=0.002$). Gene expression was generally consistent between infected and uninfected animals ($p>0.05$), however *ABCC4* gene expression was significantly higher in infected versus uninfected mice (97.4 vs 0.02 x 10^4 fold change vs GAPDH; $p<0.001$). There was little agreement between QTAP and qPCR or WB, with R^2 values ranging from 0.001 (MDR1 QTAP vs qPCR) to 0.34 (MRP1 QTAP vs WB).

This evaluation is the first to determine absolute protein concentrations of drug transporters across pre-clinical species. We observed significant differences in MDR1 and OATP2A1 concentrations between species, suggesting that the tissue exposure of their substrates, including

many ARVs, may not be equal between these models. Further, the lack of differences in transporter expression between infected and uninfected animals suggests that HIV infection does not confound ARV distribution studies. Finally, the lack of agreement between analytical techniques indicates that resources may need to be focused on generating high-throughput, downstream measures of protein expression. Taken together, these data inform the use of pre-clinical models for studying ARV distribution and the design of targeted therapies for HIV eradication.

ABSTRACT PRESENTED AT 23RD CONFERENCE ON RETROVIRUSES AND OPPORTUNISTIC INFECTIONS, BOSTON, MA.

Multispecies Differences in Drug Transporter Expression and Localization in GI Tissue

Corbin G. Thompson[1], Elias P. Rosen[1], Paige Charlins[3], Leila Mulder[3], Martina Kovarova[1], Yuri Fedoriw[1], Paul Luciw[2], J. Victor Garcia[1], Ramesh Akkina[3], and Angela DM Kashuba[1]

[1]University of North Carolina at Chapel Hill, Chapel Hill, NC, USA

[2]University of California, Davis, CA, USA

[3]Colorado State University, Fort Collins, CO, USA

HIV replication may persist during treatment within tissue reservoirs, including the gastrointestinal (GI) tract. Differences in drug transporter expression and localization may alter ARV exposure and confound the ability to translate study results between animal models, and to humans. Here, we characterize the expression and localization of transporters relevant to ARVs in 3 animal models.

Three cohorts of uninfected animals (rhesus macaques (NHP, n=3); humanized mice (BLT, n=6 and hu-HSC-Rag, n=18)) were dosed to steady-state with a combination of ARVs including tenofovir (TFV), emtricitabine (FTC), and raltegravir (RAL). Ileum and rectum were collected at necropsy and analyzed for gene (qPCR) and protein (Western blot) expression and localization (immunohistochemistry (IHC)) of ARV efflux (*ABCB1*, *ABCG2*, *ABCC1*, *ABCC2*, and *ABCC4*) and uptake (*SLC29A1*, *SLCO2A1*, *SLC22A3*) transporters. Tissue concentrations were analyzed

by LC-MS and normalized to plasma. Species comparisons were performed using ANOVA. Data are reported as mean fold expression vs GAPDH.

In the ileum, gene expression differed significantly between BLT and hu-HSC-Rag mice for *ABCB1* (5.02 vs 23.4 x 10^{-4};p=0.005), *ABCC2* (0.11 vs 0.19;p=0.01), and *ABCC4* (4.56 vs 1.91 x 10^{-6};p=0.005). Protein expression did not differ between these 2 models (p>0.05). Iliac NHP gene expression was increased over mouse for *ABCB1* & *ABCC4* (1.7 & 3.3 log;p<0.01) and decreased for *SLC22A3* (3.2 log;p<0.01). In the colorectum, gene differences were again observed between BLT and hu-HSC-Rag mice for *ABCB1* (2.08 vs 26.3 x 10^{-4};p<0.001), *SLC29A1* (0.07 vs 0.04;p=0.019), and *ABCG2* (0.11 vs 0.05;p=0.001). No interspecies differences were seen. In all species, IHC showed MDR1 localization on the luminal surface of ileac and rectal mucosa and a lack of MRP2 expression. hu-HSC-Rag TFV tissue concentrations were 13 & 8-fold greater than BLTs and NHPs (p<0.05).

This is the first study comparing the expression and localization of these transporters across animal models. Observed variability in expression suggests model-dependent ARV tissue penetration (e.g. decreased *ABCB1* and increased *ABCC4* expression in BLT mice explain the observed decrease in TFV exposure). Multi-log increases in *ABCB1* expression between NHP and mice may impact the disposition of many ARVs that use *ABCB1* for transport (e.g. TFV and RAL). Ultimately, these data can be coupled with ARV exposure data to inform inter-species drug scaling for targeting HIV reservoirs.

ABSTRACT PRESENTED AT 15TH INTERNATIONAL WORKSHOP ON CLINICAL PHARMACOLOGY OF HIV AND HEPATITIS C THERAPY, WASHINGTON, D.C.

Characterizing Antiretroviral Distribution Within Active Viral Reservoirs Using Mass Spectrometry Imaging

Corbin G. Thompson[1], Eli Rosen[2], Craig Sykes[1], Yuri Fedoriw[1], Paul Luciw[3], David C. Muddiman[2], and Angela DM Kashuba[1]

[1]University of North Carolina at Chapel Hill, Chapel Hill, NC, USA [2]North Carolina State University, Raleigh, NC, USA [3]University of California at Davis, Davis, CA, USA

HIV infection persists despite long-term antiretroviral (ARV) treatment. Inadequate ARV exposure in certain anatomic sites may contribute to continued viral replication within tissue reservoirs. Detailed evaluations of the contribution of ARV disposition to the formation and persistence of these reservoirs would greatly inform HIV cure efforts. Recent studies have demonstrated differential ARV penetration into suspected reservoirs using tissue homogenates; however this method of evaluating ARV exposure in tissues is limited in its scope and ability to describe within-tissue ARV distribution. Mass spectrometry imaging (MSI) allows for the visualization of small molecule biodistribution within anatomic sites. Here, we use a novel MSI technique to characterize the distribution of two commonly prescribed ARVs within the lymph node, which has been implicated as an active viral reservoir.

A single uninfected rhesus macaque was dosed to steady-state with 30mg/kg tenofovir disoproxil fumarate (TDF) given subcutaneously, and 200mg efavirenz (EFV) given orally once daily. At necropsy, an inguinal lymph node was removed and frozen on dry ice. A single ten micron slice from each tissue was analyzed using an infrared matrix-assisted laser desorption electrospray ionization (IR-MALDESI) source coupled to a Thermo Q-Exactive mass spectrometer. MSI data were analyzed using MSiReader software. In order to relate observed IR-MALDESI findings to tissue architecture, serial sections were fixed and stained with hematoxylin and eosin (H&E).

IR-MALDESI imaging revealed non-homogenous ARV distribution within the tissue compartment. TFV and EFV were both detected in the lymph node, though their respective signals showcased unique tissue distribution. Visual inspection of the supporting H&E stain show that TFV signal was concentrated throughout the medullary sinuses, while EFV signal was predominantly visualized near a small section of the lymph node capsule.

This is the first report of visualizing ARV distribution within a tissue implicated as a viral reservoir. Observed distributional patterns identified by IR-MALDESI, when coupled with H&E stains from serial slices, agree with tissue homogenate studies that have shown that TFV and EFV achieve measurable concentrations in the lymph nodes. The distinct distributional pattern of EFV compared to TFV suggests that ARV exposure within viral reservoirs cannot be assumed to be the same between individual agents. Further, TFV's apparent preference for the vascularized medullary sinus over the lymphoid follicles may suggest inadequate concentrations at the site of action. Importantly, the distributional variation observed between TFV and EFV would not have

been captured with standard analytical methods and showcases the advantage of using MSI for future studies. Because the tissues evaluated in this study were removed from a dosed animal, the observed results are likely representative of ARV disposition during in vivo dosing scenarios. This study provides sound proof of concept for future evaluations defining drug distribution in animals and humans.

APPENDIX 6: GRANTS AND AWARDS

September 2016	**ASCPT Presidential Trainee Award** *Scholarship awarded to top abstracts at the ASCPT conference*
November 2015	**International Antiviral Society Young Investigator Award** *Scholarship given on the basis of abstract quality. Provides free attendance at CROI 2016*
2015-2016	**AFPE Pre-Doctoral Fellowship in Pharmaceutical Sciences** *National award given to doctoral students who demonstrate promising research proposals*
November 2014	**International Antiviral Society Young Investigator Award** *Scholarship given on the basis of abstract quality. Provides free attendance at CROI 2015*
August 2014	**DPET Research Day Travel Award** *Divisional travel award given to the top three poster presenters at DPET Research Day*
2014-2015	**AFPE Pre-Doctoral Fellowship in Pharmaceutical Sciences** *National award given to doctoral students who demonstrate promising research proposals*
2012-2013	**AFPE-Rho Chi First Year Graduate School Fellowship** *National award given to two graduating pharmacy students who are pursuing a graduate degree*
2012-2013	**UNC Eshelman Fellowship** *For selected incoming students into the graduate program at UNC*

REFERENCES

1. van Sighem AI, Gras L a J, Reiss P, Brinkman K, de Wolf F. Life expectancy of recently diagnosed asymptomatic HIV-infected patients approaches that of uninfected individuals. *AIDS*. 2010;24(10):1527-1535. doi:10.1097/QAD.0b013e32833a3946.

2. Wong JK, Hezareh M, Günthard HF, et al. Recovery of replication-competent HIV despite prolonged suppression of plasma viremia. *Science*. 1997;278(5341):1291-1295. doi:10.1126/science.278.5341.1291.

3. Montaner J, Harris M, Mo T, Harrigan P. Rebound of plasma HIV viral load following prolonged suppression with combination therapy. *AIDS*. 1998;12(11):1398-1399.

4. Marshall J, Oberwinkler J, Chun T, et al. Re-emergence of HIV after stopping therapy. *Nature*. 1999;401(October):874-875.

5. Finzi D, Hermankova M, Pierson T, et al. Identification of a Reservoir for HIV-1 in Patients on Highly Active Antiretroviral Therapy. *Science (80-).* 1997;278(5341):1295-1300. doi:10.1126/science.278.5341.1295.

6. Perelson AS, Essunger P, Cao Y, Vesanen M, Hurley A. Decay characteristics of HIV-1-infected compartments during combination therapy. *Nature*. 1997;387:188-191.

7. Siliciano JD, Kajdas J, Finzi D, et al. Long-term follow-up studies confirm the stability of the latent reservoir for HIV-1 in resting CD4+ T cells. *Nat Med*. 2003;9(6):727-728. doi:10.1038/nm880.

8. Siliciano JD, Siliciano RF. A long-term latent reservoir for HIV-1: Discovery and clinical implications. *J Antimicrob Chemother*. 2004;54(1):6-9. doi:10.1093/jac/dkh292.

9. Banga R, Procopio FA, Noto A, et al. PD-1+ and follicular helper T cells are responsible for persistent HIV-1 transcription in treated aviremic individuals. *Nat Med*. 2016;22(7):754-761. doi:10.1038/nm.4113.

10. Gray LR, Roche M, Flynn JK, Wesselingh SL, Gorry PR, Churchill MJ. Is the central nervous system a reservoir of HIV-1? *Curr Opin HIV AIDS*. 2014;9(6):552-558. doi:10.1097/COH.0000000000000108.

11. Joseph AP, Kenneth HM, Seth LW, William XO, Frederick PB, DDeborah JA. Highly active antiretroviral therapy does not completely suppress HIV in semen of sexually active HIV-infected men who have sex with men. *Aids*. 2013;26(12):1535-1543. doi:10.1097/QAD.0b013e328353b11b.Highly.

12. Cu-Uvin S, DeLong AK, Venkatesh KK, et al. Genital tract HIV-1 RNA shedding among women with below detectable plasma viral load. *AIDS*. 2010;24(16):2489-2497. doi:10.1097/QAD.0b013e32833e5043.

13. Popovic M, Tenner-Racz K, Pelser C, Stellbrink HJ, van Lunzen J, Lewis G, Kalyanaraman VS, Gallo RC RP. Persistence of HIV-1 structural proteins and glycoproteins in lymph nodes of patients under highly active antiretroviral therapy. *Proc Natl Acad Sci U S A*. 2005;(102):14807-14812.

14. Wong JK, Yukl SA. Tissue reservoirs of HIV. *Curr Opin HIV AIDS*. 2016;11(4):362-370. doi:10.1097/COH.0000000000000293.

15. Cory TJ, Schacker TW, Stevenson M, Fletcher C V. Overcoming Pharmacologic Sanctuaries. *Curr Opin HIV AIDS*. 2013;8(3):190-195. doi:10.1126/scisignal.2001449.Engineering.

16. Mowat a M, Viney JL. The anatomical basis of intestinal immunity. *Immunol Rev*. 1997;156:145-166. doi:10.1111/j.1600-065X.1997.tb00966.x.

17. Veazey RS, Demaria M, Chalifoux L V, et al. Gastrointestinal Tract as a Major Site of CD4+ T Cell Depletion and Viral Replication in SIV Infection. *Science (80-).* 1998;280(April):427-430. doi:10.1007/s13398-014-0173-7.2.

18. Mattapallil JJ, Douek DC, Hill B, Nishimura Y, Martin M, Roederer M. Massive infection and loss of memory CD4+ T cells in multiple tissues during acute SIV infection. *Nature*. 2005;434(7037):1093-1097. doi:10.1542/peds.2006-0900HHHH.

19. Guadalupe M, Reay E, Sankaran S, et al. Severe CD4+ T-cell depletion in gut lymphoid tissue during primary human immunodeficiency virus type 1 infection and substantial delay in restoration following highly active antiretroviral therapy. *J Virol*. 2003;77(21):11708-11717. doi:10.1128/JVI.77.21.11708.

20. Kelley CF, Haaland RE, Patel P, et al. HIV-1 RNA rectal shedding is reduced in Men with Low plasma HIV-1 RNA viral loads and is not enhanced by sexually transmitted bacterial infections of the rectum. *J Infect Dis*. 2011;204(5):761-767. doi:10.1093/infdis/jir400.

21. Kiviat NB, Critchlow CW, Hawes SE, et al. Determinants of human immunodeficiency virus DNA and RNA shedding in the anal-rectal canal of homosexual men. *J Infect Dis*. 1998;177(3):571-578. http://www.ncbi.nlm.nih.gov/pubmed/9498434.

22. Rueda CM, Velilla PA, Chougnet CA, Montoya CJ, Rugeles MT. HIV-induced T-cell activation/exhaustion in rectal mucosa is controlled only partially by antiretroviral treatment. *PLoS One*. 2012;7(1). doi:10.1371/journal.pone.0030307.

23. Chun TW, Nickle DC, Justement JS, et al. HIV-infected individuals receiving effective antiviral therapy for extended periods of time continually replenish their viral reservoir. *J Clin Invest*. 2005;115(11):3250-3255. doi:10.1172/JCI26197.

24. Yukl S, Gianella S, Sinclair E, et al. Differences in HIV Burden and Immune Activation

within the Gut of HIV+ Patients on Suppressive Antiretroviral Therapy. *J Infect Dis*. 2010;202(10):1553-1561. doi:10.1086/656722.Differences.

25. Chun T-W, Nickle DC, Justement JS, et al. Persistence of HIV in gut-associated lymphoid tissue despite long-term antiretroviral therapy. *J Infect Dis*. 2008;197(5):714-720. doi:10.1086/527324.

26. Avettand-Fenoel V, Hocqueloux L, Muller-Trutwin M, Prazuck T. Greater Diversity of HIV DNA Variants in the Rectum Compared to Variants in the Blood in Patients Without HAART. *J Med Virol*. 2011;83:1499-1507. doi:10.1002/jmv.

27. Imamichi H, DeGray G, Dewar RL, et al. Lack of compartmentalization of HIV-1 quasispecies between the gut and peripheral blood compartments. *J Infect Dis*. 2011;204(2):309-314. doi:10.1093/infdis/jir259.

28. Evering TH, Mehandru S, Racz P, et al. Absence of HIV-1 evolution in the gut-associated lymphoid tissue from patients on combination antiviral therapy initiated during primary infection. *PLoS Pathog*. 2012;8(2). doi:10.1371/journal.ppat.1002506.

29. Lorenzo-Redondo R, Fryer HR, Bedford T, et al. Persistent HIV-1 replication maintains the tissue reservoir during therapy. *Nature*. January 2016. doi:10.1038/nature16933.

30. McBride K, Xu Y, Bailey M, et al. The majority of HIV type 1 DNA in circulating CD4+ T lymphocytes is present in non-gut-homing resting memory CD4+ T cells. *AIDS Res Hum Retroviruses*. 2013;29(10):1330-1339. doi:10.1089/AID.2012.0351.

31. Lerner P, Guadalupe M, Donovan R, et al. The gut mucosal viral reservoir in HIV-infected patients is not the major source of rebound plasma viremia following interruption of highly active antiretroviral therapy. *J Virol*. 2011;85(10):4772-4782. doi:10.1128/JVI.02409-10.

32. Rothenberger MK, Keele BF, Wietgrefe SW, et al. Large number of rebounding/founder HIV variants emerge from multifocal infection in lymphatic tissues after treatment interruption. *Proc Natl Acad Sci*. 2015;112(10):E1126-E1134. doi:10.1073/pnas.1414926112.

33. Mendoza D, Johnson SA, Peterson BA, et al. Comprehensive analysis of unique cases with extraordinary control over HIV replication Comprehensive analysis of unique cases with extraordinary control over HIV replication. *Blood*. 2012;119(20):4645-4655. doi:10.1182/blood-2011-10-381996.

34. Brenchley JM, Douek DC. HIV infection and the gastrointestinal immune system. *Mucosal Immunol*. 2008;1(1):23-30. doi:10.1038/mi.2007.1.

35. George MD, Asmuth DM. Mucosal immunity in HIV infection. *Curr Opin Infect Dis*. 2014;27(3):275-281. doi:10.1097/QCO.0000000000000059.

36. Kotler DP, Gaetz HP, Lange M, Klein E, Holt PR. Enteropathy Associated with the Acquired Immunodeficiency Syndrome. *Ann Intern Med*. 1984;101(4):421-428. doi:10.7326/0003-4819-101-4-421.

37. Griffin GE. Malabsorption, malnutrition and HIV disease. *Baillieres Clin Gastroenterol*. 1990;4(2):361-373. doi:10.1016/0950-3528(90)90006-3.

38. Raffatellu M, Santos RL, Verhoeven DE, et al. Simian immunodeficiency virus–induced mucosal interleukin-17 deficiency promotes Salmonella dissemination from the gut. *Nat Med*. 2010;14(4):421-428. doi:10.1038/nm1743.Simian.

39. Ciccone EJ, Greenwald JH, Lee PI, et al. CD4+ T cells, including Th17 and cycling subsets, are intact in the gut mucosa of HIV-1-infected long-term nonprogressors. *J Virol*. 2011;85(12):5880-5888. doi:10.1128/JVI.02643-10.

40. Guadalupe M, Sankaran S, George MD, et al. Viral suppression and immune restoration in the gastrointestinal mucosa of human immunodeficiency virus type 1-infected patients initiating therapy during primary or chronic infection. *J Virol*. 2006;80(16):8236-8247. doi:10.1128/JVI.00120-06.

41. Deeks SG, Tracy R, Douek DC. Systemic Effects of Inflammation on Health during Chronic HIV Infection. *Immunity*. 2013;39(4):633-645. doi:10.1016/j.immuni.2013.10.001.Systemic.

42. Estes JD, Wietgrefe S, Schacker T, et al. Simian immunodeficiency virus-induced lymphatic tissue fibrosis is mediated by transforming growth factor beta 1-positive regulatory T cells and begins in early infection. *J Infect Dis*. 2007;195(4):551-561. doi:10.1086/510852.

43. Mavigner M, Cazabat M, Dubois M, et al. Altered Cd4 T Cell Homing To the Gut Impairs Mucosal Immune Reconstitution in Treated Hiv Infectd Indivinduals. *J Clin Invest*. 2012;122(1):62-69. doi:10.1172/JCI59011.62.

44. Kim CJ, McKinnon LR, Kovacs C, et al. Mucosal Th17 cell function is altered during HIV infection and is an independent predictor of systemic immune activation. *J Immunol*. 2013;191(5):2164-2173. doi:10.4049/jimmunol.1300829.

45. Dandekar S, George MD, Bäumler AJ. Th17 cells, HIV and the gut mucosal barrier. *Curr Opin HIV AIDS*. 2010;5(2):173-178. doi:10.1097/COH.0b013e328335eda3.

46. Brenchley JM, Price DA, Schacker TW, et al. Microbial translocation is a cause of systemic immune activation in chronic HIV infection. *Nat Med*. 2006;12(12):1365-1371. doi:10.1038/nm1511.

47. French AL, Evans CT, Agniel DM, et al. Microbial translocation and liver disease

progression in women coinfected with HIV and hepatitis C virus. *J Infect Dis*. 2013;208(4):679-689. doi:10.1093/infdis/jit225.

48. Kelesidis T, Kendall MA, Yang OO, Hodis HN, Currier JS. Biomarkers of microbial translocation and macrophage activation: Association with progression of subclinical atherosclerosis in HIV-1 infection. *J Infect Dis*. 2012;206(10):1558-1567. doi:10.1093/infdis/jis545.

49. Chun T, Engel D, Berrey M. Early establishment of a pool of latently infected , resting CD4 ⁄ T cells during primary HIV-1 infection. *Proc Natl Acad Sci U S A*. 1998;95(July):8869-8873.

50. Strain MC, Little SJ, Daar ES, et al. Effect of treatment, during primary infection, on establishment and clearance of cellular reservoirs of HIV-1. *J Infect Dis*. 2005;191(9):1410-1418. doi:10.1086/428777.

51. Thompson CG, Cohen MS, Kashuba ADM. Antiretroviral pharmacology in mucosal tissues. *J Acquir Immune Defic Syndr*. 2013;63 Suppl 2:S240-7. doi:10.1097/QAI.0b013e3182986ff8.

52. Thompson CG, Sedykh A, Nicol MR, Muratov E, Fourches D. Short Communication : Cheminformatics Analysis to Identify Predictors. *AIDS Res Hum Retroviruses*. 2014;30(11):1058-1064. doi:10.1089/aid.2013.0254.

53. Greener B, Patterson KB, Prince HM a, Sykes C, Adams JL. Dolutegravir Pharmacokinetics in the Genital Tract and Colorectum of HIV Negative Men After Single and Multiple Dosing. *J Acquir Immune Defic Syndr*. 2013;1(64):39-44. doi:10.3851/IMP2665.Single.

54. Dinoso JB, Kim SY, Wiegand a M, et al. Treatment intensification does not reduce residual HIV-1 viremia in patients on highly active antiretroviral therapy. *Proc Natl Acad Sci U S A*. 2009;106(23):9403-9408. doi:10.1073/pnas.0903107106.

55. Gandhi RT, Zheng L, Bosch RJ, et al. The effect of raltegravir intensification on low-level residual viremia in HIV-infected patients on antiretroviral therapy: a randomized controlled trial. *PLoS Med*. 2010;7(8). doi:10.1371/journal.pmed.1000321.

56. Fletcher C V, Staskus K, Wietgrefe SW, et al. Persistent HIV-1 replication is associated with lower antiretroviral drug concentrations in lymphatic tissues. *Proc Natl Acad Sci U S A*. 2014;111(6):2307-2312. doi:10.1073/pnas.1318249111.

57. Shen L, Siliciano RF. Viral reservoirs, residual viremia, and the potential of highly active antiretroviral therapy to eradicate HIV infection. *J Allergy Clin Immunol*. 2008;122(1):22-28. doi:10.1016/j.jaci.2008.05.033.

58. Archin NM, Liberty A, Kashuba ADM, et al. Administration of vorinostat disrupts HIV-1

latency in patients on antiretroviral therapy. *Nature*. 2013;487(7408):482-485. doi:10.1038/ncomms7379.IRF8.

59. Rasmussen TA, Tolstrup M, Brinkmann CR, et al. Panobinostat, a histone deacetylase inhibitor, for latent virus reactivation in HIV-infected patients on suppressive antiretroviral therapy: A phase 1/2, single group, clinical trial. *Lancet HIV*. 2014;1(1):e13-e21. doi:10.1016/S2352-3018(14)70014-1.

60. Panel on Opportunistic Infections in HIV-Infected Adults and Adolescents. *Guidelines for the Use of Antiretroviral Agents in HIV-1-Infected Adults and Adolescents*.; 2014.

61. Kis O, Robillard K, Chan GNY, Bendayan R. The complexities of antiretroviral drug-drug interactions: role of ABC and SLC transporters. *Trends Pharmacol Sci*. 2010;31(1):22-35. doi:10.1016/j.tips.2009.10.001.

62. Robillard KR, Chan GNY, Zhang G, La Porte C, Cameron W, Bendayan R. Role of P-glycoprotein in the distribution of the HIV protease inhibitor atazanavir in the brain and male genital tract. *Antimicrob Agents Chemother*. 2014;58(3):1713-1722. doi:10.1128/AAC.02031-13.

63. Nagle M, Wu W, Eraly S, Nigam S. Organic anion transport pathways in antiviral handling in choroid plexus in Oat1 (Slc22a6) and Oat3 (Slc22a8) deficient tissue. *Neurosci Lett*. 2013;534:133-138. doi:10.1097/MPG.0b013e3181a15ae8.Screening.

64. Robillard KR, Hoque T, Bendayan R. Expression of ATP-binding cassette membrane transporters in rodent and human sertoli cells: relevance to the permeability of antiretroviral therapy at the blood-testis barrier. *J Pharmacol Exp Ther*. 2012;340(1):96-108. doi:10.1124/jpet.111.186916.

65. Huang Y, Hoque MT, Jenabian MA, et al. Antiretroviral drug transporters and metabolic enzymes in human testicular tissue – potential contribution to HIV-1 sanctuary site [in press]. *J Antimicrob Chemother*. 2016:1-12. doi:dkw046.

66. Thörn M, Finnström N, Lundgren S, Rane A, Lööf L. Cytochromes P450 and MDR1 mRNA expression along the human gastrointestinal tract. *Br J Clin Pharmacol*. 2005;60(1):54-60. doi:10.1111/j.1365-2125.2005.02389.x.

67. Drozdzik M, Gröer C, Penski J, et al. Protein abundance of clinically relevant multidrug transporters along the entire length of the human intestine. *Mol Pharm*. 2014;11(10):3547-3555. doi:10.1021/mp500330y.

68. Zhang QY. Characterization of human small intestinal cytochromes P-450. *Drug Metab Dispos*. 1999;27(7):804-809.

69. Patterson KB, Prince HM a, Stevens T, Shaheen NJ. Differential Penetration of Raltegravir throughout Gastrointestinal Tissue: Implications for Eradication and Cure.

AIDS. 2013;27(9):1413-1419. doi:10.1126/scisignal.2001449.Engineering.

70. van Marle G, Church DL, Nunweiler KD, Cannon K, Wainberg M a, Gill MJ. Higher levels of Zidovudine resistant HIV in the colon compared to blood and other gastrointestinal compartments in HIV infection. *Retrovirology*. 2010;7:74. doi:10.1186/1742-4690-7-74.

71. Nicol MR, Emerson CW, Prince HM, et al. Models for predicting effective HIV chemoprevention in women. *J Acquir Immune Defic Syndr*. 2015;68(4):369-376. doi:10.1097/QAI.0000000000000472 [doi].

72. Muller M, Pena A, Derendorf H. Issues in Pharmacokinetics and Pharmacodynamics of Anti-Infective Agents : Distribution in Tissue. *Antimicrob Agents Chemother*. 2004;48(5):1441-1453. doi:10.1128/AAC.48.5.1441.

73. Cory TJ, Winchester LC, Robbins BL, Fletcher C V. A rapid spin through oil results in higher cell-associated concentrations of antiretrovirals compared with conventional cell washing. *Bioanalysis*. 2015;7(12):1447-1455. doi:10.4155/bio.15.70.

74. Prideaux B, Stoeckli M. Mass spectrometry imaging for drug distribution studies. *J Proteomics*. 2012;75(16):4999-5013. doi:10.1016/j.jprot.2012.07.028.

75. Thompson CG, Bokhart MT, Sykes C, et al. Mass spectrometry imaging reveals heterogeneous efavirenz distribution within putative HIV reservoirs. *Antimicrob Agents Chemother*. 2015;59(5):2944-2948. doi:10.1128/AAC.04952-14.

76. Rosen EP, Thompson CG, Sykes C, Adamson L, Charlins P, Remling-Mulder L. Quantifying Intra- and Inter-species Variability of Antiretroviral (ARV) Distribution in GALT by MSI. In: *23rd Conference on Retroviruses and Opportunistic Infections*. ; 2016.

77. Bokhart MT, Rosen E, Thompson C, Sykes C, Kashuba ADM, Muddiman DC. Quantitative mass spectrometry imaging of emtricitabine in cervical tissue model using infrared matrix-assisted laser desorption electrospray ionization. *Anal Bioanal Chem*. October 2014. doi:10.1007/s00216-014-8220-y.

78. Rosen EP, Sykes C, Thompson CG, Kashuba ADM. Optimized Detection of Latency Reversing Agents in Tissue by Mass Spectrometry Imaging. In: *4th Annual Collaboratory of AIDS Researchers for Eradication Meeting, San Diego, CA*. ; 2013.

79. Huser T, Chan J. Raman spectroscopy for physiological investigations of tissues and cells. *Adv Drug Deliv Rev*. 2015;89:57-70. doi:10.1016/j.addr.2015.06.011.

80. Chuchuen O, Henderson MH, Sykes C, Kim MS, Kashuba ADM, Katz DF. Quantitative analysis of microbicide concentrations in fluids, gels and tissues using confocal raman spectroscopy. *PLoS One*. 2013;8(12):1-23. doi:10.1371/journal.pone.0085124.

81. Maher JR, Chuchuen O, Henderson MH, et al. Co-localized confocal Raman spectroscopy and optical coherence tomography (CRS-OCT) for depth-resolved analyte detection in tissue. *Biomed Opt Express*. 2015;6(6):2022. doi:10.1364/BOE.6.002022.

82. Nazari M, Muddiman DC. Cellular Level Mass Spectrometry Imaging using Infrared Matrix Assisted Laser Desorption Electrospray Ionization (IR-MALDESI) by Oversampling. *Anal Bioanal Chem*. 2015;407(8):37-54. doi:10.1016/bs.mcb.2015.01.016.Observing.

83. Zavalin A, Todd EM, Rawhouser PD, Yang J, Norris JL, Caprioli RM. Direct imaging of single cells and tissue at sub-cellular spatial resolution using transmission geometry MALDI MS. *J Mass Spectrom*. 2012;47(11):1473-1481. doi:10.1002/jms.3108.

84. Guo MT, Rotem A, Heyman J a., Weitz D a. Droplet microfluidics for high-throughput biological assays. *Lab Chip*. 2012;12(12):2146. doi:10.1039/c2lc21147e.

85. Mazutis L, Gilbert J, Ung WL, Weitz DA, Griffiths AD, Heyman JA. Single-cell analysis and sorting using droplet-based microfluidics. *Nat Protoc*. 2013;8(5):870-891. doi:10.1038/nprot.2013.046\rhttp://www.nature.com/nprot/journal/v8/n5/abs/nprot.2013.046.html#supplementary-information.

86. Hatch AC, Fisher JS, Tovar AR, et al. 1-Million droplet array with wide-field fluorescence imaging for digital PCR. *Lab Chip*. 2011;11(22):3838. doi:10.1039/c1lc20561g.

87. Shim J, Olguin LF, Whyte G, et al. Simultaneous Determination of Gene Expression and Enzymatic Activity in Individual Bacterial Cells in Microdroplet Compartments. *J Am Chem Soc*. 2009;131(42):15251-15256. doi:10.1021/ja904823z.

88. Rosen EP, Thompson CG, Sykes C, Mathews M, Adamson L. Quantifying Intra- and Inter-species Variability of ARV Distribution in GALT by MSI. In: *23rd Conference on Retroviruses and Opportunistic Infections*. ; 2016.

89. Patterson KB, Prince H a, Kraft E, et al. Penetration of tenofovir and emtricitabine in mucosal tissues: implications for prevention of HIV-1 transmission. *Sci Transl Med*. 2011;3(112):112re4. doi:10.1126/scitranslmed.3003174.

90. Lin JH, Chiba M, Balani S, et al. Species Differences a Potent in the and Metabolism of Indinavir, a Potent Human Immunodeficiency Virus Protease Inhibitor. *Drug Metab Dispos*. 1996;24(10).

91. Edagwa BJ, Zhou T, McMillan JM, Liu X-M, Gendelman HE. Development of HIV reservoir targeted long acting nanoformulated antiretroviral therapies. *Curr Med Chem*. 2014;21(36):4186-4198. doi:10.1016/j.biotechadv.2011.08.021.Secreted.

92. Parboosing R, Maguire GEM, Govender P, Kruger HG. Nanotechnology and the

treatment of HIV infection. *Viruses*. 2012;4(4):488-520. doi:10.3390/v4040488.

93. Chauhan VP, Jain RK. Strategies for advancing cancer nanomedicine. *Nat Mater*. 2013;12(11):958-962. doi:10.1038/nmat3792.

94. Kinman L, Bui T, Larsen K, et al. Optimization of Lipid Y Indinavir Complexes for Localization in Lymphoid Tissues of HIV-Infected Macaques. *J Acquir Immune Defic Syndr*. 2006;42(2):155-161. doi:10.1097/01.qai.0000214822.33905.87.

95. Namanja H, Emmert D, Davis D, Campos C. Toward Eradicating HIV Reservoirs in the Brain: Inhibiting P- glycoprotein at the Blood-Brain Barrier with Prodrug Abacavir Dimers. *J Am Chem Soc*. 2012;134(6):2976-2980. doi:10.1021/ja206867t.Toward.

96. Roy U, McMillan J, Alnouti Y, et al. Pharmacodynamic and antiretroviral activities of combination nanoformulated antiretrovirals in HIV-1-infected human peripheral blood lymphocyte- reconstituted mice. *J Infect Dis*. 2012;206(10):1577-1588. doi:10.1093/infdis/jis395.

97. Roy U, Ding H, Pilakka-Kanthikeel S, et al. Preparation and characterization of anti-HIV nanodrug targeted to microfold cell of gut-associated lymphoid tissue. *Int J Nanomedicine*. 2015;10:5819-5835. doi:10.2147/IJN.S68348.

98. Nicol MR, Fedoriw Y, Mathews M, et al. Expression of six drug transporters in vaginal, cervical, and colorectal tissues: Implications for drug disposition in HIV prevention. *J Clin Pharmacol*. 2013;(September). doi:10.1002/jcph.248.

99. Kis O, Sankaran-walters S, Walmsley SL, Dandekar S, Bendayan R. HIV-1 Alters Intestinal Expression of Drug Transporters and Metabolic Enzymes : Implications in Antiretroviral Drug Disposition. *Antimicrob Agents Chemother*. 2016;60(5):2771-2781. doi:10.1128/AAC.02278-15.

100. De Rosa MF, Robillard KR, Kim CJ, et al. Expression of membrane drug efflux transporters in the sigmoid colon of hiv-infected and uninfected men. *J Clin Pharmacol*. 2013;53(9):934-945. doi:10.1002/jcph.132.

101. Thompson CG, Fallon JK, Charlins P, Remling-Mulder L, Kovarova M. Quantitative Proteomic Analysis of Drug Transporter Expression in the GI Tract of Multiple Animal Models of HIV Infection. In: *17th Workshop on Clinical Pharmacology of HIV and Hepa*. ; :17.

102. Lin JH. Applications and limitations of interspecies scaling and in vitro extrapolation in pharmacokinetics. *Drug Metab Dispos*. 1998;26(12):1202-1212. doi:0090-9556/98/2612-1202.

103. Thompson CG, Rosen EP, Charlins P, Remling-Mulder L, Kovarova M. Multispecies Differences in Drug Transporter Expression and Localization in GI Tissue. In: *23rd*

Conference on Retroviruses and Opportunistic Infections. ; 2016.

104. Denton PW, Søgaard OS, Tolstrup M. Using animal models to overcome temporal, spatial and combinatorial challenges in HIV persistence research. *J Transl Med*. 2016;14(1):44. doi:10.1186/s12967-016-0807-y.

105. Ho YC, Shan L, Hosmane NN, et al. Replication-competent noninduced proviruses in the latent reservoir increase barrier to HIV-1 cure. *Cell*. 2013;155(3):540-551. doi:10.1016/j.cell.2013.09.020.

106. Thompson CG, Gay C, Kashuba ADM. HIV Persistence in GALT: Pharmacological Challenges and Opportunities. *AIDS Res Hum Retroviruses*. 2017.

107. Barry J a, Robichaud G, Bokhart MT, et al. Mapping Antiretroviral Drugs in Tissue by IR-MALDESI MSI Coupled to the Q Exactive and Comparison with LC-MS/MS SRM Assay. *J Am Soc Mass Spectrom*. April 2014. doi:10.1007/s13361-014-0884-1.

108. Berges BK, Wheat WH, Palmer BE, Connick E, Akkina R. HIV-1 infection and CD4 T cell depletion in the humanized Rag2-/-gamma c-/- (RAG-hu) mouse model. *Retrovirology*. 2006;3:76. doi:10.1186/1742-4690-3-76.

109. Melkus MW, Estes JD, Padgett-Thomas A, et al. Humanized mice mount specific adaptive and innate immune responses to EBV and TSST-1. *Nat Med*. 2006;12(11):1316-1322. doi:10.1038/nm1431.

110. Massud I, Aung W, Martin A, et al. Lack of prophylactic efficacy of oral maraviroc in macaques despite high drug concentrations in rectal tissues. *J Virol*. 2013;87(16):8952-8961. doi:10.1128/JVI.01204-13.

111. Shytaj IL, Norelli S, Chirullo B, et al. A highly intensified ART regimen induces long-term viral suppression and restriction of the viral reservoir in a simian AIDS model. *PLoS Pathog*. 2012;8(6):e1002774. doi:10.1371/journal.ppat.1002774.

112. Neff CP, Ndolo T, Tandon A, Habu Y, Akkina R. Oral pre-exposure prophylaxis by anti-retrovirals raltegravir and maraviroc protects against HIV-1 vaginal transmission in a humanized mouse model. *PLoS One*. 2010;5(12):e15257. doi:10.1371/journal.pone.0015257.

113. Denton PW, Krisko JF, Powell D a, et al. Systemic administration of antiretrovirals prior to exposure prevents rectal and intravenous HIV-1 transmission in humanized BLT mice. *PLoS One*. 2010;5(1):e8829. doi:10.1371/journal.pone.0008829.

114. Veselinovic M, Yang K-H, LeCureux J, et al. HIV Pre-Exposure Prophylaxis: Mucosal Tissue Drug Distribution of RT Inhibitor Tenofovir and Entry Inhibitor Maraviroc in a Humanized Mouse Model. *Virology*. 2014;0:253-263. doi:10.1016/j.virol.2014.07.008.HIV.

115. Robichaud G, Garrard KP, Barry J a, Muddiman DC. MSiReader: an open-source interface to view and analyze high resolving power MS imaging files on Matlab platform. *J Am Soc Mass Spectrom*. 2013;24(5):718-721. doi:10.1007/s13361-013-0607-z.

116. Wang F, Flanagan J, Su N, et al. RNAscope: A novel in situ RNA analysis platform for formalin-fixed, paraffin-embedded tissues. *J Mol Diagnostics*. 2012;14(1):22-29. doi:10.1016/j.jmoldx.2011.08.002.

117. Deleage C, Wietgrefe SW, Del Prete G, Morcock DR, Hao PX, Piatak M. Defining HIV and SIV Reservoirs in Lymphoid Tissues. *Pathog Immun*. 2016;1(1):68-106.

118. Thompson CG, Fallon JK, Mathews M, et al. Multispecies Differences in Drug Transporter Expression and Localization in Gastrointestinal Tissue: Implications for HIV Eradication. *J Antimicrob Chemother*. 2017.

119. Lefrançois L, Puddington L. INTESTINAL AND PULMONARY MUCOSAL T CELLS: Local Heroes Fight to Maintain the Status Quo. *Annu Rev Immunol*. 2006;24(1):681-704. doi:10.1146/annurev.immunol.24.021605.090650.

120. Kassahun K, Mcintosh I, Cui D, et al. Metabolism and Disposition in Humans of Raltegravir (MK-0518). *Pharmacology*. 2007;35(9):1657-1663. doi:10.1124/dmd.107.016196.

121. Ray AS, Cihlar T, Robinson KL, et al. Mechanism of active renal tubular efflux of tenofovir. *Antimicrob Agents Chemother*. 2006;50(10):3297-3304. doi:10.1128/AAC.00251-06.

122. Sankaran S, Guadalupe M, Reay E, et al. Gut mucosal T cell responses and gene expression correlate with protection against disease in long-term HIV-1-infected nonprogressors. *Proc Natl Acad Sci U S A*. 2005;102(28):9860-9865. doi:10.1073/pnas.0503463102.

123. Dumond JB, Yeh RF, Patterson KB, et al. Antiretroviral drug exposure in the female genital tract: implications for oral pre- and post-exposure prophylaxis. *AIDS*. 2007;21(14):1899-1907. doi:10.1097/QAD.0b013e328270385a.Antiretroviral.

124. Greener B, Patterson KB, Prince HMA, et al. Dolutegravir Pharmacokinetics in the Genital Tract and Colorectum of HIV Negative Men After Single and Multiple Dosing. *J Acquir Immune Defic Syndr*. 2013;64(1):39-44. doi:10.1016/j.molcel.2007.05.041.A.

125. Liu P, Müller M, Derendorf H. Rational dosing of antibiotics: the use of plasma concentrations versus tissue concentrations. *Int J Antimicrob Agents*. 2002;19(4):285-290. http://www.ncbi.nlm.nih.gov/pubmed/11978499.

126. Boffito M, Back DJ, Blaschke TF, et al. Protein binding in antiretroviral therapies. *AIDS*

Res Hum Retroviruses. 2003;19(9):825-835. doi:10.1089/088922203769232629.

127. Müller M, Rohde B, Kovar A, Georgopoulos A, Eichler HG, Derendorf H. Relationship between serum and free interstitial concentrations of cefodizime and cefpirome in muscle and subcutaneous adipose tissue of healthy volunteers measured by microdialysis. *J Clin Pharmacol*. 1997;37(12):1108-1113. http://www.ncbi.nlm.nih.gov/pubmed/9506005.

128. Kovar a, Dalla Costa T, Derendorf H. Comparison of plasma and free tissue levels of ceftriaxone in rats by microdialysis. *J Pharm Sci*. 1997;86(1):52-56. doi:10.1021/js960244a.

129. Palmer S, Josefsson L, Coffin JM. HIV reservoirs and the possibility of a cure for HIV infection. *J Intern Med*. 2011;270(6):550-560. doi:10.1111/j.1365-2796.2011.02457.x.

130. Smith MZ, Wightman F, Lewin SR. HIV reservoirs and strategies for eradication. *Curr HIV/AIDS Rep*. 2012;9(1):5-15. doi:10.1007/s11904-011-0108-2.

131. Zuckerman R a, Whittington WLH, Celum CL, et al. Higher concentration of HIV RNA in rectal mucosa secretions than in blood and seminal plasma, among men who have sex with men, independent of antiretroviral therapy. *J Infect Dis*. 2004;190(1):156-161. doi:10.1086/421246.

132. Neely M, Benning L, Xu J, Strickler H. Cervical Shedding of HIV-1 Among Women With Low Levels of Viremia While Receiving Highly Active Antiretroviral Therapy. *J Acquir Immune Defic Syndr*. 2011;44(1):38-42. doi:10.1097/01.qai.0000248352.18007.1f.Cervical.

133. Damouche A, Lazure T, Avettand-Fènoël V, et al. Adipose Tissue Is a Neglected Viral Reservoir and an Inflammatory Site during Chronic HIV and SIV Infection. *PLoS Pathog*. 2015;11(9):e1005153. doi:10.1371/journal.ppat.1005153.

134. Hu M, Cost M, Poloyac S. Expression of Transporters and Metabolizing Enzymes in the Female Lower Genital Tract : Implications for Microbicide Research. *AIDS Res Hum Retroviruses*. 2013;29(0). doi:10.1089/aid.2013.0032.

135. Thompson CG, Fallon JK, Nicol MR, Smith PC, Kashuba ADM. Quantification of Drug Transporters in Vaginal and Cervical Tissue Using a Novel Targeted Proteomics Approach: Implications for Small Molecule Disposition in Viral Reservoirs. In: *20th International AIDS Conference. Melbourne, Australia*. ; 2014.

136. Uchida Y, Zhang Z, Tachikawa M, Terasaki T. Quantitative targeted absolute proteomics of rat blood-cerebrospinal fluid barrier transporters: comparison with a human specimen. *J Neurochem*. 2015;134(6):1104-1115. doi:10.1111/jnc.13147.

137. Denton PW, Olesen R, Choudhary SK, et al. Generation of HIV latency in humanized BLT mice. *J Virol*. 2012;86(1):630-634. doi:10.1128/JVI.06120-11.

138. North TW, Higgins J, Deere JD, et al. Viral sanctuaries during highly active antiretroviral therapy in a nonhuman primate model for AIDS. *J Virol*. 2010;84(6):2913-2922. doi:10.1128/JVI.02356-09.

139. Schmittgen TD, Livak KJ. Analyzing real-time PCR data by the comparative CT method. *Nat Protoc*. 2008;3(6):1101-1108. doi:10.1038/nprot.2008.73.

140. Higgins JW, Bao JQ, Ke AB, et al. Utility of oatp1a/1b-knockout and OATP1B1/3-humanized mice in the study of OATP-mediated pharmacokinetics and tissue distribution: Case studies with pravastatin, atorvastatin, simvastatin, and carboxydichlorofluorescein. *Drug Metab Dispos*. 2014;42(1):182-192. doi:10.1124/dmd.113.054783.

141. Fallon JK, Smith PC, Xia CQ, Kim MS. Quantification of Four Efflux Drug Transporters in Liver and Kidney Across Species Using Targeted Quantitative Proteomics by Isotope Dilution NanoLC-MS/MS. *Pharm Res*. 2016;33(9):2280-2288. doi:10.1007/s11095-016-1966-5.

142. Lan P, Tonomura N, Shimizu A, Wang S, Yang Y-G. Reconstitution of a functional human immune system in immunodeficient mice through combined human fetal thymus/liver and CD34+ cell transplantation. *Blood*. 2006;108(2):487-492. doi:10.1182/blood-2005-11-4388.

143. Melkus MW, Estes JD, Padgett-Thomas A, et al. Humanized mice mount specific adaptive and innate immune responses to EBV and TSST-1. *Nat Med*. 2006;12(11):1316-1322. doi:10.1038/nm1431.

144. Massud I, Martin A, Dinh C, et al. Pharmacokinetic profile of raltegravir, elvitegravir and dolutegravir in plasma and mucosal secretions in rhesus macaques. *J Antimicrob Chemother*. 2015;70(5):1473-1481. doi:10.1093/jac/dku556.

145. MacPhee DJ. Methodological considerations for improving Western blot analysis. *J Pharmacol Toxicol Methods*. 2010;61(2):171-177. doi:10.1016/j.vascn.2009.12.001.

146. Fallon JK, Harbourt DE, Maleki SH, Kessler FK, Ritter JK, Smith PC. Absolute quantification of human uridine-diphosphate glucuronosyl transferase (UGT) enzyme isoforms 1A1 and 1A6 by tandem LC-MS. *Drug Metab Lett*. 2008;2(3):210-222. doi:10.2174/187231208785425764.

147. Asher GN, Fallon JK, Smith PC. UGT concentrations in human rectal tissue after multidose, oral curcumin. *Pharmacol Res Perspect*. 2016;4(2):n/a-n/a. doi:10.1002/prp2.222.

148. Uchida Y, Toyohara T, Ohtsuki S, Moriyama Y, Abe T, Terasaki T. Quantitative Targeted Absolute Proteomics for 28 Transporters in Brush-Border and Basolateral Membrane Fractions of Rat Kidney. *J Pharm Sci*. 2016;105(2):1011-1016. doi:10.1002/jps.24645.

149. Aebersold R, Burlingame AL, Bradshaw R a. Western Blots vs. SRM Assays: Time to turn the tables? *Mol Cell Proteomics*. 2013:2381-2382. doi:10.1074/mcp.E113.031658.

150. Anderson PL, Kiser JJ, Gardner EM, Rower JE, Meditz A, Grant RM. Pharmacological considerations for tenofovir and emtricitabine to prevent HIV infection. *J Antimicrob Chemother*. 2011;66(2):240-250. doi:10.1093/jac/dkq447.

151. WHO. The Top 10 Causes of Death. World Health Organization Fact Sheet. http://www.who.int/mediacentre/factsheets/fs310/en/index.html. Published 2011.

152. Romano J, Kashuba A, Becker S, Cummins J, Turpin J, Veronese F. Pharmacokinetics and pharmacodynamics in HIV prevention; current status and future directions: a summary of the DAIDS and BMGF sponsored think tank on pharmacokinetics (PK)/pharmacodynamics (PD) in HIV prevention. *AIDS Res Hum Retroviruses*. 2013;29(11):1418-1427. doi:10.1089/aid.2013.0122.

153. Division of AIDS. Table for grading the severity of adult and pediatric adverse events. 2009;(August).

154. Zembruski NCL, Büchel G, Jödicke L, Herzog M, Haefeli WE, Weiss J. Potential of novel antiretrovirals to modulate expression and function of drug transporters in vitro. *J Antimicrob Chemother*. 2011;66(4):802-812. doi:10.1093/jac/dkq501.

155. Hijazi K, Cuppone AM, Smith K, et al. Expression of genes for drug transporters in the human female genital tract and modulatory effect of antiretroviral drugs. *PLoS One*. 2015;10(6):1-18. doi:10.1371/journal.pone.0131405.

156. Brown KC, Patterson KB, Malone S a, et al. Single and multiple dose pharmacokinetics of maraviroc in saliva, semen, and rectal tissue of healthy HIV-negative men. *J Infect Dis*. 2011;203(10):1484-1490. doi:10.1093/infdis/jir059.

157. Patterson KB, Prince HA, Kraft E, et al. Penetration of Tenofovir and Emtricitabine in Mucosal Tissues: Implications for Prevention of HIV-1 Transmission. *Sci Transl Med*. 2012;3(July 2010). doi:10.1126/scitranslmed.3003174.Penetration.

158. Babusis D, Phan TK, Lee WA, Watkins WJ, Ray AS. Mechanism for effective lymphoid cell and tissue loading following oral administration of nucleotide prodrug GS-7340. *Mol Pharm*. 2013;10(2):459-466. doi:10.1021/mp3002045.

159. Buseyne F, Le Gall S, Boccaccio C, et al. MHC-I – restricted presentation of HIV-1 virion antigens without viral replication. *Nat Med*. 2001;7(3):5-10. doi:Doi 10.1038/85493.

160. Frank I, Santos JJ, Mehlhop E, et al. Presentation of exogenous whole inactivated simian immunodeficiency virus by mature dendritic cells induces CD4+ and CD8+ T-cell responses. *J Acquir Immune Defic Syndr*. 2003;34(1):7-19.

http://www.ncbi.nlm.nih.gov/pubmed/14501788.

161. Eriksson S, Graf EH, Dahl V, et al. Comparative Analysis of Measures of Viral Reservoirs in HIV-1 Eradication Studies. *PLoS Pathog*. 2013;9(2). doi:10.1371/journal.ppat.1003174.

162. Spina CA, Anderson J, Archin NM, et al. An In-Depth Comparison of Latent HIV-1 Reactivation in Multiple Cell Model Systems and Resting CD4+ T Cells from Aviremic Patients. *PLoS Pathog*. 2013;9(12):1-15. doi:10.1371/journal.ppat.1003834.

163. Thompson CG, Rosen E, Sykes C, Fedoriw Y, Luciw P, Muddiman DC KA. Characterizing Antiretroviral Distribution Within Active Viral Reservoirs Using Mass Spectrometry Imaging. *15th Int Work Clin Pharmacol HIV Hepat C Ther*. 2014.

164. Ni X, Li L, Pan G. HDAC inhibitor-induced drug resistance involving ATP-binding cassette transporters (Review). *Oncol Lett*. 2015;9(2):515-521. doi:10.3892/ol.2014.2714.

165. Podany AT, Winchester LC, Robbins BL, Fletcher C V. Quantification of cell-associated atazanavir, darunavir, lopinavir, ritonavir, and efavirenz concentrations in human mononuclear cell extracts. *Antimicrob Agents Chemother*. 2014;58(5):2866-2870. doi:10.1128/AAC.02551-13.

166. Robichaud G, Barry JA, Garrard KP, Muddiman DC. Infrared Matrix-Assisted Laser Desorption Electrospray Ionization (IR-MALDESI) Imaging Source Couple to a FT-ICR Mass Spectrometer. *J Am Soc Mass Spectrom*. 2013;24(1):92-100. doi:10.1007/s13361-012-0505-9.INFRARED.

167. Gratton S, Cheynier R, Dumaurier M-J, Oksenhendler E. Highly restricted spread of HIV-1 and multiply infected cells within splenic germinal centers. *Proc Natl Acad Sci U S A*. 2000;97(26):14566-14571.

168. Burton GF, Keele BF, Estes JD, Thacker TC. Follicular dendritic cell contributions to HIV pathogenesis. *Immunology*. 2002;14:275-284. doi:10.1016/S1044.

169. Zink MC, Clements JE. A novel simian immunodeficiency virus model that provides insight into mechanisms of human immunodeficiency virus central nervous system disease. *J Neurovirol*. 2002;8 Suppl 2:42-48. doi:10.1080/13550280290101076.

170. Rompay KKA Van. The Use of Nonhuman Primate Models of HIV Infection for the Evaluation of Antiviral Strategies. *AIDS Res Hum Retroviruses*. 2012;28(1):16-35. doi:10.1089/aid.2011.0234.

171. North TW, Rompay KKA Van, Higgins J, et al. Suppression of Virus Load by Highly Active Antiretroviral Therapy in Rhesus Macaques Infected with a Recombinant Simian Immunodeficiency Virus Containing Reverse Transcriptase from Human Immunodeficiency Virus Type 1. *J Virol*. 2005;79(12):7349-7354. doi:10.1128/JVI.79.12.7349.

172. Hofman MJ, Higgins J, Matthews TB, et al. Efavirenz Therapy in Rhesus Macaques Infected with a Chimera of Simian Immunodeficiency Virus Containing Reverse Transcriptase from Human Immunodeficiency Virus Type 1. *Antimicrob Agents Chemother*. 2004;48(9):3483-3490. doi:10.1128/AAC.48.9.3483.

173. Kessner D, Chambers M, Burke R, Agus D, Mallick P. ProteoWizard: open source software for rapid proteomics tools development. *Bioinformatics*. 2008;24(21):2534-2536. doi:10.1093/bioinformatics/btn323.

174. Liu X, Natta K Van, Yeo H, et al. Unbound Drug Concentration in Brain Homogenate and Cerebral Spinal Fluid at Steady State as a Surrogate for Unbound Concentration in Brain Interstitial Fluid ABSTRACT : *Drug Metab Dispos*. 2009;37(4):787-793. doi:10.1124/dmd.108.024125.throughput.

175. de Lange E, Danhof M. Cerebrospinal Fluid Pharmacokinetics to Predict Brain Target Concentrations in the Clinical Setting Implications of the Barriers Between Blood and Brain. *Clin Pharmacokinet*. 2002;41(10):691-703.

176. Peroni RN, Di Gennaro SS, Hocht C, et al. Efavirenz is a substrate and in turn modulates the expression of the efflux transporter *ABCG2*/BCRP in the gastrointestinal tract of the rat. *Biochem Pharmacol*. 2011;82(9):1227-1233. doi:10.1016/j.bcp.2011.07.081.

177. Fellay J, Marzolini C, Meaden ER, et al. Response to antiretroviral treatment in HIV-1-infected individuals with allelic variants of the multidrug resistance transporter 1 : a pharmacogenetics study. *Lancet*. 2002;359:30-36.